Multiscale Views of Multi-agent Interactions in the Context Of Collective Behavior

Subhradeep Roy

Dissertation submitted to the Faculty of the
Virginia Polytechnic Institute and State University
in partial fulfillment of the requirements for the degree of

Doctor of Philosophy
in
Engineering Mechanics

Nicole T. Abaid, Chair
Romesh C. Batra
Mark S. Cramer
James Hanna
Michael R. Taaffe

June 19, 2017
Blacksburg, Virginia

Keywords: multi-agent systems, consensus, synchronization, directed information transfer, real-world networks

Multiscale Views of Multi-agent Interactions in the Context Of Collective Behavior

Subhradeep Roy

Abstract

In nature, many social species demonstrate collective behavior ranging from coordinated motion in flocks of birds and schools of fish to collective decision making in humans. Such distinct behavioral patterns at the group level are the consequence of local interactions among the individuals. We can learn from these biological systems, which have successfully evolved to operate in noisy and fault-prone environments, and understand how these complex interactions can be applied to engineered systems where robustness remains a major challenge. This dissertation addresses a two-scale approach to study these interactions- one in larger scale, where we are interested in the information exchange in a group and how it enables the group to reach a common decision, and the other in a smaller scale, where we are focused in the presence and directionality in the information exchange in a pair of individuals. To understand the interactions at large scale, we use a graph theoretic approach to study consensus or synchronization protocols over two types of biologically-inspired interaction networks. The first network captures both collaborative and antagonistic interactions and the second considers the impact of dynamic leaders in presence of purely collaborative interactions. To study the interactions at small scale, we use an information theoretic approach to understand the directionality of information transfer in a pair of individual using a real-world data-set of animal group motion. Finally, we choose the issue of same-sex marriage in the United States to demonstrate that collective opinion formation is not only a result of negotiations among the individuals, but also reflects inherent spatial and political similarities and temporal delays.

Multiscale Views of Multi-agent Interactions in the Context Of Collective Behavior

Subhradeep Roy

General Audience Abstract

Social animals exhibit coordination often referred to as 'collective behavior' that results from interactions among individuals in the group. This dissertation has demonstrated how interactions can be studied using mathematical modeling, at the same time reveals that real-world interactions are even more complex. Mathematical modeling provides capabilities to introduce biologically inspired phenomena, for example, the implementation of both friendly and hostile interactions that may coexist; and the presence of leader-follower interactions, which is another determinant of collective behavior. The results may find applications in real-world networks, where hostile and leader-follower interactions are prevalent, for example international relations, online social media sites, neural networks, and biologically inspired robotic interactions. We further extend our knowledge regarding interactions by choosing real world systems, the first to understand human decision making, for example in public policies; and the second in animal group motion. Public policy adoption is generally complex and depends on a variety of factors, and no exception is same-sex marriage in the United States which has been a volatile subject for decades until nationwide legalization on June 26, 2015. We target this timely issue and explore the opinion formation of senators and state-law as they evolve over two decades to identify factors that may have affected the dynamics. We unravel geographic proximity, and state-government ideology are significant contributors to the senators opinions and the state-law adoption. Moreover, we build a state-law adoption model which captures these driving factors, and demonstrates predictive power. This study will help to understand or model other public policies that propagate via social and political change. Next we choose the system of bats to investigate navigational leadership roles as they fly in pairs from direct observation of bat swarms in flight. Pairs of bats were continuously tracked in a mountain cave in Shandong Province, China, from which three-dimensional path points are extracted and converted to one-dimensional curvature time series. The study allows us to answer the question of whether individuals fly independently of each other or interact to plan flight paths.

This work was supported by the National Science Foundation under grant CMMI-1342176 and by the Institute for Critical Technology and Applied Science at Virginia Tech.

To Ria

Acknowledgments

First and foremost, I would like to thank my advisor, Dr. Nicole Abaid, for her thorough guidance, encouragement, and continuous support during my doctoral studies. She always prioritized the responsibility in her role as a mentor and provided insights and suggestions on any topic of discussion. She provided freedom to think and explore ideas on my own which helped me to explore different ongoing research but at the same time steered me in the right direction whenever she thought I needed it. Her keen attention to details in editing the manuscripts helped me to improve my written communication skills. She demonstrated how challenges can be overcome with positivity, and she will always be my role model as I pursue my future career.

I am grateful to my PhD committee members, Dr. Romesh Batra, Dr. Mark Cramer, Dr. James Hanna, and Dr. Michael Taaffe, who were always been very responsive to meet in person and in a group, providing insightful suggestions, feedback and critical comments that improved my understating and depth of my knowledge.

The dream of pursuing my PhD at Virginia Tech was possible because of the constant support of my advisor at IIT Kanpur, Dr. Sovan Das. I thank him for developing in me the interest towards applied mathematics. He always encouraged me to explore new areas of research which played a crucial role in determining my PhD research area.

I would like to thank my lab mate, Masoud for providing such a wonderful working environment. The times of frustration and exhaustion were easy to deal with because of his great sense of humor. I would like to thank Kayla for her thorough tutorial in using the tracking system. She has been a wonderful person to work with and is always keen to help.

I would especially like to thank my family. I got my best friend, Ria included in my family on July 22nd, 2013 by getting married to her which has been the best moment of my life. There are no proper words to convey my deep gratitude to her. She has been extremely supportive of me throughout this entire process, and her intense care, endless patience and love helped me get to this point. My parents, Sudhangshu Roy and Krishna Roy deserve special thanks for their continued support, and the sacrifices they made to help me succeed. I deeply thank my parents-in-law Dr. Amalendu Basu and Debjani Basu, who have also been generous with their love and encouragement. I also thank my entire family including my in-laws for the encouragement despite the long distance between us. Finally, I thank the entire Blacksburg

family, including the Bengali Student Association, for making this place like a home away from home.

Contents

List of Figures

List of Tables

Chapter 1

Introduction

Collective behavior in social groups describes the emergence of group level behavior from interaction and negotiation of the individuals to reach an agreement. Examples of collective behavior include collective opinion formation in humans [1] and coordinated motion in flocks of birds [2], school of fish [3], and swarms of insects [4]. In nature, social animals benefit from collective behavior in avoiding predators [5], finding a mate [6], foraging [7], and migration [8]. Interaction among the individuals is a strong determinant of collective behavior, whereby information propagates across the group and the result is the group-level coordination. In particular, individual members in the group act based on local information available to them from neighbors. In this dissertation, we study these interactions; one in large scale, where we use a modeling approach to capture the emergence of collective behavior based on local interactions, and the other in a small scale, where we use real-world datasets to identify pairwise information exchange that drive the group level behavior.

1.1 Large scale view of interaction using modeling approach

Mathematical modeling of collective behavior has drawn interest within the study of distributed systems. One common motivation is to learn from the biological systems, which have successfully evolved to operate in noisy and fault-prone environments, and to understand these complex interactions that can be applied to engineered systems where robustness remains a major challenge. Animal groups may be considered as a collection of individuals, wherein the underlying interaction network among group mates plays a central role in driving the individuals to reach to a common state of agreement. In terms of dynamical systems, collective behavior may be modeled as a synchronization or consensus problems. Synchronization is a phenomenon where individuals in a group interact among themselves to reach a time-varying accordant state. Consensus on the other hand is a specialized case

of synchronization where the accordant state is time-invariant. The interaction among the individuals, also called agents, are generally modeled using graph theory. The interactions among the individuals are represented by networks or graphs, wherein the node or vertex denotes each individual, and the directed edges connecting the nodes represent the neighbors of each individual with whom negotiation is performed.

In recent years, synchronization has been the subject of intensive study in a variety of disciplines. Within the literature, synchronization of dynamical systems is studied varying characteristics of the agent interaction network. In [9, 10, 11, 12, 13], the topology of the interaction network and the coupling strength are assumed to be constant in time and results on conditions to achieve synchronization are presented. The concept of the master stability function (MSF) approach introduced in [12] has been an effective tool for studying synchronization over static network models. Synchronization over dynamic network topologies is relatively less explored and has been studied in [14, 15], where topologies updating from deterministic sequences are considered and in [16, 17, 18, 19, 20, 21], where topologies updating from realizations of a random variable (stochastic) are considered. A review of several recent works on evolving dynamical networks may be found in [22]; synchronization over blinking networks, where coupling strength and the connection topology varies with time, is highlighted along with applications to real-world systems, for example, cellular neural networks, epidemic spreading, and opinion dynamics to mention a few. Motivated by real-world networks, synchronization is studied in [23], where coupling strength is varied, and in [24], where the cardinality of the agents' neighbor sets are varied. Synchronization over time varying numerosity constrained (NC) networks, which constrains the network by prescribing a limit on number perception of the individuals, has been studied in detail in [25] and closed form results are provided for stochastic synchronization.

On the other hand, consensus problems in multi-agent systems have received more attention based in part on their wide range of applications, such as unmanned aerial vehicles [26, 27], autonomous underwater vehicles (AUVs) [28, 29, 30, 31], air traffic control [32, 33] and wireless sensor networks [34, 35]. Consensus problems are supported by a large theoretical literature exploring these problems [36, 37, 38, 39, 40, 41, 42, 43, 44, 45]. Consensus protocols are studied considering static network topologies in [40, 45], dynamic network topologies with deterministic switching in [41, 42], and stochastic topologies in [37, 39, 43]. A variety of metrics for consensus and stochastic synchronization conditions are developed from stability concepts, including mean square stability [37], almost sure stability [44], and MSF [12] of the disagreement among agents. Within both the consensus and synchronization literature, closed form results for consensus and synchronization conditions are limited to a few well studied topologies, such as consensus over Erdős-Rényi random networks in [36] and NC networks in [37, 38] and stochastic synchronization in [25].

Furthermore, interaction networks can be used to incorporate another striking feature of social groups which is leadership by an individual or subset of the group, and has been studied for example in fish schools [46]. This group behavior may be modeled as leader-follower consensus and synchronization protocols, which partition the agents into two types: leaders

and followers [38, 47]. In general, the leaders have access to more information and attempt to drive the entire system to a desired common state through their updating protocol. It is noteworthy that leaders whose states are time-variant and update dynamically according to a consensus or synchronization protocols are rarely considered in the literature [48] and closed form expressions relating the convergence speed among leaders to that of the whole system are particularly absent. In addition, the nature of interaction among the individuals can also be varied by modifying properties of the edges connecting the nodes. For example, hostile and friendly interactions among the individuals can be simultaneously modeled by implementing a signed graph, which uses both positive and negatively weighted edges [49, 50, 51]. In summary, by varying both edges and nodes, this modeling approach has the capability of reproducing a wide variety of collective behaviors that we observe in nature.

In this dissertation, we study consensus and synchronization over two types of biologically-inspired interaction networks. The first captures both collaborative and antagonistic interactions and the second considers the impact of dynamic leaders in presence of purely collaborative interactions. Although static or deterministically switching networks have received attention in the literature based on the tractability of these problems, in this work we target randomly switching networks to model the more realistic scenario that individuals in social groups share information with a dynamic and stochastic set of peers. We establish closed form results for the rate of convergence to consensus and conditions for stochastic synchronization over each network type.

1.2 Small scale view of interaction using data-driven approach

Consensus and synchronization protocols provide an approach to study collective behavior relying on a priori assumptions that individuals seek agreement on a quantity of interest through iterated negotiations. However, a deeper understanding regarding the nature of unknown interactions triggers the need for an alternate approach which uses evidences from real-world phenomenon. For example, collective opinion formation in humans have attracted researchers from different discipline to fully understand and identify the factors that might shape the opinion space using real data from social networks platforms [52, 53, 54]. Opinion dynamics in general is a very complex process and lot of underlying factors affect how individuals form opinion and make decisions. To attain a quantitative assessment of opinion dynamics, recent availability of real-world data set has been very useful. In this dissertation, we choose two real-world datasets, first, the issue of same-sex marriage to study collective opinion formation in humans and second, system of bats to study the role of pairwise interactions.

Public policies are perfect examples where opinion formation span both individual and population scales [55, 56, 57]. One such example is same-sex marriage in the United States.

Same-sex marriage in the United States has been a volatile subject for decades until nationwide legalization on June 26, 2015. We target this timely issue and explore the opinion formation of senators and state-law as they evolve over two decades to identify factors that may have affected the dynamics. We identify change in opinion not only results from negotiations among individuals, but also reflects inherent spatial and political similarities and temporal delays. Drawing on the results of the data-based analysis, we provide a state-law adoption model with which we seek to identify when states switch from banning to legalizing same-sex marriage. There are several mathematical models that incorporate protocols motivated from real-world phenomena, and are important to understand the dynamics of opinion formation and for their predictive power. For example, the "voter model" [58] which is relevant in predicting election results; the "majority rule model" [59, 60, 61] where the position of the majority determines the group level opinion. However, in our study we use "social impact model", [62, 63] which is grounded on a psychological theory that considers the influence of the group size, their convincing power, and the distance from a target opinion. We demonstrate that a distance-based social impact model is able to capture the evolution of the state-laws and shows a good predictive power in terms of correctly identifying the states that switch from banning to legalizing the same-sex marriage.

To further our study in understanding interactions at small scale, we use information theoretic approaches to understand the directionality of information transfer in a pair of individuals using a real-world dataset of animal group motion. Particularly, we target bats, which are unique among such social animals in that they use active sensory echolocation or bio-sonar. In other words, they emit ultrasonic waves and sense echoes to detect and navigate surroundings. In real bat swarms, understanding navigational leadership roles is a challenge, and quantitative assessment of leadership appears to be relatively less explored. Given the broadcast nature of bio-sonar, the active sensing promotes information sharing which allows bats to potentially send information forward in space, whereas vision or passive sensing may not. We seek to understand navigational leadership in bats from direct observation of bat swarms in flight. Pairs of bats were continuously tracked in a mountain cave in Shandong Province, China, from which 3D path points are extracted and converted to 1D curvature time series. We explore two recent tools from dynamical systems to extract causal relationships between these time series, namely transfer entropy (TE) and convergent cross mapping (CCM). These tools measure the directional information transfer between two random processes. TE is formulated in terms of resolution of uncertainty and is a measure of directional information transfer between two time series. The principal difficulty to calculate TE from experimental data is in estimating the probability distributions as it is a data hungry process. TE has been successfully applied to a large variety of subject areas including neuroscience [64], economics [65], and social media [66]. On the other hand, convergent cross mapping (CCM) is relatively recent tool to determine causality between two time series [67] which can be extended to nonlinear, non-separable dynamical systems, involving weakly coupled variables and in presence of third variable. We use these tools to identify the direction of information transfer between a pair of bats flying together, which allows us to answer the question of whether individuals fly independently of each other or

interact to plan flight paths. We find that the identified causal relationships between bats is sensitive to the selected mathematical tools and parameters.

This dissertation is organized as follows. In Chapter 2, we develop a mathematical model capturing collaborative and antagonistic interactions over randomly switching network and study the convergence of consensus and synchronization protocols. In Chapter 3, we study a leader-follower model in purely collaborative framework and provide closed form results for the rate of convergence to consensus and conditions for stochastic synchronization. In Chapter 4, we explore the issue of the same-sex marriage in United States, to identify the factors that play important role in real-world opinion formation. In Chapter 5, we use information theoretic approaches to investigate the navigational leadership of bats using direct observation of swarms in flight. Chapter 6 is reserved for conclusion.

1.3 References

[1] Daron Acemoglu and Asuman Ozdaglar. Opinion dynamics and learning in social networks. *Dynamic Games and Applications*, 1(1):3–49, 2011.

[2] Michele Ballerini, Nicola Cabibbo, Raphael Candelier, Andrea Cavagna, Evaristo Cisbani, Irene Giardina, Vivien Lecomte, Alberto Orlandi, Giorgio Parisi, and Andrea Procaccini. Interaction ruling animal collective behavior depends on topological rather than metric distance: Evidence from a field study. *Proceedings of the National Academy of Sciences*, 105(4):1232–1237, 2008.

[3] Roland W Tegeder and Jens Krause. Density dependence and numerosity in fright stimulated aggregation behaviour of shoaling fish. *Philosophical Transactions of the Royal Society of London. Series B: Biological Sciences*, 350(1334):381–390, 1995.

[4] John Stodart Kennedy. The migration of the desert locust (schistocerca gregaria forsk.). i. the behaviour of swarms. ii. a theory of long-range migrations. *Philosophical Transactions of the Royal Society of London B: Biological Sciences*, 235(625):163–290, 1951.

[5] Birgitta Sillen-Tullberg and Olof Leimar. The evolution of gregariousness in distasteful insects as a defense against predators. *American Naturalist*, pages 723–734, 1988.

[6] David P Cowan. Group living in the european rabbit (oryctolagus cuniculus): mutual benefit or resource localization? *The Journal of Animal Ecology*, pages 779–795, 1987.

[7] Timothy M Casey, Barbara Joos, Terrence D Fitzgerald, Mary E Yurlina, and Paula A Young. Synchronized group foraging, thermoregulation, and growth of eastern tent caterpillars in relation to microclimate. *Physiological Zoology*, pages 372–377, 1988.

[8] Eberhard Gwinner. Circannual rhythms in bird migration. *Annual Review of Ecology and Systematics*, 8:381–405, 1977.

[9] Xiwei Liu and Tianping Chen. Cluster synchronization in directed networks via intermittent pinning control. *IEEE Transactions on Neural Networks*, 22(7):1009–1020, 2011.

[10] Alex Arenas, Albert Diaz-Guilera, Jurgen Kurths, Yamir Moreno, and Changsong Zhou. Synchronization in complex networks. *Physics Reports*, 469(3):93–153, 2008.

[11] Francesco Sorrentino, Mario di Bernardo, Franco Garofalo, and Guanrong Chen. Controllability of complex networks via pinning. *Physical Review E*, 75(4):046103, 2007.

[12] Louis M Pecora and Thomas L Carroll. Master stability functions for synchronized coupled systems. *Physical Review Letters*, 80(10):2109, 1998.

[13] Yang-Yu Liu, Jean-Jacques Slotine, and Albert-Laszlo Barabasi. Controllability of complex networks. *Nature*, 473(7346):167–173, 2011.

[14] Daniel J Stilwell, Erik M Bollt, and D Gray Roberson. Sufficient conditions for fast switching synchronization in time-varying network topologies. *SIAM Journal on Applied Dynamical Systems*, 5(1):140–156, 2006.

[15] Jun Zhao, David J Hill, and Tao Liu. Synchronization of complex dynamical networks with switching topology: a switched system point of view. *Automatica*, 45(11):2502–2511, 2009.

[16] Bo Shen, Zidong Wang, and Xiaohui Liu. Bounded synchronization and state estimation for discrete time-varying stochastic complex networks over a finite horizon. *IEEE Transactions on Neural Networks*, 22(1):145–157, 2011.

[17] Maurizio Porfiri, Daniel J Stilwell, and Erik M Bollt. Synchronization in random weighted directed networks. *IEEE Transactions on Circuits and Systems I: Regular Papers*, 55(10):3170–3177, 2008.

[18] Maurizio Porfiri, Daniel J Stilwell, Erik M Bollt, and Joseph D Skufca. Random talk: Random walk and synchronizability in a moving neighborhood network. *Physica D: Nonlinear Phenomena*, 224(1):102–113, 2006.

[19] Maurizio Porfiri. Stochastic synchronization in blinking networks of chaotic maps. *Physical Review E*, 85(5):056114, 2012.

[20] Andrzej Stefanski, Jerzy Wojewoda, Tomasz Kapitaniak, and Serhiy Yanchuk. Simple estimation of synchronization threshold in ensembles of diffusively coupled chaotic systems. *Physical Review E*, 70(2):026217, 2004.

[21] Arturo Buscarino, Luigi Fortuna, Mattia Frasca, and Alessandro Rizzo. Synchronization in networks of mobile agents. In *Modelling, Estimation and Control of Networked Complex Systems*, pages 3–25. Springer, 2009.

[22] Igor Belykh, Mario di Bernardo, Jurgen Kurths, and Maurizio Porfiri. Evolving dynamical networks. *Physica D: Nonlinear Phenomena*, 267:1–6, 2014.

[23] Changsong Zhou, Adilson E Motter, and Jurgen Kurths. Universality in the synchronization of weighted random networks. *Physical Review Letters*, 96(3):034101, 2006.

[24] Takashi Nishikawa, Adilson E Motter, Ying-Cheng Lai, and Frank C Hoppensteadt. Heterogeneity in oscillator networks: Are smaller worlds easier to synchronize? *Physical Review Letters*, 91(1):014101, 2003.

[25] Nicole Abaid and Maurizio Porfiri. Synchronous dynamics over numerosity-constrained stochastic networks. In *Applications of Chaos and Nonlinear Dynamics in Science and Engineering-Vol. 2*, pages 95–121. Springer, 2012.

[26] Randal W Beard, Timothy W McLain, Michael A Goodrich, and Erik P Anderson. Coordinated target assignment and intercept for unmanned air vehicles. *IEEE Transactions on Robotics and Automation*, 18(6):911–922, 2002.

[27] Michael A Kovacina, Daniel Palmer, Guang Yang, and Ravi Vaidyanathan. Multi-agent control algorithms for chemical cloud detection and mapping using unmanned air vehicles. In *IEEE/RSJ International Conference on Intelligent Robots and Systems*, volume 3, pages 2782–2788, 2002.

[28] Qiuling Jia and Guangwen Li. Formation control and obstacle avoidance algorithm of multiple autonomous underwater vehicles (AUVs) based on potential function and behavior rules. In *IEEE International Conference on Automation and Logistics*, pages 569–573, 2007.

[29] Maurizio Porfiri, D Gray Roberson, and Daniel J Stilwell. Tracking and formation control of multiple autonomous agents: A two-level consensus approach. *Automatica*, 43(8):1318–1328, 2007.

[30] Ratnesh Kumar and James A Stover. A behavior-based intelligent control architecture with application to coordination of multiple underwater vehicles. *IEEE Transactions on Systems, Man and Cybernetics, Part A: Systems and Humans*, 30(6):767–784, 2000.

[31] Darren K Maczka, Davide Spinello, Daniel J Stilwell, Aditya S Gadre, and Wayne L Neu. Coordinated tracking of an acoustic signal by a team of autonomous underwater vehicles. In *AUVSI's Unmanned Systems North America*, 2009.

[32] Bo Chen and Harry H Cheng. A review of the applications of agent technology in traffic and transportation systems. *IEEE Transactions on Intelligent Transportation Systems*, 11(2):485–497, 2010.

[33] Minh Nguyen-Duc, J-P Briot, and Alexis Drogoul. An application of multi-agent coordination techniques in air traffic management. In *IEEE/WIC International Conference on Intelligent Agent Technology*, pages 622–625, 2003.

[34] Min Chen, Sergio Gonzalez, and Victor CM Leung. Applications and design issues for mobile agents in wireless sensor networks. *IEEE Wireless Communications*, 14(6):20–26, 2007.

[35] Kemal Akkaya and Mohamed Younis. A survey on routing protocols for wireless sensor networks. *Ad Hoc Networks*, 3(3):325–349, 2005.

[36] Silvana Silva Pereira. Mean square convergence of consensus algorithms in random WSNs. *IEEE Transactions on Signal Processing*, 58(5):2866–2874, 2010.

[37] Nicole Abaid and Maurizio Porfiri. Consensus over numerosity-constrained random networks. *IEEE Transactions on Automatic Control*, 56(3):649–654, 2011.

[38] Nicole Abaid and Maurizio Porfiri. Leader-follower consensus over numerosity-constrained random networks. *Automatica*, 48(8):1845–1851, 2012.

[39] Yuko Hatano and Mehran Mesbahi. Agreement over random networks. *IEEE Transactions on Automatic Control*, 50(11):1867–1872, 2005.

[40] Jianquan Lu, Daniel WC Ho, and Jurgen Kurths. Consensus over directed static networks with arbitrary finite communication delays. *Physical Review E*, 80(6):066121, 2009.

[41] Wei Ren and Randal Beard. *Distributed consensus in multi-vehicle cooperative control: theory and applications*. Springer, 2007.

[42] Reza Olfati-Saber, J Alex Fax, and Richard M Murray. Consensus and cooperation in networked multi-agent systems. *Proceedings of the IEEE*, 95(1):215–233, 2007.

[43] Wei Ren and Randal W Beard. Consensus seeking in multiagent systems under dynamically changing interaction topologies. *IEEE Transactions on Automatic Control*, 50(5):655–661, 2005.

[44] Maurizio Porfiri and Daniel J Stilwell. Consensus seeking over random weighted directed graphs. *IEEE Transactions on Automatic Control*, 52(9):1767–1773, 2007.

[45] Rifat Sipahi and Artug Acar. Stability analysis of three-agent consensus dynamics with fixed topology and three non-identical delays. In *ASME Dynamic Systems and Control Conference*, pages 1483–1490, 2008.

[46] Iain D Couzin, Christos C Ioannou, Guven Demirel, Thilo Gross, Colin J Torney, Andrew Hartnett, Larissa Conradt, Simon A Levin, and Naomi E Leonard. Uninformed individuals promote democratic consensus in animal groups. *Science*, 334(6062):1578–1580, 2011.

[47] Ran Xiaohong and Wu Qinghe. Leader-follower consensus for multi-agent systems based on error predictor. In *International Conference on Measuring Technology and Mechatronics Automation*, pages 681–684, 2013.

[48] Qiang Song, Fang Liu, Jinde Cao, and Wenwu Yu. *M*-matrix strategies for pinning-controlled leader-following consensus in multiagent systems with nonlinear dynamics. *IEEE Transactions on Cybernetics*, 43(6):1688–1697, 2013.

[49] Claudio Altafini and Gabriele Lini. Predictable dynamics of opinion forming for networks with antagonistic interactions. *IEEE Transactions on Automatic Control*, 60(2):342–357, 2015.

[50] Claudio Altafini. Consensus problems on networks with antagonistic interactions. *IEEE Transactions on Automatic Control*, 58(4):935–946, 2013.

[51] Claudio Altafini. Dynamics of opinion forming in structurally balanced social networks. *PloS ONE*, 7(6):e38135, 2012.

[52] Abhimanyu Das, Sreenivas Gollapudi, and Kamesh Munagala. Modeling opinion dynamics in social networks. In *Proceedings of the 7th ACM international conference on Web search and data mining*, pages 403–412. ACM, 2014.

[53] Felipe Bravo-Marquez, Daniel Gayo-Avello, Marcelo Mendoza, and Barbara Poblete. Opinion dynamics of elections in twitter. In *Web Congress (LA-WEB), 2012 Eighth Latin American*, pages 32–39. IEEE, 2012.

[54] Walter Quattrociocchi, Guido Caldarelli, and Antonio Scala. Opinion dynamics on interacting networks: media competition and social influence. *Scientific reports*, 4:4938, 2014.

[55] Stuart N Soroka and Christopher Wlezien. Opinionpolicy dynamics: public preferences and public expenditure in the united kingdom. *British Journal of Political Science*, 35(04):665–689, 2005.

[56] David Protess and Maxwell E McCombs. *Agenda setting: Readings on media, public opinion, and policymaking*. Routledge, 2016.

[57] Benjamin I Page and Robert Y Shapiro. Effects of public opinion on policy. *American political science review*, 77(01):175–190, 1983.

[58] Vishal Sood, Tibor Antal, and Sidney Redner. Voter models on heterogeneous networks. *Physical Review E*, 77(4):041121, 2008.

[59] Serge Galam. Minority opinion spreading in random geometry. *The European Physical Journal B-Condensed Matter and Complex Systems*, 25(4):403–406, 2002.

[60] Claudio J Tessone, Raul Toral, Pau Amengual, Horacio S Wio, and Maxi San Miguel. Neighborhood models of minority opinion spreading. *The European Physical Journal B-Condensed Matter and Complex Systems*, 39(4):535–544, 2004.

[61] R Lambiotte. How does degree heterogeneity affect an order-disorder transition? *EPL (Europhysics Letters)*, 78(6):68002, 2007.

[62] Bibb Latane. The psychology of social impact. *American Psychologist*, 36(4):343, 1981.

[63] Maciej Lewenstein, Andrzej Nowak, and Bibb Latane. Statistical mechanics of social impact. *Physical Review A*, 45(2):763, 1992.

[64] Alexander G Dimitrov, Aurel A Lazar, and Jonathan D Victor. Information theory in neuroscience. *Journal of computational neuroscience*, 30(1):1–5, 2011.

[65] Okyu Kwon and Jae-Suk Yang. Information flow between composite stock index and individual stocks. *Physica A: Statistical Mechanics and its Applications*, 387(12):2851–2856, 2008.

[66] Greg Ver Steeg and Aram Galstyan. Information transfer in social media. In *Proceedings of the 21st international conference on World Wide Web*, pages 509–518. ACM, 2012.

[67] George Sugihara, Robert May, Hao Ye, Chih-hao Hsieh, Ethan Deyle, Michael Fogarty, and Stephan Munch. Detecting causality in complex ecosystems. *science*, 338(6106):496–500, 2012.

Chapter 2

On the effect of collaborative and antagonist interactions on synchronization and consensus in networks of conspecific agents

The contents of this chapter have appeared partially in a conference paper at the ASME 2015 Dynamic Systems and Control Conference in Columbus, Ohio, USA.

2.1 Abstract

While the vast majority of work on consensus and synchronization considers only collaborative interactions among the agents, antagonistic interactions may play important roles in coordination of social systems. In this work, we define a composite model over a stochastically-switching network capturing both collaborative and antagonistic interactions. We consider a general class of agents, so-called conspecifics, defined in terms of a common distribution for their interaction capacity and the weights they ascribe to interactions. We find closed form expressions for necessary and sufficient conditions for consensus, the rate of convergence to consensus, and conditions for stochastic synchronization. This model is further extended to composite topologies capable of capturing any number of independent interaction modes. Results demonstrate the presence of antagonistic interactions may help the system to achieve consensus and synchronization which is not possible in presence of only

collaborative interactions and, at times, enables convergence at a faster rate.

2.2 Introduction

The vast majority of work on synchronization and consensus among networked agents considers agents to be collaborative, which ignores potentially hostile interactions that drive the group state away from agreement. However, it has been recently discovered that social relations among the individuals may be composed of different modes [1], for example, friendly and hostile relations. One such situation is the effect of jamming in groups of animals that use active sensory systems [2]. For example, bats echolocate by emitting ultrasonic waves and sensing echoes to navigate and detect surroundings [2]. Jamming occurs when multiple bats are echolocating and each individuals' calls become difficult to distinguish, which may lead to misinterpretation of their environment [2]. Other examples of antagonistic and collaborative interactions can be found in different social networks [3, 4]. A particularly relevant example is in [1], where real-world networks with negative interactions between pairs of individuals are studied; the empirical data in this Chapter shows instances where both collaborative and antagonistic interactions are present between the same pair of individuals. These different interaction modes can be captured by the superposition of multiple interaction networks representing each unique relation, where one mode of interaction may result in collaboration and another may result in driving the states of the agents apart. This may be particularly relevant in modeling bat-inspired robotic interactions, where the vision of the bats and jamming of acoustic signals may be represented by the collaborative and antagonistic communication topologies, respectively. This model includes the case that an agent may be simultaneously collaborative and antagonistic to another agent. For example, if a robotic bat sees a live bat and follows it (collaborative vision), the live bat's echolocation may lead to jamming (antagonistic acoustics).

Antagonistic and collaborative interaction networks can be modeled by implementing a signed graph, which uses both positive and negatively weighted edges. Antagonistic interactions modeled in this way are explored to some extent across the literature. Consensus problems in the presence of antagonistic agents over static networks are considered in [5, 6, 7]. Results in [6, 7] demonstrate how bipartite consensus is achieved, in which all agents converge to same magnitude but opposite in sign. The signed graph is also studied over a gossiping model in [8], and over deterministically switching signed random networks in [9]. The coexistence of collaborative and antagonistic interactions between a pair of individuals at the same time has been identified as a more complex and realistic problem in [10]. In particular, such a study has been proposed as a future work which may have applications, for example, in game theory. We target this timely problem by building the antagonistic interaction network independently of the collaborative interaction network and superimpose to obtain the composite network topology. This framework is further generalized by extending to composite topologies capable of capturing any number of independent modes of

interaction. The generalization in terms of agents is obtained by assuming the agents to be conspecific, which can be specified to network topologies studied in the literature.

Modeling of consensus protocols considering conspecific agents is first introduced in [11], where agents are defined in terms of the same common random variable and are thus called "conspecific". More specifically, these agents draw traits from independent realizations of the same bivariate distribution for the cardinality of their neighbor set and the averaging weight parameter assigned to their neighbors at each time step. The conspecific model offers a general case of the recent work in [12], where the concept of activity potential distribution is related to the network degree distribution and results with various real-world networks are compared. The authors mention that deviations from the empirical data result from constant edge weights in the network, a condition which should be relaxed in the future to capture more realistic scenarios. The conspecific model here considers exactly this case, since edge weights vary as realizations of a random variable.

The objective of the present study is to gain insight into the role of antagonistic interactions in consensus and synchronization. The results demonstrate that the presence of antagonistic interactions may help the system to achieve consensus and stochastic synchronization, which is not possible in presence of collaborative interactions only. The fact that negative interactions improve synchronization is also been established in [13], where the results show that synchronization over a static interaction network can be optimized by targeted edge removal or by adding negatively weighted edges. This work differs from the present study in that the interaction network in [13] is neither randomly generated nor switching during the synchronization protocol, so that the condition for convergence depends on the static network topology. Conversely, the condition for convergence derived in this work is a function of multiple moments of a probability distribution describing both the network construction and interaction weights.

In this work, we establish a necessary and sufficient condition for convergence of a collaborative-antagonistic network of conspecific agents to consensus, which automatically gives the convergence rate, and we adapt this result to a necessary and sufficient condition for synchronization in analogously coupled dynamical systems. These conditions are defined in terms of the mean square stability of the disagreement among agents. The closed form results are further extended for a composite topology expressed as a linear combination of independent networks. We choose numerosity-constrained (NC) networks [14] as an exemplary protocol to illustrate our results.

In the rest of the Chapter, we use the following notation: $\rho(\cdot)$ for the spectral radius of a matrix; $\mathbf{E}[\cdot]$ for expected value; $\otimes$ and $\oplus$ for the Kronecker product and the sum, respectively; superscript T for matrix transposition; I_N for the N-dimensional identity matrix; $e_i \in \mathbb{R}^N$ for ith column of I_N; $1_N \in \mathbb{R}^N$ for the N-dimensional vector with all entries equal to one; and $0_N \in \mathbb{R}^N$ for the N-dimensional vector with all entries equal to zero.

2.3 Problem statement

In our present model, we define two directed graphs for the interaction topology to incorporate collaborative and antagonistic interactions among the agents, and we call them the "helping graph" and "hurting graph", respectively. The composite communication topology is then given by additively combining these two graphs. Agents average their states with "neighbors" defined by shared edges in this composite topology. The helping graph is so named since this topology incorporates collaboration among the agents, which may result in the convergence of the agents' states to synchronization or consensus when considered alone. On the other hand, averaging over the hurting graph alone always results in divergence of the state. In the rest of the Chapter, the subscript 1 is used to denote the variables associated with the helping graph and subscript 2 to denote that of the hurting graph.

In this protocol, we target a generalized random network consisting of conspecific agents [11] which may be specialized to such networks as NC and Erdos-Renyi models. In the conspecific model, agents are randomly assigned two traits as a realization of a bivariate distribution at every time step; these traits are the cardinality of their neighbor sets and the weight they assign to their neighbors. At each time step, an agent's neighbor set is randomly selected from all other agents according to a uniform distribution, with the cardinality fixed by the bivariate distribution. All agents in the network are subject to the same bivariate distribution, which warrants their definition as "conspecifics".

Here, we explain how we build collaborative and antagonistic interactions into a network of conspecific agents. At every time step, the cardinality of each agent's neighbor set is independent realizations of the random variable $\mathcal{D}_1$ for helping graph and by $\mathcal{D}_2$ for hurting graph. The averaging weight, also called persuasibility, assigned by each agent to its neighbors is generated realizations of the random variables $\mathcal{E}_1$ and $\mathcal{E}_2$ for helping and hurting graph, respectively. The term "persuasibility" is used since small values of this quantity mean that an agent's updated state is dominated by its previous state, as opposed to information from neighbors as is the case when this quantity is large. We note that the topology of the helping graph is independent to that of the hurting graph. The jointly distributed random variables, $\mathcal{D}_i$ and $\mathcal{E}_i$ for $i = 1, 2$, are assumed to have bivariate distribution $g_{\mathcal{D}_1,\mathcal{E}_1}(d_1, \epsilon_1)$ for the helping graph and $g_{\mathcal{D}_2,\mathcal{E}_2}(d_2, \epsilon_2)$ for the hurting graph, where $d_1, d_2 \in \{0, 1, \ldots, N-1\}$ and $\epsilon_1, \epsilon_2 \in \mathbb{R}^+$.

To build the interaction network in discrete time with time step $k \in \mathbb{Z}^+$, we define two independent and identically distributed random matrices $M_i(k) \in \mathbb{R}^{N\times N}$ for $i = 1, 2$. The random variable $M(k)$ is given by the relation $M(k) = M_1(k) - M_2(k)$ to incorporate the helping and hurting topologies in the composite graph. The ith row of a realization of the matrix M_1 has diagonal entry equal to $\epsilon_{1i}d_{1i}$ and off-diagonal entries in $\{0, -\epsilon_{1i}\}$, where d_{1i} and ϵ_{1i} are realizations of $\mathcal{D}_1$ and $\mathcal{E}_1$, respectively, for the ith agent. Among the off-diagonal entries, there are d_{1i} nonzero entries and $N - d_{1i} - 1$ zero entries, making the M_1 matrix a type of graph Laplacian where each row is multiplied by a different constant value. In a

similar fashion, ith row of a realization of the matrix M_2 has diagonal entry equal to $\epsilon_{2i}d_{2i}$ and off-diagonal entries in $\{0, -\epsilon_{2i}\}$, where d_{2i} and ϵ_{2i} are realizations of random variables $\mathcal{D}_2$ and $\mathcal{E}_2$, respectively. Note that both $M_1(k)$ and $M_2(k)$ have the property $M_i(k)1_N = 0_N$, for $i = 1, 2$, which implies $M(k)1_N = 0_N$. We comment that M_2 is modeled independently of M_1, and the negative edges of the composite network are then introduced by multiplying all the entries of M_2 by negative one. That is why M is denoted by the difference of M_2 from M_1, instead of summing them up. Summing up the construction above, the ith row of a realization of the state matrix M has diagonal entry equal to $(\epsilon_{1i}d_{1i}) - (\epsilon_{2i}d_{2i})$ and off-diagonal entries in $\{0, -\epsilon_{1i},\ \epsilon_{2i},\ (-\epsilon_{1i} + \epsilon_{2i})\}$ and every permutation of these zero and non-zero off-diagonal entries is equally likely. We comment that each row of this matrix is dictated by identically distributed random variables which are independent over both agents and time steps. Preliminary work on consensus in this model has been presented in [15].

2.4 Results

2.4.1 Consensus

We consider N conspecific agents with state $x(k) \in \mathbb{R}^N$ at time k updating according to discrete-time consensus protocol

$$x(k+1) = W(k)x(k), \tag{2.1}$$

where $W(k) = I_N - M(k) \in \mathbb{R}^{N\times N}$ is the state matrix with the property $W(k)1_N = 1_N$. Following the methodology in [14], we project the consensus problem (2.1) on the disagreement space in terms of a disagreement variable $\xi(k)$, which updates as

$$\xi(k+1) = \widetilde{W}(k)\xi(k), \tag{2.2}$$

where $\xi_k = Q^T x_k \in \mathbb{R}^{N-1}$ and $\widetilde{W} = Q^T W Q$. The matrix $Q \in \mathbb{R}^{N\times(N-1)}$ is not unique, but has the properties $Q^T 1_N = 0_N$, $Q^T Q = I_{N-1}$, and $QQ^T = R = I_N - 1_N {1_N}^T$. To quantify the rate of decay of the disagreement dynamics, the asymptotic convergence factor is defined, following [16], as

$$r_a = \sup_{\|\xi_0\|\neq 0} \lim_{k\to\infty} \left(\mathbf{E}\left[\|\xi_k\|^2\right] / \|\xi_0\|^2\right)^{1/k}.$$

We consider the mean square stability of the disagreement dynamics in (3.7), although this problem can be equivalently phrased in terms of exponential mean square stability and stochastic stability, and implying almost sure stability [17, 18]. The asymptotic convergence factor can be expressed as $r_a = \rho\left(\mathbf{E}[\widetilde{W} \otimes \widetilde{W}]\right)$, or as $r_a = \rho\left(G\right)$ following from the definition of the disagreement system, where

$$G = (R \otimes R)(I_{N^2} - (\mathbf{E}[M] \oplus \mathbf{E}[M]) + \mathbf{E}[M \otimes M]). \tag{2.3}$$

We recall from [11, 14, 19] that a necessary and sufficient condition for mean square consentability for the consensus problem in (2.1) is $r_a = \rho(G) < 1$ and that r_a gives the speed of convergence to consensus when it is attained.

Theorem 1. *For a consensus protocol* (2.1) *with number of agents* $N \geq 3$*, the spectral radius of the matrix* G *in* (2.3) *is given by* $\rho(G) = \left(1 - \frac{N\eta_1}{N-1}\right)^2 - \frac{N}{N-1}\left({\phi_1}^2 + {\psi_1}^2\right)$

$$+ (\phi_2 + \psi_2) + (\phi_3 + \psi_3)\,, \tag{2.4}$$

where $\phi_1 = \mathbf{E}[\mathcal{E}_1\mathcal{D}_1], \phi_2 = \mathbf{E}[{\mathcal{E}_1}^2{\mathcal{D}_1}^2]$, $\phi_3 = \mathbf{E}[{\mathcal{E}_1}^2\mathcal{D}_1]$, $\psi_1 = \mathbf{E}[\mathcal{E}_2\mathcal{D}_2], \psi_2 = \mathbf{E}[{\mathcal{E}_2}^2{\mathcal{D}_2}^2]$, $\psi_3 = \mathbf{E}[{\mathcal{E}_2}^2\mathcal{D}_2]$, *and* $\eta_1 = \phi_1 - \psi_1$.

Proof. The proof of the theorem relies on verifying ansatz for the eigenvalues and vectors of auxiliary matrices F_1 and F_2, and then relating them to G's eigenstructure. Then we show that the provided eigenvalues equal the full spectrum of G by noticing that the eigenspaces are orthogonal and their dimensions sum to N^2. Thus, we determine the spectral radius.

First, we compute an expression for G based on a counting argument, following a technique also used in [11]. In our present model, $M = M_1 - M_2$, and $\mathbf{E}[M_1] = NR\phi_1/(N-1)$ and $\mathbf{E}[M_2] = NR\psi_1/(N-1)$, which can be verified by the definitions entries of M_1 and M_2. Using the property of independence of M_1 and M_2, it follows that $(R \otimes R)(\mathbf{E}[M] \oplus \mathbf{E}[M]) = (2N\eta_1/(N-1))(R \otimes R)$, and $(R \otimes R)\mathbf{E}[M \otimes M] = (N\eta_1/(N-1))^2(R \otimes R) + (I_N \otimes R)\,(F_1 + F_2)$. For both F_1 and F_2, the matrices $F^{(1)}$, $F^{(2)}$, and $F^{(3)}$ are identical and have diagonal blocks $F^{(1)}_{ii} = -I_N - N(N-2)e_i(Re_i)^T$, $F^{(2)}_{ii} = I_N/N + ((N^2 - 3N + 1)/(N-1))e_i(Re_i)^T$, $F^{(3)}_{ii} = -I_N/N + e_i(Re_i)^T$, and off-diagonal blocks with $i \neq j$, $F^{(1)}_{ij} = -I_N + Ne_i(Re_i)^T + Ne_j(Re_j)^T$, $F^{(2)}_{ij} = I_N/N + (1/(N-1))e_i(e_i - e_j)^T - (N/(N-1))e_i(Re_i)^T - e_j(Re_j)^T$, $F^{(3)}_{ij} = -I_N/N + e_i(e_i - e_j)^T + (Ne_i + e_j)(Re_j)^T$, where $i = 1, \ldots, N$.

The eigenvectors and corresponding eigenvalues F can be related to those of the matrix G. We define $\Gamma^{(1)} = \{v \in \mathbb{R}^{N^2} : v \in (\ker(R \otimes R))\}$ and its orthogonal complement ${\Gamma^{(1)}}^{\perp}$. It can be verified if $v \in {\Gamma^{(1)}}^{\perp}$ is an eigenvector of $(I_N \otimes R)\,(F_1 + F_2)$ with eigenvalue $\hat{\lambda} \in \mathbb{R}$, then v is an eigenvector of G with eigenvalue $\lambda = (1 - N\eta_1/(N-1))^2 + \hat{\lambda}$. The reader is directed to [11, 14] for a detailed proof of this fact.

We notice that $\Gamma^{(1)}$ is the null space of G and hence has the corresponding eigenvalue $\lambda^{(1)} = 0$. It further can be verified that $(I_N \otimes R)\,(F_1 + F_2)$ has eigenvalues $\hat{\lambda}^{(2)} = -N(N-2)/(N-1)^2\left({\phi_1}^2 + {\psi_1}^2\right) + (\phi_2 + \psi_2) - 1/(N-1)\,(\phi_3 + \psi_3)\,$, $\hat{\lambda}^{(3)} = 0$, $\hat{\lambda}^{(4)} = -N/(N-1)\left({\phi_1}^2 + {\psi_1}^2\right) + (\phi_2 + \psi_2) + (\phi_3 + \psi_3)$ and the corresponding eigenvectors have the form $v = [{v_1}^T {v_2}^T \cdots {v_N}^T]^T$

in the eigenspaces

$$\Gamma^{(2)} = \Big\{ v \in \mathbb{R}^{N^2} : v_i = \mu_i Re_i - \frac{1}{N}\sum_{j=1}^{N} \mu_j Re_j, \text{ with}$$
$$\mu_1 \dots \mu_N \in \mathbb{R} \text{ such that } \sum_{j=1}^{N} \mu_j = 0 \text{ for } i = 1, \dots, N \Big\},$$
$$\Gamma^{(3)} = \Big\{ v \in \mathbb{R}^{N^2} : \sum_{i=1}^{N} v_i = 0_N,\ v_i^T 1_N = 0, \text{ and } e_i^T v_i = 0, \text{ for } i = 1, \dots, N \Big\},$$
$$\Gamma^{(4)} = \Big\{ v \in \mathbb{R}^{N^2} : v_i = \mu Re_i \text{ for } i = 1, \dots, N \text{ and } \mu \in \mathbb{R} \Big\}$$

which satisfy the eigenvalue equation $(I_N \otimes R)(F_1 + F_2)\, v = \hat{\lambda}^{(i)} v$ for $v \in \Gamma^{(i)}$, $i = 2, 3, 4$. The four distinct eigenvalues of G are given by $\lambda^{(1)} = 0$, and $\lambda^{(i)} = (1 - N\eta_1/(N-1))^2 + \hat{\lambda}^{(i)}$, $i = 2, 3, 4$ with the corresponding eigenspaces $\Gamma^{(1)}, \Gamma^{(2)}, \Gamma^{(3)}$, and $\Gamma^{(4)}$. The eigenspaces have dimensions $2N-1, N-1, N^2-3N+1$, and 1, respectively, and it can be directly verified that they are mutually orthogonal. Furthermore, their dimensions sum to N^2, which implies that the spectrum of G equals $\{\lambda^{(1)}, \lambda^{(2)}, \lambda^{(3)}, \lambda^{(4)}\}$. Using the inequalities ${\phi_1}^2 \leq \phi_2 \leq (N-1)\phi_3$ and ${\psi_1}^2 \leq \psi_2 \leq (N-1)\psi_3$, it follows that $\lambda^{(4)} \geq \lambda^{(3)}$, $\lambda^{(4)} + \lambda^{(2)} \geq 0$, and $\lambda^{(4)} - \lambda^{(2)} \geq 0$. Hence $\lambda^{(4)}$ is the spectral radius of G and has the form given in (2.4). □

Corollary 1. *For a composite topology given by the superposition of q graphs, the random variable $M(k)$ at any time k can be expressed as $M(k) = \sum_{i=1}^{q} \alpha_i M_i(k)$. The coefficients α_i can assume any real values, where positive and negative weights denote collaborative and antagonistic interactions, respectively. The spectral radius for this network is given by*

$$\rho(G) = \left(1 - \frac{N\Gamma}{N-1}\right)^2 - \frac{N}{N-1}\left(\sum_{i=1}^{q} {\alpha_i}^2 {\phi_1^i}^2\right) + \left(\sum_{i=1}^{q} {\alpha_i}^2 \phi_2^i\right) + \left(\sum_{i=1}^{q} {\alpha_i}^2 \phi_3^i\right).$$

Here, $\phi_1^i = \mathbf{E}[\mathcal{E}_i \mathcal{D}_i], \phi_2^i = \mathbf{E}[{\mathcal{E}_i}^2 {\mathcal{D}_i}^2]$, and $\phi_3^i = \mathbf{E}[{\mathcal{E}_i}^2 \mathcal{D}_i]$ for ith network topology and $\Gamma = \sum_{i=1}^{q} \alpha_i \phi_1^i$.

Proof. The proof directly follows that of Theorem 2. □

This result is useful for modeling systems where more than two modes of interaction are considered, such as simultaneous sensing cues from vision, hearing, and flow sensing, where each topology is built independently of the other modes. Moreover, this composite model may well represent the real-world networks studied in [1], where six different interaction modes are found to be prevalent among pairs of individuals, namely collaboration (friendship, communication, trade) and antagonism (enmity, armed aggression, punishment).

2.4.2 Synchronization

Considering the synchronization problem, we define N coupled oscillators whose states are denoted with $x_i(k) \in \mathbb{R}^m,\ i = 1, \ldots, N$. The individual dynamics of each oscillator in the absence of coupling is described by $x_i(k+1) = f(x_i(k))$, where $f : \mathbb{R}^m \to \mathbb{R}^m$ is a nonlinear function, k is the time variable, and $x_i(0)$ is the initial condition. The dynamics of a networked oscillator is given by

$$x_i(k+1) = f(x_i(k)) - \sum_{j=1}^{N} [M]_{ij}(k) f(x_j(k)). \tag{2.5}$$

Here, the nonlinear function f is assumed to be the same for the individual dynamics and inner coupling among the oscillators. We say the oscillator states synchronize if $x_1(k) = \ldots = x_N(k) = s(k)$ for all k, where s is a solution of individual oscillator dynamics satisfying $s(k+1) = f(s(k))$.

The spectral radius of G also gives insight into the synchronization of coupled dynamical systems over a network defined by M. For the synchronization problem in (3.2), following the results in [20, 21], the necessary and sufficient condition for the system to be stochastically stable is

$$\ln(\rho(G)) + 2h_{\max} < 0, \tag{2.6}$$

where $h_{\max}$ is the largest Lyapunov exponent of the individual dynamics $f(x)$. We note that this condition is based on linearizing the system dynamics near synchronization, and is thus locally defined.

In summary, for stochastic consensus of the system in (2.1), we require $\log(\rho(G)) < 0$, and for stochastic synchronization of the system in (3.2), the condition is $\ln(\rho(G)) < -2h_{\max}$.

2.5 Discussion

2.5.1 Numerical validation

We numerically validate the closed form result for the spectral radius given in (2.4) through Monte Carlo simulations on the consensus protocol of conspecific agents in (2.1). We define two joint probability mass functions for $N = 10$ conspecific agents

$$g_{\mathcal{D}_1,\mathcal{E}_1}(d_1, \epsilon_1) = \begin{cases} 1/10 \ \text{ for } \ d_1 = 0, \epsilon_1 = 0.01, \\ 1/10 \ \text{ for } \ d_1 = 3, \epsilon_1 = 0.01, \\ 1/10 \ \text{ for } \ d_1 = 2, \epsilon_1 = 0.03, \\ 7/10 \ \text{ for } \ d_1 = 6, \epsilon_1 = 0.03, \end{cases} \tag{2.7}$$

for helping graph and

$$g_{\mathcal{D}_2,\mathcal{E}_2}(d_2,\epsilon_2) = \begin{cases} 1/10 \text{ for } d_2 = 0, \epsilon_2 = 0.01, \\ 1/10 \text{ for } d_2 = 1, \epsilon_2 = 0.01, \\ 1/10 \text{ for } d_2 = 3, \epsilon_2 = 0.03, \\ 7/10 \text{ for } d_2 = 2, \epsilon_2 = 0.03, \end{cases} \tag{2.8}$$

for hurting graph. The agents draw realizations from these bivariate distributions for the cardinality of the neighbor set and the averaging weight they ascribe to the neighbors' opinions at each time step independent to the interaction network at the previous time steps and to other agents. The matrix M_1 corresponds to the collaborative interaction network built from the distribution in (2.7) and the matrix M_2 corresponds to the antagonistic interaction network built from the distribution in (2.8). The initial conditions are chosen randomly and held constant for 100 realizations. We find that the magnitude of the disagreement vector decreases linearly in a logarithmic scale. The best fit line is computed over time steps $[35, 45]$. We find the disagreement norm squared decreases as 0.834^k and the value of the asymptotic convergence factor calculated by (2.4) is 0.832^k, thus confirming the analytical results.

2.5.2 Closed form approximations for a large number of agents and sensitivity analysis of the disturbance topology

The closed form result in (2.4) can be further simplified by considering the limit as the number of agents goes to infinity. For large number of agents, $\rho(G)$ in (2.4) is approximated as

$$\rho(G) \simeq (1-\eta_1)^2 - \left({\phi_1}^2 + {\psi_1}^2\right) + (\phi_2 + \psi_2) + (\phi_3 + \psi_3)\,.$$

An alternative approximation for the main result can be computed considering the composite topology as a perturbation of the collaborative topology, i.e., $M = M_1 - \delta M_2$, for $\delta << 1$. In [22], spectral impact was defined to measure the relative change in the largest eigenvalue of the adjacency matrix due to addition or removal of edges or nodes in the case of fixed topology. The corresponding change in the spectral radius, neglecting $\mathcal{O}(\delta^2)$ terms, is given by $\Delta\rho(G) = \rho(G)\big|_{M_1-\delta M_2} - \rho(G)\big|_{M_1} = \delta\left(2N\psi_1/(N-1) - 2N^2\phi_1\psi_1/(N-1)^2\right)$, and in the presence of a large numbers of agents, $\Delta\rho(G) \simeq 2\delta\psi_1\left(1-\phi_1\right)$. We notice that $\Delta\rho(G)$ changes sign depending on the magnitude of ϕ_1, meaning that the addition of a disturbing topology can either benefit or hinder consensus or synchronization.

2.5.3 Exemplary protocol: NC networks

We demonstrate the results on collaborative and antagonistic interactions with NC networks, which is a specialized class of conspecific agents that require the number of neighbors for every

agent and the averaging weight to both be constants [14]. Therefore, we fix $\mathcal{D}_1$ and $\mathcal{D}_2$ to be constants n_1, $n_2 \in \{1, 2, \ldots, N-1\}$ for the helping and the hurting graph, respectively. We keep the averaging weight constant for both the graphs and denote it as $\mathcal{E}_1 = \mathcal{E}_2 = \hat{\epsilon} \in \mathbb{R}^+$. Thus the moments of $g_{\mathcal{D}_1,\mathcal{E}_1}(d_1, \epsilon_1)$ and $g_{\mathcal{D}_2,\mathcal{E}_2}(d_2, \epsilon_2)$ are $\phi_1 = \hat{\epsilon}n_1$, $\phi_2 = \hat{\epsilon}^2{n_1}^2$, $\phi_3 = \hat{\epsilon}^2 n_1$, $\psi_1 = \hat{\epsilon}n_2$, $\psi_2 = \hat{\epsilon}^2{n_2}^2$, and $\psi_3 = \hat{\epsilon}^2 n_2$. Hence, the spectral radius from equation (2.4) is given by

$$\rho(G) = \left(1 - \frac{\hat{\epsilon}nN}{N-1}\right)^2 + \frac{\hat{\epsilon}^2\left((n_1+n_2)(N-1) - (n_1^2+n_2^2)\right)}{N-1}$$

where $n = n_1 - n_2$. For large numbers of agents, $\rho(G)$ can be approximated as $\rho(G) \simeq (1-\hat{\epsilon}n)^2 + \hat{\epsilon}^2(n_1+n_2)$. This is consistent with the large network approximation with collaborative interactions in [11].

Synchronization over NC networks can be enabled by antagonistic interactions in cases where sychronization is not possible with only collaboration

To study the synchronization over NC networks with our present model, we consider a logistic map for individual dynamics. The dynamics of the individual logistic map is given by $x(k+1) = 3.9x(k)(1-x(k))$, and random initial conditions are used. The largest Lyapunov exponent $h_{\max}$ is 0.485 for logistic maps [20] and, from (3.11), stochastic synchronization is achieved if and only if the natural logarithm of the spectral radius of G is less than -0.970.

For illustration, we consider two cases of 200 coupled logistic maps connected over two NC networks, one in the absence of a hurting graph with $n_2 = 0$ and the other in the presence of hurting graph with $n_2 = 3$. In both the cases, $n_1 = 10$ is constant.

Figure 2.1a shows variation of $\ln[\rho(G)]$ with $\hat{\epsilon}$ predicted by the main result and the numerical threshold required for stochastic synchronization of logistic maps. Similarly to the results in [20, 14], the analytical curve for r_a has a characteristic shape, with a decrease from 0 to a minimum value as $\hat{\epsilon}$ increases from 0, followed by an unbounded increase as $\hat{\epsilon}$ goes to ∞. The bounded interval within which the system is synchronizable is when the green triangles and blue squares are less than the black diamonds for logistic maps. In these examples, this interval is approximately equal to $[0.039, 0.142]$ in the absence of hurting graph and $[0.060, 0.167]$ in the presence of hurting graph with $n_2 = 3$. Remarkably, when $\hat{\epsilon} = 0.15$, we observe that the synchronization is achieved in the presence of the hurting graph (Figure 2.1b), which is otherwise not possible in the absence of the same (Figure 2.1c). These results are consistent with the predictions from the main theoretical result depicted in Figure 2.1a.

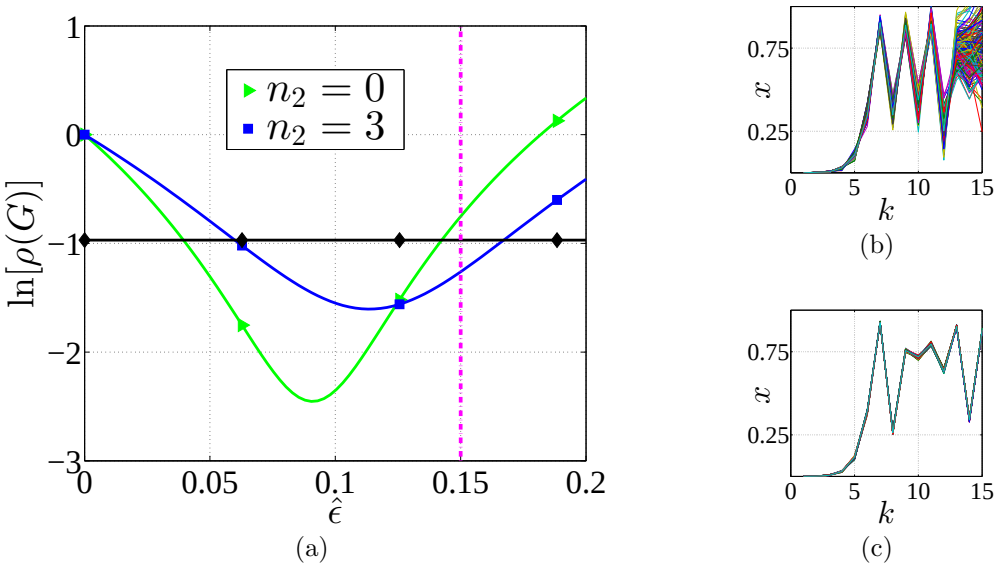

(a) (b) (c)

Figure 2.1: (a) Asymptotic convergence factor over a NC network with $N = 200$ and $n_1 = 10$ as a function of $\hat{\epsilon}$. The case when $n_2 = 0$ is denoted by green line (triangles) and $n_2 = 3$ is denoted by blue line (squares). Black line (diamonds) correspond to $-2h_{\max}$ of logistic map. The vertical dash-dot line corresponds to $\hat{\epsilon} = 0.15$. Time series with fixed $\hat{\epsilon} = 0.15$ are shown for (b) $n_2 = 0$, and (c) $n_2 = 3$.

Cases where antagonism enables consensus, and optimal network parameters for these cases, can be found from the closed form expression for $\rho(G)$

To study the influence of the hurting graph on consensus, we compute the contour plot with $N = 10$ and $n_1 = 8$, and vary n_2 and $\hat{\epsilon}$ in Figure 2.2. We plot $\log[r_a]$ varying n_2 from zero to eight and $\hat{\epsilon}$ from zero to one. Observing the level curve corresponding to $\log[r_a] = 0$, we note that $\hat{\epsilon}$ has a limit slightly greater than 0.2 within which consensus is achieved when $n_2 = 0$. But increasing $\hat{\epsilon}$ beyond 0.2 requires an increase of n_2 in order to maintain consensus. In summary, the presence of the hurting graph enables a broader range of $\hat{\epsilon}$ to admit consensus, but the maximum possible convergence speed is decreased in these cases compared to when $n_2 = 0$ However, when $\log[r_a]$ is compared with $n_2 = 0$ and $n_2 = 4$, we observe consensus can be achieved in both cases, but in presence of antagonism, convergence speed increases since $\log[r_a]$ decreases.

We quantify this interaction between the parameters by providing n_2^{opt}, which we derive by taking the derivative of the asymptotic convergence factor with respect to n_2 and solving the resultant expression equated to zero. The optimum value of n_2 calculated in terms of the remaining system parameters corresponds to the point where r_a is minimum, which assures fastest possible convergence in the presence of antagonistic interactions. This is given by

$$n_2^{\text{opt}} = \text{rnd}^+\left(\frac{1}{1+N(N-1)}\left(N(1+n_1N) \quad -\frac{1}{2}(1+N^2) - \frac{N(N-1)}{\hat{\epsilon}}\right)\right), \tag{2.9}$$

where $\text{rnd}^{+}(\cdot)$ denotes rounding the argument to the nearest nonnegative integer, which satisfies the conditions on the definition of n_2.

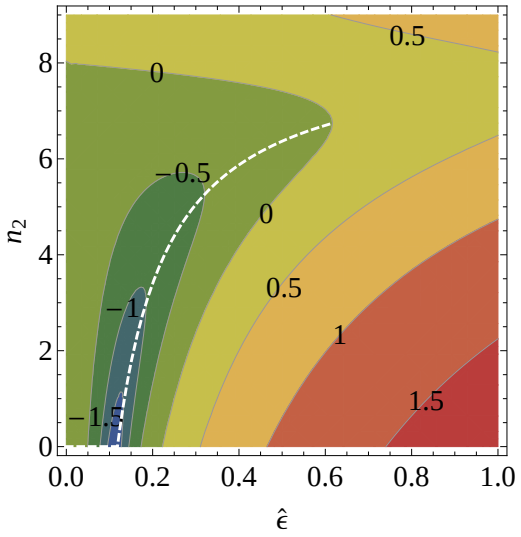

Figure 2.2: Contour plot of $\log[r_a]$ for $N = 10$ agents coupled over NC networks with $n_1 = 8$, and n_2 and $\hat{\epsilon}$ varying. n_2^{opt} is denoted by the dashed white line.

We see that n_2^{opt} increases with increasing values of $\hat{\epsilon}$ when N and n_1 are kept constant. For very small values of $\hat{\epsilon}$, n_2^{opt} is zero, which means that the presence of antagonistic interactions is not able to improve the possible convergence speed. For $\hat{\epsilon}$ greater than some critical value, n_2^{opt} begins to increase; the rate of increase of n_2^{opt} with $\hat{\epsilon}$ is greater for small values of $\hat{\epsilon}$ and approaches zero as $\hat{\epsilon}$ goes to infinity. In other words, the difference between small values of persuasibility corresponds to large changes in hurting graph's numerosity to attain the best convergence speed. On the other hand, the value of persuasibility has less of an impact on the optimal n_2 when $\hat{\epsilon}$ is larger.

Antagonistic edges reduce the effective persuasibility, thus enabling a system to reach consensus/synchronization that would otherwise be unattainable

Since we are interested in whether systems reach consensus/synchronization, and their convergence speed in the case that they do, we only discuss the region where n_2^{opt} gives systems that converge. We comment that, for systems that converge, i.e. with $\log[r_a] < 0$ for consensus, and with $\ln[r_a] < -2h_{max}$ for synchronization, it can be shown directly from the expression in (2.9) that the value of $n_2^{\text{opt}} < n_1$. This suggests that the mechanism by which the hurting graph creates a larger region of $\hat{\epsilon}$ wherein convergence can be achieved (as compared to the helping graph by itself) is based on cancellation between antagonistic and collaborative interactions in the expected network. More specifically, in cases when $\hat{\epsilon}$ is too large to admit convergence for the helping graph independently, the introduction of

the hurting graph cancels some collaborative edges, thus lessening the effective persuasibility of the agents and allowing the system to converge. This interpretation is in line with the finding that, to help the system converge, the hurting graph must have less edges than the helping graph on average.

2.6 Conclusion

Here, we define and study consensus and synchronization of a composite model over a stochastically-switching network capturing both collaborative and antagonistic interactions among the agents. Results demonstrate that system parameters may be chosen so that the presence of antagonistic interactions among the agents enables the system to achieve both consensus and synchronization which is otherwise not possible and, at times, helps to achieve convergence at a relatively faster rate. We identify critical values of system parameter that give maxima in convergence speed for NC networks. Although the present study has biological inspiration, the results find applications in the control of robotic teams with multiple sensing modalities. The theoretical results developed here may help design control algorithms to enable such robots to attain collective behavior at a broader range of persuasibilty.

2.7 References

[1] Michael Szell, Renaud Lambiotte, and Stefan Thurner. Multirelational organization of large-scale social networks in an online world. *Proceedings of the National Academy of Sciences*, 107(31):13636–13641, 2010.

[2] Nachum Ulanovsky, M Brock Fenton, Asaf Tsoar, and Carmi Korine. Dynamics of jamming avoidance in echolocating bats. *Proceedings of the Royal Society of London. Series B: Biological Sciences*, 271(1547):1467–1475, 2004.

[3] David Easley and Jon Kleinberg. *Networks, crowds, and markets: Reasoning about a highly connected world*. Cambridge University Press, 2010.

[4] Tibor Antal, Paul L Krapivsky, and Sidney Redner. Social balance on networks: The dynamics of friendship and enmity. *Physica D: Nonlinear Phenomena*, 224(1):130–136, 2006.

[5] Claudio Altafini and Gabriele Lini. Predictable dynamics of opinion forming for networks with antagonistic interactions. *IEEE Transactions on Automatic Control*, 60(2):342–357, 2015.

[6] Claudio Altafini. Consensus problems on networks with antagonistic interactions. *IEEE Transactions on Automatic Control*, 58(4):935–946, 2013.

[7] Claudio Altafini. Dynamics of opinion forming in structurally balanced social networks. *PloS ONE*, 7(6):e38135, 2012.

[8] Guodong Shi, Mikael Johansson, and Karl Henrik Johansson. How agreement and disagreement evolve over random dynamic networks. *IEEE Journal on Selected Areas in Communications*, 31(6):1061–1071, 2013.

[9] Guodong Shi, Alexandre Proutiere, Mikael Johansson, J Baras, and K Johansson. Emergent behaviors over signed random dynamical networks: State-flipping model. *IEEE Transactions on Control of Network Systems*, 2014.

[10] Jiangping Hu and Wei Xing Zheng. Emergent collective behaviors on coopetition networks. *Physics Letters A*, 378(26):1787–1796, 2014.

[11] Nicole Abaid, Irina Igel, and Maurizio Porfiri. On the consensus protocol of conspecific agents. *Linear Algebra and its Applications*, 437(1):221–235, 2012.

[12] Nicola Perra, Bruno Goncalves, Romualdo Pastor-Satorras, and Alessandro Vespignani. Activity driven modeling of time varying networks. *Scientific Reports*, 2, 2012.

[13] Takashi Nishikawa and Adilson E Motter. Network synchronization landscape reveals compensatory structures, quantization, and the positive effect of negative interactions. *Proceedings of the National Academy of Sciences*, 107(23):10342–10347, 2010.

[14] Nicole Abaid and Maurizio Porfiri. Consensus over numerosity-constrained random networks. *IEEE Transactions on Automatic Control*, 56(3):649–654, 2011.

[15] Subhradeep Roy and Nicole Abaid. Consensus of conspecific agents via collaborative and antagonistic interactions. In *ASME Dynamic Systems and Control Conference*, Columbus, Ohio, USA, 2015.

[16] Jing Zhou and Qian Wang. Convergence speed in distributed consensus over dynamically switching random networks. *Automatica*, 45(6):1455–1461, 2009.

[17] Maurizio Porfiri and Daniel J Stilwell. Consensus seeking over random weighted directed graphs. *IEEE Transactions on Automatic Control*, 52(9):1767–1773, 2007.

[18] Xiangbo Feng, Kenneth A Loparo, Yuandong Ji, and Howard Jay Chizeck. Stochastic stability properties of jump linear systems. *IEEE Transactions on Automatic Control*, 37(1):38–53, 1992.

[19] Nicole Abaid and Maurizio Porfiri. Leader-follower consensus over numerosity-constrained random networks. *Automatica*, 48(8):1845–1851, 2012.

[20] Nicole Abaid and Maurizio Porfiri. Synchronous dynamics over numerosity-constrained stochastic networks. In *Applications of Chaos and Nonlinear Dynamics in Science and Engineering-Vol. 2*, pages 95–121. Springer, 2012.

[21] Maurizio Porfiri. A master stability function for stochastically coupled chaotic maps. *EPL (Europhysics Letters)*, 96(4):40014, 2011.

[22] Attilio Milanese, Jie Sun, and Takashi Nishikawa. Approximating spectral impact of structural perturbations in large networks. *Physical Review E*, 81(4):046112, 2010.

Chapter 3

Leader-follower consensus and synchronization in numerosity-constrained networks with dynamic leadership

The contents of this chapter have appeared in Chaos: An Interdisciplinary Journal of Nonlinear Science, 26(11), 116309, 2016 and partially in a conference paper in the Proceedings of the International Conference of Control, Dynamic Systems, and Robotics, Ottawa, Ontario, Canada, 2015.

3.1 Abstract

In this work, we study leader-follower consensus and synchronization protocols over a stochastically switching network. The agents representing the followers can communicate with any other agent, whereas the agents serving as leaders are restricted to interact only with the other leaders. The model incorporates the phenomenon of numerosity, which limits the perceptual capacity of the agents while allowing for shuffling with whom each individual interacts at each time step. We derive closed form expressions for necessary and sufficient conditions for consensus, the rate of convergence to consensus, and conditions for stochastic synchronization in terms of the asymptotic convergence factor. We provide simulation results to validate the theoretical findings and to illustrate the dependence of this factor on system parameters. The closed form results enable us to study the factors affecting the feasibility of consensus. We show that agents' traits can be chosen for an engineered system to maximize the convergence speed and that protocol speed is enhanced as the proportion of the leaders increases in certain cases. These results may find application in the design and

control of an engineered leader-follower system, where consensus or synchronization at the fastest possible rate is desired.

3.2 Introduction

Collective behavior in social groups is an emergent phenomenon where interaction negotiated through communication among the individuals drives coordinated motion [1]. In the physical world, the communication between individuals may not be all-to-all, due to a variety of constraints. These constraints may be physical (e.g. communication signals which attenuate with increasing distance between the individuals [2]) and psychological (e.g. species-based constraint on the number perception observed in animal groups [3]). Among these constraints, the perception of numbers necessarily impacts collective behavior, since animal groups comprise many individuals. The so-called numerosity constraint on number perception, defined in [4, 5], provides an upper limit on the cardinality of groups which may be accurately perceived, and above which the group's cardinality is imprecisely perceived as "many". This perceptual phenomenon impacts a variety of social species, including fish [5], birds [3], and humans [4].

Collective behavior can be formalized as a process where individuals exchange their state information with other group members and reach an agreement through an iterative process of negotiation [6]. We model this behavior as a consensus protocol, defined as an algorithm for a multi-agent system with an equilibrium when all agents hold a common state [7, 8]. In recent years, consensus problems in multi-agent systems have become a pervasive topic of research based in part on their wide range of applications, such as unmanned aerial vehicles [9, 10], autonomous underwater vehicles (AUVs) [11, 12], air traffic control [13], wireless sensor networks [14, 15] and coordinated decision making in economic systems [16].

The wide range of engineering and science applications for consensus protocols is supported by a large theoretical literature exploring these problems [7, 8, 17, 18, 19, 20, 21, 22, 23, 24, 25, 26, 27, 28]. Within this literature, conditions to reach consensus have been studied varying characteristics of the agent interaction network. Networks may be static [17, 27] or switching over time. Switching networks may be further divided into those updating from a deterministic or arbitrary sequence [8, 28] or from realizations of a random variable [7, 20, 21, 25, 26]. Convergence analysis under both static and switching network topologies are considered in [29] where necessary and sufficient conditions for consensus are provided. In addition, agent dynamics are considered updating in continuous [19] or discrete time [20]. A variety of metrics for consensus are developed from stability concepts, including mean square stability [20] and almost sure stability [22, 25] of the disagreement among agents. We comment that, within the literature, closed form results for consensus conditions and convergence speed are generally lacking, except for Erdos-Renyi random networks in [23, 30] and for numerosity-constrained (NC) networks in [20, 24, 31]. Although static or deterministically switching networks have received attention in the literature based on the

tractability of these problems, this work targets randomly switching networks to model the more realistic scenario that individuals in social groups share information with a dynamic and stochastic set of peers. Thus, we select NC networks for our present study, which quantify a critical limit to the number perception observed in social groups [20].

Within social groups, leadership by an individual or subset of the group is a strong determinant of collective behavior and is prevalent across different species, for example, fish schools [32], pigeon flocks [33, 34], and human crowds [35]. This group behavior may be modeled as a specialized type of consensus problem, called leader-follower consensus, which partitions the agents into two types: leaders and followers [24, 36, 37]. In general, the followers have access to less information and the leaders more so; the leaders attempt to drive the entire system to a desired common state through their updating protocol. Conditions for achieving leader-follower consensus have been studied for a variety of systems, including those with static [38] and deterministically switching [37, 39] interaction topologies. In addition, randomly switching topologies are studied in [24], where the NC networks considered in this Chapter are used. The rate at which consensus is reached has also been explored in [36]. In terms of the followers' dynamics, both linear [36, 24] and nonlinear [40] dynamics have been considered, as well as systems whose agents have first-order dynamics [24], second-order dynamics [38, 40], and both first- and second-order dynamics [41] in a mixed or heterogenous system. Nevertheless, leaders whose state varies dynamically according to a consensus protocol are rarely considered in the literature [40, 41, 42] and closed form expressions relating the consensus among leaders to that of the whole system are notably absent.

Synchronization is a generalization of the consensus concept, where individuals in a group interact among themselves to reach a time-varying accordant state. Synchronization of coupled dynamical systems is studied varying characteristics of the agent interaction network. For example, in [43, 44], the topology of the interaction network and the coupling strength are assumed to be constant in time and results on conditions to achieve synchronization are presented. The concept of the master stability function (MSF) [44] has been an effective tool for studying synchronization over static network models. Pinning control schemes for controlled synchronization based on MSF has been studied in [45]. Synchronization over switching network topologies is relatively less explored and has been studied in [46, 47, 48], where topologies updating from deterministic sequences are considered, and in [49, 50, 51], where topologies updating from realizations of a random variable (stochastic) are considered. A review of several recent studies on evolving dynamical networks may be found in [52]; synchronization over blinking networks, where coupling strength and the connection topology varies with time, is highlighted along with applications to real-world systems, for example, cellular neural networks, epidemic spreading, and opinion dynamics. Synchronization over time-varying NC networks has been studied in detail in [53] and closed form results are provided for stochastic synchronization. A recent study of consensus and synchronization considering both collaborative and antagonistic interactions among the agents can be found in [31], where closed form expressions for necessary and sufficient conditions for consensus, the rate of convergence to consensus, and conditions for stochastic synchronization

are derived. The results in [31] demonstrate that the antagonistic interactions can enable the system to attain consensus and synchronization which is otherwise not possible.

In this Chapter, we study leader-follower consensus and synchronization protocols over a stochastically-switching network inspired by the numerosity constraint. In the present work, the leaders have dynamic states and reach consensus by interacting only among themselves, while the followers interact with both the leaders and other followers by definition. This problem statement defines the dynamic leaders to be more influential than followers as they only negotiate with a subset of the total group, while their states propagate through the entire system via the unidirectional interaction they may have with the followers. This setup acts as a model of a representative democracy, where policies are decided upon by a subset of representatives whose decisions are disseminated to the entire populace [54]. In this idealized system, consensus among representatives is required for making public policy and consensus among all agents represents a populace whose opinions align with its representatives, which may be the goal of a democracy, as modeled similarly in [42]. With this work, we target modeling this representative democratic leader-follower system through a consensus protocol incorporating the numerosity constraint.

Here, we establish necessary and sufficient conditions for consensus and synchronization of such a system with dynamic leaders and we study the rate of convergence to consensus and stochastic synchronization of the entire system in terms of the mean square stability of the disagreement among agents. A closed form expression for the asymptotic convergence factor, which measures this rate, is established. A similar model for consensus has been studied in [24], where the leaders have a common state which is constant with time. We comment that, in [24], the state of consensus of the entire system was pre-determined by the set leaders' common state, whereas in this work the leaders' states start from random initial conditions and converge over time. The technique used to derive the closed form results is similar to [24, 20], but consideration of dynamic leaders in the present model introduces more general phrasing of the problem that allows leaders' states to evolve.

The Chapter is organized as follows. In section 3.3, we describe the setup of the problem. In section 3.4, we define the asymptotic convergence factor for measuring the rate to reach consensus using results on stochastic stability and derive its closed form expression for the stated problem. We also present necessary and sufficient conditions for consensus and stochastic synchronization. In section 3.5, we provide a simulation study to validate the main result and present exemplary systems with three different proportions of leaders and followers. We provide results for synchronization demonstrating logistic maps. Finally, we draw our conclusions in Section 3.6. Section A is left for Appendix.

3.3 Problem statement

3.3.1 Network model

We consider a system of N agents, with l agents acting as leaders and f agents as followers, with $l+f = N$ and $f, l \geq 3$. The sets $\mathcal{L}$, $\mathcal{F}$, and $\mathcal{N}$ denote the indices of leaders, followers, and total agents, respectively, and we write $\mathcal{F} = \{1, 2, \cdots, f\}$, $\mathcal{L} = \{f+1, f+2, \cdots, N\}$, and $\mathcal{N} = \mathcal{F} \cup \mathcal{L}$. The agents communicate at discrete time steps over a stochastically-switching directed network which is numerosity constrained [20]. According to the numerosity constrained model, at each time step, agents communicate with n randomly selected neighbors and $n \in \{1, \ldots, l-1\}$ is constant over all time steps and agents in the system. Leaders are assumed to communicate with n other leaders, whereas the followers communicate with n neighbors which are selected from both leaders and followers. At each time step $k \in \mathbb{Z}^+$, the communication network is defined through the graph Laplacian $L(k) \in \mathbb{R}^{N \times N}$. The first f rows of $L(k)$, i.e. row $i \in \mathcal{F}$, represent the followers' interaction graph, since each row defines how a follower is connected to the rest of the $(N-1)$ agents in the system. The last l rows of $L(k)$ represent the leaders' subgraph, i.e. when $i \in \mathcal{L}$, and show the connections restricted to the leaders. By definition of the numerosity constrained topology, each row of $L(k)$ has a diagonal entry equal to n and off-diagonal entries comprising n "-1's" and $N-n-1$ "0's". More specifically, when $i \in \mathcal{F}$, the appearance of -1's along the $N-1$ off-diagonal positions is equally likely, whereas when $i \in \mathcal{L}$, the first f columns are 0's and -1 can appear in the remaining $l-1$ off-diagonal positions with equal probability. Note the first f columns in the leaders' sub-system has all the elements equal to zero, since leaders do not receive information from the followers. We observe that $L(k)$ is not necessarily symmetric due to unidirectional communication among the agents, but it has zero row sum. Thus, $L(k)\mathbf{1}_N = \mathbf{0}_N$, with $\mathbf{1}_N \in \mathbb{R}^{N \times 1}$ having all entries equal to 1 and $\mathbf{0}_N \in \mathbb{R}^{N \times 1}$ having all entries equal to zero. In Figure 3.1, we provide a schematic of one realization of the interaction network for $l = 3, f = 4$, and $n = 2$ and the corresponding graph Laplacian is given as

$$L(k) = \begin{bmatrix} 2 & 0 & 0 & -1 & -1 & 0 & 0 \\ 0 & 2 & -1 & -1 & 0 & 0 & 0 \\ -1 & 0 & 2 & 0 & 0 & 0 & -1 \\ 0 & 0 & -1 & 2 & 0 & 0 & -1 \\ 0 & 0 & 0 & 0 & 2 & -1 & -1 \\ 0 & 0 & 0 & 0 & -1 & 2 & -1 \\ 0 & 0 & 0 & 0 & -1 & -1 & 2 \end{bmatrix}.$$

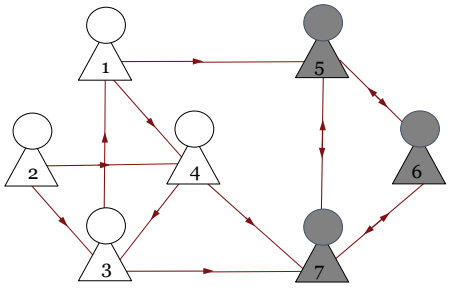

Figure 3.1: A single realization of the interaction network for the system parameters $l = 3, f = 4$, and $n = 2$. Leaders are grey and followers are white.

3.3.2 Consensus

At time step k, the state of the agents is given by the vector $\boldsymbol{x}(k) = [\boldsymbol{x}^f(k)^T \boldsymbol{x}^l(k)^T]^T \in \mathbb{R}^{N\times 1}$, where $\boldsymbol{x}^f(k) \in \mathbb{R}^{f\times 1}$ is the state vector for the followers and $\boldsymbol{x}^l(k) \in \mathbb{R}^{l\times 1}$ is the state vector for the leaders. The full state vector is updated according to the discrete-time consensus protocol

$$\boldsymbol{x}(k+1) = (I_N - \epsilon L(k))\boldsymbol{x}(k), \tag{3.1}$$

where $\boldsymbol{x}(0)$ is a random initial condition, I_N is an identity matrix of size N, and $\epsilon > 0$. The parameter ϵ acts as a weighting parameter, also called persuasibility, which determines how the agents update their states using the information received from the neighbors at each time step. This quantity can be viewed both as an averaging weight which quantifies the relative influence of each agent's state and as a time step capturing the characteristic time step of the updating protocol. We say the consensus is reached when agents share a common state, $\boldsymbol{x} = s\mathbf{1}_N$, where $s \in \mathbb{R}$.

3.3.3 Synchronization

For the synchronization problem, we consider N coupled oscillators whose states are denoted with $\boldsymbol{x}_i(k) \in \mathbb{R}^m,\ i = 1, \ldots, N$. The individual dynamics of each oscillator in the absence of coupling at time step k, is described by

$$\boldsymbol{x}_i(k+1) = f(\boldsymbol{x}_i(k)),$$

where $f : \mathbb{R}^m \to \mathbb{R}^m$ is a nonlinear function in general, and $\boldsymbol{x}_i(0)$ corresponds to the initial condition. The dynamics of a networked oscillator is given by

$$\boldsymbol{x}_i(k+1) = f(\boldsymbol{x}_i(k)) - \epsilon \sum_{j=1}^{N} L_{ij}(k) f(\boldsymbol{x}_j(k)), \tag{3.2}$$

where $i = 1, \ldots, N$. The nonlinear function f is assumed to be same for the individual dynamics and inner coupling among the oscillators. We say the oscillator states have synchronized if the state vectors for all oscillators are identical, that is, $\boldsymbol{x}_1(k) = \ldots = \boldsymbol{x}_N(k) = \boldsymbol{s}(k)$ for all $k \in \mathbb{N}$, where $\boldsymbol{s}$ satisfies $\boldsymbol{s}(k+1) = f(\boldsymbol{s}(k))$.

3.4 Analysis

In this section, we relate the consensus problem (3.1) to a stochastic stability problem. We define and derive the closed form expression for the so-called asymptotic convergence factor to capture the rate of convergence to consensus for the consensus protocol in (3.1). We establish a necessary and sufficient condition for convergence to consensus in terms of the so-called asymptotic convergence factor, and adapt this result to a necessary and sufficient condition for synchronization protocol in (3.2), in analogously coupled dynamical systems.

3.4.1 Preliminary results on consentability

For a general discrete-time linear system, we write

$$\boldsymbol{x}(k+1) = W(k)\boldsymbol{x}(k), \tag{3.3}$$

where $W(k) \in \mathbb{R}^{N\times N}$ are independent, identically distributed random matrices, and we denote the common random variable as W. In other words, at each time step k, the rows of the matrix $W(k)$ are realizations of identically distributed random variables, which are pairwise independent and independent in time [20]. The asymptotic convergence factor [55] for (3.3) is defined as

$$r_a(W) = \sup_{\|\boldsymbol{x}(0)\|\neq 0} \lim_{k\to\infty} \left(\frac{\mathbf{E}\left[\|\boldsymbol{x}(k)\|^2\right]}{\|\boldsymbol{x}(0)\|^2} \right)^{1/k}, \tag{3.4}$$

where $\mathbf{E}[\bullet]$ is the expected value. The factor can be written in terms of the statistical properties of W as

$$r_a(W) = \rho(\mathbf{E}[W \otimes W]), \tag{3.5}$$

where $\otimes$ denotes Kronecker product and $\rho(\bullet)$ is the spectral radius of a matrix, as in [20].

Proposition 1. *The necessary and sufficient condition for the system* (3.3) *to be mean square stable (MSS), is* $r_a(W) < 1$ *and, when the system is MSS,* r_a *gives the convergence rate.*

For (3.3) to be a consensus protocol, $W(k)$ must have the property

$$W(k)\mathbf{1}_N = \mathbf{1}_N, \tag{3.6}$$

making span($\mathbf{1}_N$) an equilibrium of the system. We project the consensus problem (3.1) on the disagreement space to measure the closeness of the system to consensus in terms of a disagreement variable $\boldsymbol{\xi}(k)$ defined as $\boldsymbol{\xi}(k) = Q^T\boldsymbol{x}(k) \in \mathbb{R}^{N-1}$. Here, the matrix $Q \in \mathbb{R}^{N\times(N-1)}$ has the properties $Q^T\mathbf{1}_N = \mathbf{0}_{N-1}$, $Q^TQ = I_{N-1}$, and $QQ^T = R$ for $R = I_N - \mathbf{1}_N\mathbf{1}_N{}^T$. Thus, $\boldsymbol{x}(k) = \bar{x}(k)\mathbf{1}_N + Q\boldsymbol{\xi}(k)$, where the arithmetic mean of $\boldsymbol{x}(k)$ is $\bar{x}(k) = (1/N)\mathbf{1}_N^T\boldsymbol{x}(k)$. Hence, the disagreement dynamics can be written as

$$\boldsymbol{\xi}(k+1) = \tilde{W}(k)\boldsymbol{\xi}(k), \tag{3.7}$$

where $\tilde{W}(k) = Q^TW(k)Q \in \mathbb{R}^{(N-1)\times(N-1)}$.

By Proposition 1, the necessary and sufficient condition for the disagreement dynamics (3.7) to be MSS is given as

$$\begin{aligned} r_a(\tilde{W}) &= \sup_{\|\boldsymbol{\xi}(0)\|\neq 0} \lim_{k\to\infty} \left(\frac{\mathbf{E}\left[\|\boldsymbol{\xi}(k)\|^2\right]}{\|\boldsymbol{\xi}(0)\|^2}\right)^{1/k} \\ &= \rho(\mathbf{E}[Q^TWQ \otimes Q^TWQ]) \\ &= \rho((R\otimes R)\mathbf{E}[W\otimes W]) \\ &< 1. \end{aligned} \tag{3.8}$$

Definition 1. *If the disagreement dynamics in* (3.7) *is MSS, then the protocol in* (3.3) *with condition* (3.6) *is said to be mean square consentible.*

These results can be specified to study the consentibility of the leader-follower system in (3.1). Substituting $W = I_N - \epsilon L$ in the expression, $(R\otimes R)\mathbf{E}[W\otimes W]$, we get

$$G = (R\otimes R)(I_{N^2} - \epsilon(\mathbf{E}[L]\oplus\mathbf{E}[L]) + \epsilon^2\mathbf{E}[L\otimes L]), \tag{3.9}$$

where $\oplus$ denotes Kronecker sum.

Proposition 2. *Following from* (3.5) *and* (3.9)*, the asymptotic convergence factor of the consensus protocol in* (3.1) *is given by the spectral radius of* G*, i.e.,*

$$r_a = \rho(G). \tag{3.10}$$

3.4.2 Preliminary results on synchronization

The spectral radius of G also gives insight into the synchronization of coupled dynamical systems over a network defined by W summarized in the following proposition.

Proposition 3. *For the synchronization problem in* (3.2)*, following the results in [53, 56], the necessary and sufficient condition for the system to be stochastically stable is*

$$\ln(\rho(G)) + 2h_{\max} < 0, \tag{3.11}$$

where $h_{\max}$ is the largest Lyapunov exponent of the individual dynamics $f(\boldsymbol{x})$. This condition is based on linearizing the system dynamics near synchronization, and is thus locally defined.

In summary, the necessary and sufficient condition for stochastic consensus of the system in (3.3) with the condition in (3.6) is $\log(\rho(G)) < 0$, and the necessary and sufficient condition for stochastic synchronization of the system in (3.2) is $\ln(\rho(G)) < -2h_{\max}$.

In the next subsections and associated Appendices, we will calculate r_a through the following steps. First, we will compute the matrix G by a counting technique. Then, we will calculate the eigenvalues of G and associated eigenvectors. Finally, we will show G is diagonalizable to get that G^k can be calculated using spectral decomposition, from which we will determine its spectral radius.

3.4.3 Computation of $\mathbf{E}[L]$ and $\mathbf{E}[L \otimes L]$

To compute r_a, we must find the expressions for $\mathbf{E}[L]$ and $\mathbf{E}[L \otimes L]$. We denote the set of all possible distinct Laplacian matrices as $\hat{L} = \{L^{(1)}, L^{(2)}, \cdots, L^{(p)}\}$, where p corresponds to the total number of unique realizations of the Laplacian matrices given l, f, and n. In line with previous studies in [20, 24, 56, 57], we calculate $\mathbf{E}[L]$ and $\mathbf{E}[L \otimes L]$ using a counting technique assuming that the appearance of each of these p matrices is equally likely. The diagonal components of $\mathbf{E}[L]$ are equal to n and the off-diagonal $ij-$th components, where $i \neq j$, are given by $-n/(N-1)$, when $i \in \mathcal{F}$ and $j \in \mathcal{N}$; $-n/(l-1)$, when $i \in \mathcal{L}$ and $j \in \mathcal{L}$; and 0, when $i \in \mathcal{L}$ and $j \in \mathcal{F}$. Therefore,

$$\mathbf{E}[L] = \frac{nN}{N-1} R_f + \frac{nl}{l-1} R_l, \tag{3.12}$$

where $R_f = \sum_{q=1}^{f} \boldsymbol{e}_q \boldsymbol{e}_q^T - \frac{1}{N} \mathbf{1}_f \mathbf{1}_N^T$ and $R_l = \sum_{q=f+1}^{N} \boldsymbol{e}_q \boldsymbol{e}_q^T - \frac{1}{l} \mathbf{1}_l \mathbf{1}_l^T$, the elementary vector $\boldsymbol{e}_q \in \mathbb{R}^{N \times 1}$ has 1 in the qth row and zeros in the remaining rows, and $\mathbf{1}_f = \sum_{q=1}^{f} \boldsymbol{e}_q$, and $\mathbf{1}_l = \sum_{q=f+1}^{N} \boldsymbol{e}_q$.

To compute $\mathbf{E}[L \otimes L]$, we notice that $L_{ij} \in \{0, -1, n\}$. Hence $L \otimes L$, which has terms of the form $L_{ij} L_{km}$ from the definition of Kronecker product, can have values $0, 1, -n, n^2$. We consider the following six possible cases for the indices i, j, k, and m which yield distinct values for elements of $\mathbf{E}[L \otimes L]$: 1) $i = j$, $k = m$; 2) $i = j, k \neq m$; 3) $i \neq j, k = m$; 4) $i \neq j, k \neq m, i = k, j = m$; 5) $i \neq j, k \neq m, i = k, j \neq m$; and 6) $i \neq j, k \neq m, i \neq k$. The distinct values for terms of these forms are given in Table A.1. In general, the diagonal blocks of $\mathbf{E}[L \otimes L]$ are of the form,

$$\mathbf{E}[L \otimes L]_{ii} = \frac{n^2 N}{N-1} R_f + \frac{n^2 l}{l-1} R_l \text{ when } i \in \mathcal{N}, \tag{3.13}$$

and the off-diagonal blocks can have three different forms, depending on the values of i and j :

$$\mathbf{E}[L\otimes L]_{ij} = \frac{-n^2N}{(N-1)^2}R_f - \frac{n^2l}{(N-1)(l-1)}R_l + \Delta_1 \boldsymbol{e}_i\boldsymbol{e}_j^T$$
$$- \frac{\Delta_1}{N-1}\boldsymbol{e}_i(\mathbf{1}_N^T - \boldsymbol{e}_i^T), \text{ when } i\in\mathcal{F}, \text{ and } j\in\mathcal{N}; \tag{3.14a}$$
$$\mathbf{E}[L\otimes L]_{ij} = 0, \text{ when } i\in\mathcal{L}, \text{ and } j\in\mathcal{F}; \tag{3.14b}$$
$$\mathbf{E}[L\otimes L]_{ij} = \frac{-n^2N}{(N-1)(l-1)}R_f - \frac{n^2l}{(l-1)^2}R_l + \Delta_2 \boldsymbol{e}_i\boldsymbol{e}_j^T$$
$$- \frac{\Delta_2}{l-1}\boldsymbol{e}_i(\mathbf{1}_l^T - \boldsymbol{e}_i^T), \text{ when } i\in\mathcal{L}, \text{ and } j\in\mathcal{L}; \tag{3.14c}$$

where $\Delta_1 = \dfrac{n(N-n-1)}{(N-1)(N-2)}$ and $\Delta_2 = \dfrac{n(l-n-1)}{(l-1)(l-2)}$.

3.4.4 Computation of G

We substitute (3.13) and (3.14a) to (3.14c) in (3.9) to derive G in block form. We retain the indices i and j for the $N\times N$ blocks, where $i,j = 1,\cdots,N$, and we notice that the blocks have six cases: diagonal blocks G_{ii} can have $i\in\mathcal{F}$ or $i\in\mathcal{L}$ and off-diagonal blocks can have i and j belonging to either $\mathcal{F}$ or $\mathcal{L}$. We define G considering the forms for each of the cases.

For the blocks of G with both i and $j\in\mathcal{F}$, we get,

$$\underset{(i\in\mathcal{F})}{G_{ii}} = \theta_1 I_N + \theta_2\mathbf{1}_N\mathbf{1}_N^T + \theta_3\hat{I}_f + \theta_4\mathbf{1}_f\mathbf{1}_N^T + \theta_5\mathbf{1}_N\mathbf{1}_f^T + \theta_6\hat{I}_l + \theta_7\mathbf{1}_l\mathbf{1}_l^T + \theta_8\mathbf{1}_f\boldsymbol{e}_i^T + \theta_9\mathbf{1}_N\boldsymbol{e}_i^T$$
$$+ \theta_{10}\boldsymbol{e}_i\boldsymbol{e}_i^T + \theta_{11}\boldsymbol{e}_i\mathbf{1}_f^T + \theta_{12}\boldsymbol{e}_i\mathbf{1}_l^T + \theta_{13}\mathbf{1}_l\boldsymbol{e}_i^T + \theta_{14}\mathbf{1}_N\mathbf{1}_l^T; \tag{3.15a}$$
$$\underset{(i,j\in\mathcal{F},\, i\neq j)}{G_{ij}} = \theta_{29}I_N + \theta_{30}\mathbf{1}_N\mathbf{1}_N^T + \theta_{31}\hat{I}_f + \theta_{32}\mathbf{1}_f\mathbf{1}_N^T + \theta_{33}\mathbf{1}_N\mathbf{1}_f^T + \theta_{34}\hat{I}_l + \theta_{35}\mathbf{1}_l\mathbf{1}_l^T + \theta_{36}\boldsymbol{e}_i\boldsymbol{e}_j^T +$$
$$\theta_{37}\mathbf{1}_N\boldsymbol{e}_j^T + \theta_{38}\boldsymbol{e}_i\mathbf{1}_N^T + \theta_{39}\boldsymbol{e}_i\boldsymbol{e}_i^T + \theta_{40}\mathbf{1}_N\boldsymbol{e}_i^T + \theta_{41}\mathbf{1}_f\boldsymbol{e}_j^T + \theta_{42}\boldsymbol{e}_j\boldsymbol{e}_j^T + \theta_{43}\boldsymbol{e}_j\mathbf{1}_f^T + \theta_{44}\boldsymbol{e}_j\mathbf{1}_l^T$$
$$+ \theta_{45}\mathbf{1}_l\boldsymbol{e}_j^T + \theta_{46}\mathbf{1}_N\mathbf{1}_l^T + \theta_{47}\boldsymbol{e}_i\mathbf{1}_l^T; \tag{3.15b}$$

where $\hat{I}_f, \hat{I}_l \in \mathbb{R}^{N\times N}$ are diagonal matrices where $\hat{I}_f$ has first f diagonal elements equal to one and the remaining zeros, and $\hat{I}_l$ has last l diagonal elements equal to one and the remaining zeros. For G_{ii}, when $i\in\mathcal{L}$, the form of (3.15a) is retained and the coefficients $\theta_1,\ldots,\theta_{14}$ become $\theta_{15},\ldots,\theta_{28}$. Similarly, for the off-diagonal blocks of G when $i\in\mathcal{F}$ and $j\in\mathcal{L}$; $i\in\mathcal{L}$ and $j\in\mathcal{F}$; and $i\in\mathcal{L}$ and $j\in\mathcal{L}$ the form is same as that of (3.15b) and the coefficients $\theta_{29},\ldots,\theta_{47}$ become respectively $\theta_{48},\ldots,\theta_{66}$; $\theta_{67},\ldots,\theta_{85}$; and $\theta_{86},\ldots,\theta_{104}$. The definitions of the coefficients, θ_i for $i = 1,\ldots,104$ can be found in the Appendix A.3.

3.4.5 The spectral radius of G

Following Proposition 2, we must find the spectrum of G to determine the spectral radius. The full spectrum of G and corresponding eigenspaces are provided in the Appendix A.2. It can be verified that the eigenspaces are all pairwise linearly independent and have dimensions summing to N^2, see Appendix A.2, and hence G can be diagonalized using a spectral decomposition. In this section, we exploit the diagonalizability of G to derive the spectral radius of G , which gives the closed form expression of the asymptotic convergence factor.

Lemma 1. *For the matrix G in* (3.15) *with eigenvalues in* (A.1a) *to* (A.1j) *and eigenspaces in* (A.2a) *to* (A.2j)*, the expected value of the disagreement norm can be written as*

$$\mathbf{E}\left[\|\boldsymbol{\xi}(k)\|^2\right] = A_1\lambda_1^k + A_2\lambda_2^k + A_6\lambda_6^k, \tag{3.16}$$

where A_1, A_2, and A_6 are constant scalar coefficients.

Proof. We notice that the expected value of the disagreement norm

$$\mathbf{E}\left[\|\boldsymbol{\xi}(k)\|^2\right] = \mathrm{vec}(I_N)^T\mathrm{vec}(\mathbf{E}\left[\boldsymbol{\xi}(k)\boldsymbol{\xi}(k)^T\right]) = \mathrm{vec}(I_N)^T\mathrm{vec}(\mathbf{E}\left[(Q\boldsymbol{\xi}(k))(\boldsymbol{Q}\boldsymbol{\xi}(k))^T\right]),$$

where the function vec($\bullet$) stacks the columns of an $N\times M$ matrix to form an $NM\times 1$ column vector. By iteratively applying (3.7), we find that

$$\begin{aligned}\mathbf{E}\left[\|\boldsymbol{\xi}(k)\|^2\right] &= \mathrm{vec}(I_N)^T\mathbf{E}\left[\tilde{W}\otimes\tilde{W}\right]^k\mathrm{vec}(\boldsymbol{\xi}(0)\boldsymbol{\xi}(0)^T)\\ &= \mathrm{vec}(I_N)^T G^k\mathrm{vec}((Q\boldsymbol{\xi}(0))(Q\boldsymbol{\xi}(0))^T).\end{aligned} \tag{3.17}$$

Since G can be diagonalized, we can write $G = V\Lambda U$, where $\Lambda\in\mathbb{R}^{N^2\times N^2}$ is a diagonal matrix with the eigenvalues of G along the diagonal. The matrices V and U consist of N^2 linearly independent right column and left row eigenvectors of G, respectively, ordered in correspondence to these eigenvalues and scaled so that $UV = I_{N^2}$. We can find the closed form expression for the eigenstructure of G reported in the Appendix A.2. It can be verified that the eigenvectors in $\Gamma^{(i)}$ for $i = 1,\cdots,12$, $i\neq 1,2,6,11$, are orthogonal to vec(I_N). Hence, $\mathrm{vec}(I_N)^T G = \mathrm{vec}(I_N)^T(\lambda_1\boldsymbol{v}_1\boldsymbol{u}_1^T + \lambda_2\boldsymbol{v}_2\boldsymbol{u}_2^T + \lambda_6\boldsymbol{v}_6\boldsymbol{u}_6^T + \lambda_{11}\boldsymbol{v}_{11}\boldsymbol{u}_{11}^T)$, where $\boldsymbol{v}_i\in\Gamma^{(i)}$, $\boldsymbol{u}_i$ is the left eigenvector corresponding to λ_i, and

$$\lambda_1 = \epsilon^2\kappa_2 n + \sqrt{\epsilon^4\kappa_3 n^2 - \epsilon^3\kappa_5 n^2 + \epsilon^2\kappa_4 n^2} - \epsilon\kappa_1 n + 1, \tag{3.18a}$$

$$\lambda_2 = \epsilon^2\kappa_7 n - \epsilon\kappa_6 n + 1, \tag{3.18b}$$

$$\lambda_6 = \epsilon^2\kappa_2 n - \sqrt{\epsilon^4\kappa_3 n^2 - \epsilon^3\kappa_5 n^2 + \epsilon^2\kappa_4 n^2} - \epsilon\kappa_1 n + 1, \tag{3.18c}$$

$$\lambda_{11} = 0. \tag{3.18d}$$

Since, $\lambda_{11} = 0$, $\mathbf{E}\left[\|\boldsymbol{\xi}(k)\|^2\right]$ in (3.17) is of the desired form in (3.16). □

Claim 1. *The eigenvalue λ_6 is not the spectral radius of G.*

Proof. The claim can be directly showed by verifying that $\lambda_1 > |\lambda_6|$ from their expressions in (3.18a) and (3.18c). □

As a result, we only need to consider λ_1 and λ_2 as candidates for the spectral radius of G and, thus, the asymptotic convergence factor r_a.

Lemma 2. *For the matrix G in* (3.15) *with eigenvalues in* (A.1a) *to* (A.1j) *and eigenspaces in* (A.2a) *to* (A.2j)*, the eigenvalues λ_1 and λ_2 of G are positive and have exactly one non-zero intersection at $\epsilon = \epsilon_{cr}$, which is one of the following two expressions given by*

$$\epsilon_{cr1,cr2} = \frac{\pm\sqrt{\kappa_{12}^2 - 4\kappa_{10}\kappa_{11}} - \kappa_{12}}{2\kappa_{10}}$$

that satisfies the condition $(\kappa_1 - \kappa_6) + \epsilon(\kappa_7 - \kappa_2) > 0$. We define regime I as $\epsilon \in [0, \epsilon_{cr}]$ and regime II as $\epsilon \in [\epsilon_{cr}, \infty)$.

Proof. The eigenvalues λ_1 and λ_2 are always greater than zero, which can be checked using the full expressions with coefficients from the Appendix A.3. Next, we equate $\lambda_1 = \lambda_2$ and solving for ϵ. We find $\epsilon = 0$ is a root and, from (3.18a) and (3.18b), both λ_1 and λ_2 are equal to 1 at $\epsilon = 0$. Solving for the non-zero solutions for ϵ leads to the following equation

$$\sqrt{\epsilon^2\kappa_3 - \epsilon\kappa_5 + \kappa_4} = (\kappa_1 - \kappa_6) + \epsilon(\kappa_7 - \kappa_2). \tag{3.19}$$

We start by squaring the equation (3.19) and get two solutions, called ϵ_{cr1} and ϵ_{cr2}. Therefore, ϵ_{cr1} and ϵ_{cr2} are the solutions for $\pm\sqrt{\epsilon^2\kappa_3 - \epsilon\kappa_5 + \kappa_4} = (\kappa_1 - \kappa_6) + \epsilon(\kappa_7 - \kappa_2)$, however only one of them satisfies the additional condition that $(\kappa_1 - \kappa_6) + \epsilon(\kappa_7 - \kappa_2) > 0$ which enforces the positivity of the square root term in equation (3.19). We define $\epsilon = \epsilon_{cr}$ as the non-zero intersection of λ_1 and λ_2 that satisfies this condition. □

Theorem 2. *For the NC leader-follower consensus protocol in* (3.1)*, with $f, l \geq 3$, $n \in \{1, \ldots, l-1\}$, the asymptotic convergence factor is the spectral radius of G in* (3.15)*, and is given by λ_1 and λ_2 when ϵ is in regime I and regime II, respectively.*

Proof. Following Lemma 1, Lemma 2, and Claim 1, it is enough to show that that λ_1 is greater in magnitude than λ_2 in regime I and λ_2 is greater in magnitude than λ_1 in regime II. From (3.18a) and (3.18b), both λ_1 and λ_2 are equal to 1 at $\epsilon = 0$. Next, we take the derivative of both eigenvalue expressions with respect to ϵ, and find that both λ_1 and λ_2 have negative derivative as $\epsilon \to 0$ and $\text{abs}(\frac{\partial\lambda_2}{\partial\epsilon}\big|_{\epsilon\to 0^+}) > \text{abs}(\frac{\partial\lambda_1}{\partial\epsilon}\big|_{\epsilon\to 0^+})$. In other words, λ_1 and λ_2 start from the same point and then λ_2 decreases at a faster rate than λ_1 as ϵ increases from zero. Also, λ_1 and λ_2 are always greater than zero. Hence λ_1 is greater than λ_2 as $\epsilon \to 0^+$. However, $\lim_{\epsilon\to\infty}(\lambda_2 - \lambda_1) > 0$. Again from Lemma 2, λ_1 and λ_2 have exactly one intersection. This means that the order of the eigenvalues must change, and this reversal occurs at their intersection point ϵ_{cr}.

Therefore, we conclude $\lambda_1 > \lambda_2$ in regime I and $\lambda_2 > \lambda_1$ in regime II. From the definition of the asymptotic convergence factor [20] and from (3.8), we find that $r_a = \lambda_1$ for $\epsilon \leq \epsilon_{cr}$ and $r_a = \lambda_2$ for $\epsilon \geq \epsilon_{cr}$, which completes the proof. □

Remark 1. *It is noteworthy that the expression for λ_1 is same as that of the asymptotic convergence factor derived in [24], where the followers converge at pre-determined leaders common state. In our model, we observe that in regime I, when ϵ is smaller than ϵ_{cr}, the leaders' sub-system converges at a faster rate and then the followers converge to the leaders' state of consensus. Thus, the two expressions being equal is in confirmation with the dynamics.*

Remark 2. *The expression for λ_2 is the same as that of the asymptotic convergence factor derived in [20], where l replaces the total number of agents. This means that the leaders' sub-system executing the consensus protocol over the NC subgraph takes precedence over the dynamics of the followers' sub-system in the regime II. In other words, when ϵ is greater than ϵ_{cr}, the asymptotic convergence factor depends on only the number of leaders present in the system.*

3.5 Results and Discussion

3.5.1 Numerical validation

We validate the expression for r_a numerically when ϵ in both regimes I and II. In Figure 3.2, we present Monte Carlo simulations for a network with $f = 4,\ l = 8,\ n = 3$, and fixed initial conditions. The parameter $\epsilon = 0.1$ is used for targeting $r_a = \lambda_1$ and $\epsilon = 0.32$ is used for targeting $r_a = \lambda_2$. These ϵ values reside in regimes I and II, respectively, since $\epsilon_{cr} = 0.291$ for the selected model parameters. We find that the magnitude of the disagreement vector decreases linearly on a logarithmic scale as the disagreement system converges to zero for both ϵ values.

For $\epsilon = 0.1$ and $\epsilon = 0.32$, we compute a best fit line in logarithmic scale over time steps $[5, 15]$ in each case. We find that the square of the disagreement norm decreases as $(0.57)^k$ for $\epsilon = 0.1$ and $(0.19)^k$ for $\epsilon = 0.32$. From the result in Theorem 2, we find that the asymptotic convergence factor is 0.61 for $\epsilon = 0.1$ and 0.19 for $\epsilon = 0.32$, thus confirming the analytical prediction.

3.5.2 Dependence of asymptotic convergence factor on system parameters

With the validated analytical form for the asymptotic convergence factor, we explore the dependence of this quantity on model parameters. Figure 3.3 shows λ_1 and λ_2 varying with

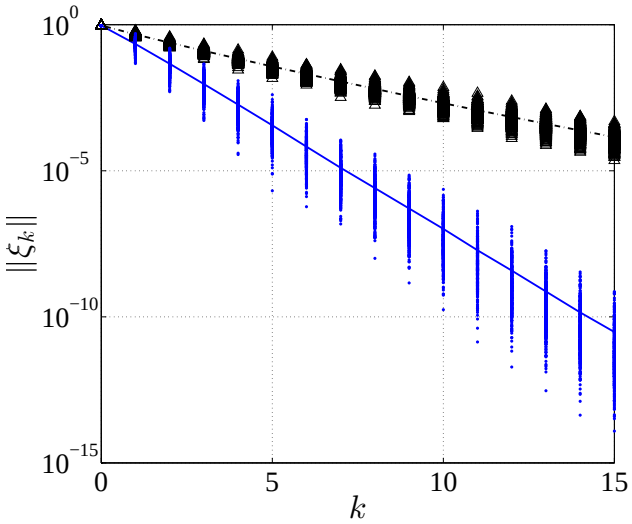

Figure 3.2: Magnitude of the disagreement vector for Monte Carlo simulations with constant initial conditions and $f = 4,\ l = 8,\ n = 3$. Individual markers show five hundred different realizations and the line depicts the average disagreement with $\epsilon = 0.1$ (blue dots and solid line) and $\epsilon = 0.32$ (black triangles and dashed line). Note that these values of ϵ are in regimes I and II, respectively, for the selected parameters.

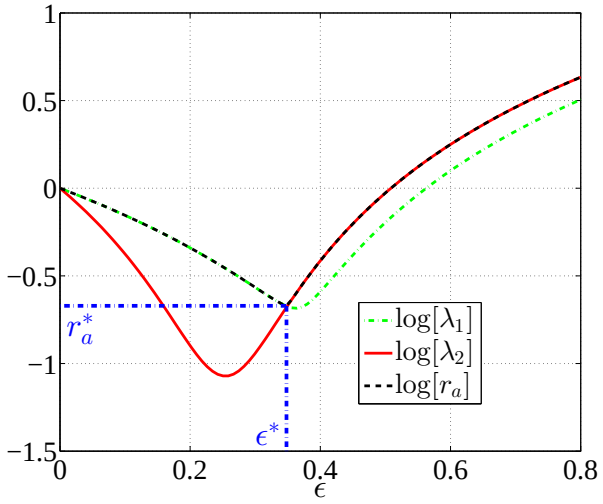

Figure 3.3: Base-ten logarithm of λ_1, λ_2, and r_a varying with ϵ and $f = l = 6,\ n = 3$. The horizontal blue dash-dot line shows the maximum convergence rate r_a^* and the corresponding persuasibility ϵ^*, which equals to ϵ_{cr} in this case.

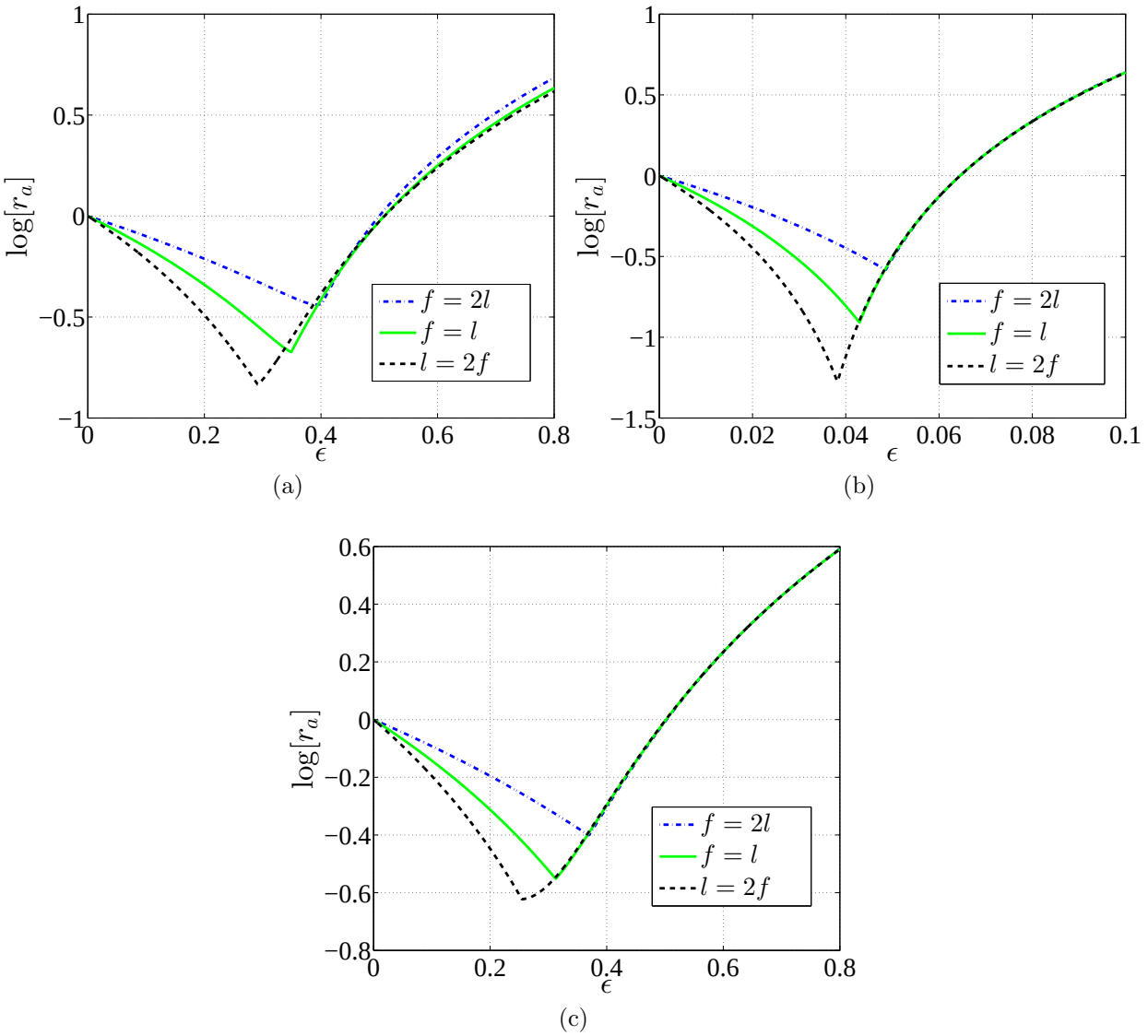

Figure 3.4: Comparative study of the asymptotic convergence factor for three different proportions of leaders and followers and (a) $N = 12$ and $n = 3$, (b) $N = 120$ and $n = 30$, (c) $N = 120$ and $n = 3$.

ϵ for a system with $f = l = 6$ and $n = 3$. The shape of these curves follows from the proof of the Theorem 2. In particular, both $\log[\lambda_1]$ and $\log[\lambda_2]$ equal zero when $\epsilon = 0$, decrease to a minimum as ϵ increases, and then increase unbounded as $\epsilon \to \infty$. The eigenvalues λ_1 and λ_2 intersect at approximately $\epsilon = 0.34$, which can be found from the expression of ϵ_{cr} substituting in these system parameters. As proved earlier, λ_1 is the asymptotic convergence factor in regime I and λ_2 is the asymptotic convergence factor in regime II, which is supported by Figure 3.3.

From the proof of Theorem 2, and from the shapes of λ_1 and λ_2, it follows that the asymptotic convergence factor decreases from unity up to a certain value of ϵ, and then increases above unity to infinity. We know that convergence speed increases as r_a decreases by definition and that systems with $r_a > 1$ do not converge to consensus. Therefore, there exists a maximum convergence speed r_a^*, where r_a is minimum, and its corresponding persuasibility ϵ^*. We follow the evolution of these features as we study the dependence of r_a on the system parameters.

We explore the behavior of the asymptotic convergence factor by varying the distribution of leaders and followers, as well as the total number of agents in the system and their numerosity. We consider for three specific cases: (a) followers are twice the number of leaders $f = 2l$, (b) leaders are twice the number of followers $l = 2f$, and (c) number of leaders is same as that of the followers $l = f$.

Effect of increasing the proportion of leaders

In Figure 3.4a, Figure 3.4b, and Figure 3.4c, we plot the asymptotic convergence factor in base-ten logarithmic scale for the three aforementioned cases keeping N and n fixed. In each of these plots, we observe that the maximum convergence speed increases as we increase the relative number of leaders with all other system parameters held constant. This can be seen as $\log[{r_a}^*]$ decreases as the proportion of leaders increases in each system. These features are supported by experimental results on a fish shoal in [58], which demonstrates increasing the proportion of experienced individuals in the group results in more effective leadership.

In addition, ϵ^* decreases as we increase the proportion of leaders, demonstrating that agents must be less persuasible and thus more stubborn to attain maximum convergence speed in the presence of higher proportions of leaders. The tactic of increasing stubbornness to achieve consensus is bolstered by the biological literature across species. Experiments on homing pigeons reveal that leadership originates as the individuals become more stubborn in the situation of conflicting opinions [34]. Moreover, results in [59, 60] indicate, in situations of conflicts, individuals become more stubborn and attempt to influence the group movement by strategically changing behavioral parameters. Results in [32] demonstrate stubborn leaders, though minority in numbers, can dictate the group outcome in simulations of animal groups.

Nevertheless, increasing the relative number of leaders is not always beneficial for system

performance at a set stubbornness (or value of ϵ). This is demonstrated in Figure 3.4a, where we observe that increasing the proportion of leaders results in a slight decrease of convergence speed when $\epsilon = 0.4$. Also, in Figure 3.4b, and Figure 3.4c, there exists ranges of ϵ ($[0.05, \infty)$ and $[0.37, \infty)$, respectively) where $\log[r_a]$ is insensitive to different proportion of leaders. This is consistent with the numerical results in [61] and experimental study on humans in [35], where it is reported only a small proportion of informed individuals leads a large group as well as a large proportion. To summarize, increasing the proportion of leaders may dramatically improve system performance in terms of convergence speed when agents are relatively stubborn, but this effect is dulled when agents are too persuasible.

Effect of increasing the group size

Next, we study the effect of group size on these trends and features of the asymptotic convergence factor. By increasing group size, we observe maximum convergence speed increases as numerosity is kept proportionally constant, but persuasibility must be lessened to achieve it. Comparing every case of Figure 3.4a with the corresponding case in Figure 3.4b, we observe that r_a^* and ϵ^* decrease when numerosity is increased proportionally with group size, which supports this argument. These results are analogously supported by biological observation. Experiments on homing pigeons in [62] demonstrate an increase in directional accuracy and decrease in homing times for flocks as compared to individuals. Also in [63], a study on fish reveals increase in improved decision-making accuracy as the group size increases. Furthermore, [64] and [65] explain how the 'many-wrongs principle'– that zero-mean random noise cancels in large populations– contributes to the navigational accuracy of animal groups increasing with group size.

We further observe, as each agent interacts with a larger group, maximum convergence speed decreases if the informational capacity of each agent (i.e. the numerosity) is not increased. These features are illustrated in Figure 3.4a and Figure 3.4c, where numerosity is kept constant and the group size is increased, which results in a slight decrease of maximum convergence speed and corresponding persuasibility. This result is in line with the studies in [62, 66, 67], which show evidence that the number of individuals contributing to the decision increases with group size. In other words, increase in group size demands increasing numerosity for better accuracy. The results of this work indicate that interacting with larger groups requires the agents to be more stubborn to achieve faster convergence. To summarize, larger systems may achieve consensus faster even among a larger number of agents if the numerosity scales with the group size and persuasibility is reduced accordingly.

Effect of increasing numerosity

Finally, we explore the dependence of asymptotic convergence factor on the numerosity of individuals in the group keeping the other system parameters constant. Comparing Fig-

ure 3.4b, and Figure 3.4c, where we fix the group size and vary numerosity, we observe that increasing numerosity for each agent results in a faster maximum convergence speed at a dramatically lower value of persuasibility, since r_a^* and ϵ^* decrease between the figures. In other words, enabling the agents to increase information exchange by increasing numerosity always results in faster maximum convergence speed, while simultaneously requiring that the agents be more stubborn.

Comparison to previous work

We compare the results of our present model with that of the model considering static leaders in [24] and briefly point out some of the main differences regarding the effect of parameters on the asymptotic convergence factor. The results in [24] demonstrate increasing leaders always results in faster convergence speed, which is not necessarily the case when the dynamic leaders are taken into account, as pointed out in Section 3.5.2. In addition, results in [24] indicate that, for fixed values of l/N, ϵ^* decreases as n/N increases, which means that increasing numerosity necessitates being less stubborn. This contradicts the results of the present model, as demonstrated by comparing each case of Figure 3.4a to that of Figure 3.4c.

The results of this model can be described in two regimes that emerge when leaders are considered to be dynamic, which are generalized from the previous literature. In regime I, the leaders' sub-system converges at a faster rate and the followers then converge to leaders' converged state, as shown in Figure 3.5a with the same system parameters as that of in Figure 3.3. In regime I, the expression of the asymptotic convergence factor is same as that derived in [24]. However, in regime II, the leaders dictate the convergence speed as shown in Figure 3.5b. The expression of the asymptotic convergence factor in this regime is same as that derived in [20], where parameters for the leaders' sub-system are used to compute the asymptotic convergence factor.

3.5.3 Synchronization

To demonstrate the results for synchronization over NC networks with our present model, we consider a logistic map similar to [53] for individual dynamics. The individual dynamics of the logistic map is given by

$$x(k+1) = 3.9x(k)(1 - x(k)), \tag{3.20}$$

with random initial conditions. The largest Lyapunov exponent $h_{\max}$ is 0.485 for logistic maps [53]. From Proposition 3, stochastic synchronization is achieved if and only if the natural logarithm of the spectral radius of G is smaller than -0.970 for logistic maps.

We consider 260 coupled oscillators connected over NC networks with $f = 180, l = 80$, and $n = 30$. Figure 3.6 shows variation of $\ln[\rho(G)]$ with ϵ and the numerical threshold required for

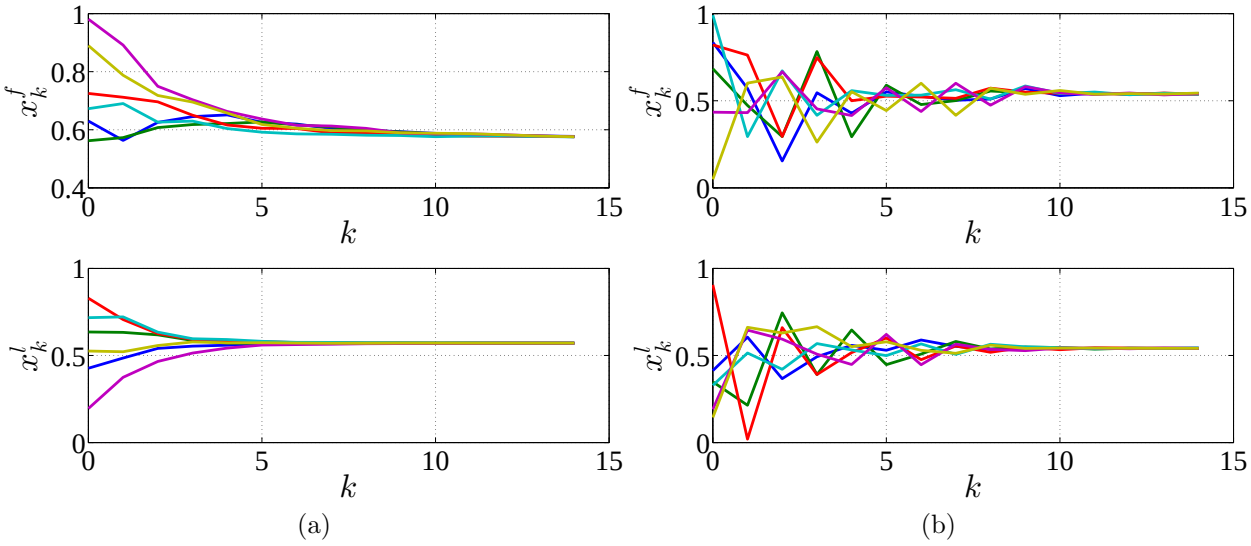

Figure 3.5: Time series evolution of leaders and followers connected over NC network with $f = l = 6, n = 3$ and (a) $\epsilon = 0.15$ (regime I), (b) $\epsilon = 0.45$ (regime II).

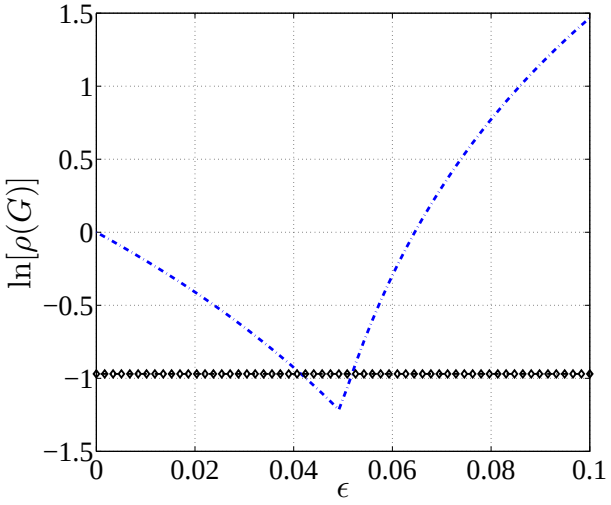

Figure 3.6: Spectral radius of G over a NC network with $f = 180, l = 80$, and $n = 30$ as a function of ϵ, drawn as blue dash-dot line. Black line (diamonds) corresponds to $-2h_{\max}$ of the logistic maps.

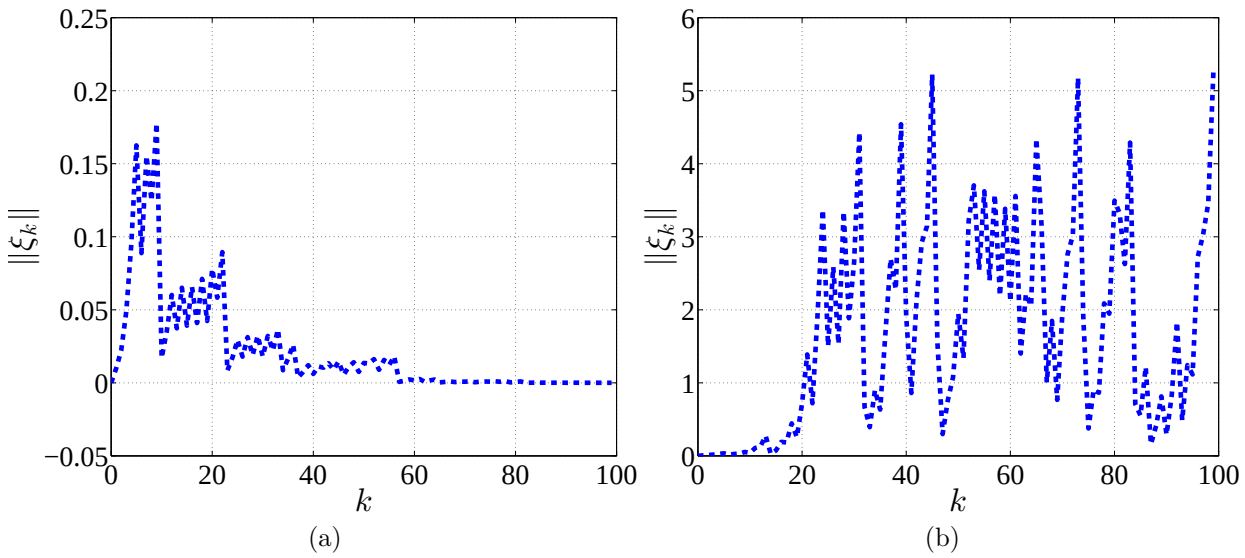

Figure 3.7: Magnitude of the disagreement vector for 260 logistic maps coupled over NC network with $f = 180, l = 80, n = 30$ and (a) $\epsilon = 0.05$ and (b) $\epsilon = 0.02$.

stochastic synchronization of logistic maps. The bounded interval within which the system is synchronizable is when the blue dash-dot line is less than the black diamonds. In this example, this interval is equal to $[0.04, 0.52]$.

For illustration, we consider the same coupled logistic maps above with random initial conditions selected uniformly in $[0, 0.001]$. We vary the coupling strength so that ϵ lies in two different regions, corresponding to Figure 3.6. In the Figure 3.7a, we choose $\epsilon = 0.05$. This corresponds to the regime where $\ln[\rho(G)]$ lies inside the bounded region. We observe the system synchronizes as the disagreement vector goes to zero with time but does not synchronize as shown in Figure 3.7b if ϵ is outside of the bounded region ($\epsilon = 0.02$). Hence, these results are consistent with the predictions from the main result. Here, we comment that the effect of the system parameters on synchronization is the same as that of the above study with respect to asymptotic convergence factor.

3.6 Conclusion

In conclusion, we define discrete-time leader-follower consensus and synchronization protocols over a stochastic NC network, where the leaders' states are dynamically changing. We determine closed form expressions for the rate of convergence to consensus and conditions for stochastic synchronization in terms of system parameters, which are group size, proportion of leaders, numerosity, and persuasibility. The closed form expression gives an insight of the underlying dynamics and helps to study how these different parameters effect the

convergence rate. We find that there exists a broad range of persuasibility within which consensus may be achieved and, for a subset of persuasibilities, the convergence rate is dictated by only the number of leaders present in the system. With an increasing proportion of leaders, maximum possible convergence speed increases and it occurs at a lower value of persuasibility; in addition, increasing the proportion of leaders has a limited effect on convergence rate when agents are more persuasible. Furthermore, maximum convergence rate is only achieved by either increasing numerosity or decreasing persuasibility when group size is increased. Finally, we find that increasing the numerosity is always beneficial for faster maximum convergence speed.

These results are supported by behaviorial studies of animal groups exhibiting collective behavior and capitalizes on these evolutionary-refined social interaction. Such biological systems can be used to inspire engineering solutions. For example, the selection of NC interaction networks is particularly relevant to engineered systems, such as wireless sensor networks, where communication links vary stochastically in time [68, 69]. While physical occlusions barring interaction between agents may not influence such systems, the total energy an agent can use for communication is capped in an analogous fashion to the numerosity constraint. Thus, the results of this work may be applied to design and control artificial leaders for multi-agent systems to enable achieving faster convergence.

3.7 References

[1] David JT Sumpter. The principles of collective animal behaviour. *Philosophical Transactions of the Royal Society B: Biological Sciences*, 361(1465):5–22, 2006.

[2] Rodolphe Sepulchre, Derek A Paley, and Naomi Ehrich Leonard. Stabilization of planar collective motion with limited communication. *IEEE Transactions on Automatic Control*, 53(3):706–719, 2008.

[3] Michele Ballerini, Nicola Cabibbo, Raphael Candelier, Andrea Cavagna, Evaristo Cisbani, Irene Giardina, Vivien Lecomte, Alberto Orlandi, Giorgio Parisi, and Andrea Procaccini. Interaction ruling animal collective behavior depends on topological rather than metric distance: Evidence from a field study. *Proceedings of the National Academy of Sciences*, 105(4):1232–1237, 2008.

[4] Manuela Piazza and Vronique Izard. How humans count: numerosity and the parietal cortex. *The Neuroscientist*, 15(3):261–273, 2009.

[5] Roland W Tegeder and Jens Krause. Density dependence and numerosity in fright stimulated aggregation behaviour of shoaling fish. *Philosophical Transactions of the Royal Society of London. Series B: Biological Sciences*, 350(1334):381–390, 1995.

[6] Larissa Conradt and Timothy J Roper. Group decision-making in animals. *Nature*, 421(6919):155–158, 2003.

[7] Yuko Hatano and Mehran Mesbahi. Agreement over random networks. *IEEE Transactions on Automatic Control*, 50(11):1867–1872, 2005.

[8] Reza Olfati-Saber and Richard M Murray. Consensus problems in networks of agents with switching topology and time-delays. *IEEE Transactions on Automatic Control*, 49(9):1520–1533, 2004.

[9] Randal W Beard, Timothy W McLain, Michael A Goodrich, and Erik P Anderson. Coordinated target assignment and intercept for unmanned air vehicles. *IEEE Transactions on Robotics and Automation*, 18(6):911–922, 2002.

[10] Michael A Kovacina, Daniel Palmer, Guang Yang, and Ravi Vaidyanathan. Multi-agent control algorithms for chemical cloud detection and mapping using unmanned air vehicles. In *IEEE/RSJ International Conference on Intelligent Robots and Systems*, volume 3, pages 2782–2788, 2002.

[11] Maurizio Porfiri, D Gray Roberson, and Daniel J Stilwell. Tracking and formation control of multiple autonomous agents: A two-level consensus approach. *Automatica*, 43(8):1318–1328, 2007.

[12] Darren K Maczka, Davide Spinello, Daniel J Stilwell, Aditya S Gadre, and Wayne L Neu. Coordinated tracking of an acoustic signal by a team of autonomous underwater vehicles. In *AUVSI's Unmanned Systems North America*, 2009.

[13] Minh Nguyen-Duc, J-P Briot, and Alexis Drogoul. An application of multi-agent coordination techniques in air traffic management. In *IEEE/WIC International Conference on Intelligent Agent Technology*, pages 622–625, 2003.

[14] Min Chen, Sergio Gonzalez, and Victor CM Leung. Applications and design issues for mobile agents in wireless sensor networks. *IEEE Wireless Communications*, 14(6):20–26, 2007.

[15] Kemal Akkaya and Mohamed Younis. A survey on routing protocols for wireless sensor networks. *Ad Hoc Networks*, 3(3):325–349, 2005.

[16] Shmuel Nitzan and Jacob Paroush. *Collective decision making: an economic outlook*. CUP Archive, 1985.

[17] Jianquan Lu, Daniel WC Ho, and Jurgen Kurths. Consensus over directed static networks with arbitrary finite communication delays. *Physical Review E*, 80(6):066121, 2009.

[18] Wei Ren and Randal Beard. *Distributed consensus in multi-vehicle cooperative control: theory and applications*. Springer, 2007.

[19] Reza Olfati-Saber, J Alex Fax, and Richard M Murray. Consensus and cooperation in networked multi-agent systems. *Proceedings of the IEEE*, 95(1):215–233, 2007.

[20] Nicole Abaid and Maurizio Porfiri. Consensus over numerosity-constrained random networks. *IEEE Transactions on Automatic Control*, 56(3):649–654, 2011.

[21] Wei Ren and Randal W Beard. Consensus seeking in multiagent systems under dynamically changing interaction topologies. *IEEE Transactions on Automatic Control*, 50(5):655–661, 2005.

[22] Maurizio Porfiri and Daniel J Stilwell. Consensus seeking over random weighted directed graphs. *IEEE Transactions on Automatic Control*, 52(9):1767–1773, 2007.

[23] Silvana Silva Pereira. Mean square convergence of consensus algorithms in random WSNs. *IEEE Transactions on Signal Processing,*, 58(5):2866–2874, 2010.

[24] Nicole Abaid and Maurizio Porfiri. Leader-follower consensus over numerosity-constrained random networks. *Automatica*, 48(8):1845–1851, 2012.

[25] Tuncer Can Aysal and Kenneth E Barner. Convergence of consensus models with stochastic disturbances. *IEEE Transactions on Information Theory*, 56(8):4101–4113, 2010.

[26] Alireza Tahbaz-Salehi and Ali Jadbabaie. A necessary and sufficient condition for consensus over random networks. *IEEE Transactions on Automatic Control*, 53(3):791–795, 2008.

[27] Rifat Sipahi and Artug Acar. Stability analysis of three-agent consensus dynamics with fixed topology and three non-identical delays. In *ASME Dynamic Systems and Control Conference*, pages 1483–1490, 2008.

[28] Zhong Wang, Jianxiang Xi, Zhicheng Yao, and Guangbin Liu. Guaranteed cost consensus for multi-agent systems with switching topologies. *International Journal of Robust and Nonlinear Control*, 2014. doi: 10.1002/rnc.3252.

[29] Wei Ren and Ella Atkins. Distributed multi-vehicle coordinated control via local information exchange. *International Journal of Robust and Nonlinear Control*, 17:1002–1033, 2007.

[30] Subhradeep Roy and Nicole Abaid. Consensus of conspecific agents via collaborative and antagonistic interactions. In *ASME 2015 Dynamic Systems and Control Conference*, pages V003T37A004–V003T37A004, 2015.

[31] Subhradeep Roy and Nicole Abaid. On the effect of collaborative and antagonist interactions on synchronization and consensus in networks of conspecific agents. *IEEE Transactions on Automatic Control*, 2016.

[32] Iain D Couzin, Christos C Ioannou, Guven Demirel, Thilo Gross, Colin J Torney, Andrew Hartnett, Larissa Conradt, Simon A Levin, and Naomi E Leonard. Uninformed individuals promote democratic consensus in animal groups. *Science*, 334(6062):1578–1580, 2011.

[33] Mate Nagy, Zsuzsa Akos, Dora Biro, and Tamas Vicsek. Hierarchical group dynamics in pigeon flocks. *Nature*, 464(7290):890–893, 2010.

[34] Dora Biro, David JT Sumpter, Jessica Meade, and Tim Guilford. From compromise to leadership in pigeon homing. *Current Biology*, 16(21):2123–2128, 2006.

[35] John RG Dyer, Anders Johansson, Dirk Helbing, Iain D Couzin, and Jens Krause. Leadership, consensus decision making and collective behaviour in humans. *Philosophical Transactions of the Royal Society B: Biological Sciences*, 364(1518):781–789, 2009.

[36] Ran Xiaohong and Wu Qinghe. Leader-follower consensus for multi-agent systems based on error predictor. In *International Conference on Measuring Technology and Mechatronics Automation*, pages 681–684, 2013.

[37] Jiangping Hu and Gang Feng. Distributed tracking control of leader-follower multi-agent systems under noisy measurement. *Automatica*, 46(8):1382–1387, 2010.

[38] Zhi-Hong Guan, Feng-Lan Sun, Yan-Wu Wang, and Tao Li. Finite-time consensus for leader-following second-order multi-agent networks. *IEEE Transactions on Circuits and Systems I: Regular Papers*, 59(11):2646–2654, 2012.

[39] Bo Liu, Tianguang Chu, Long Wang, and Guangming Xie. Controllability of a leader-follower dynamic network with switching topology. *IEEE Transactions on Automatic Control*, 53(4):1009–1013, 2008.

[40] Qiang Song, Fang Liu, Jinde Cao, and Wenwu Yu. *M*-matrix strategies for pinning-controlled leader-following consensus in multiagent systems with nonlinear dynamics. *IEEE Transactions on Cybernetics*, 43(6):1688–1697, 2013.

[41] Jae Man Kim, Jin Bae Park, and Yoon Ho Choi. Leaderless and leader-following consensus for heterogeneous multi-agent systems with random link failures. *IET Control Theory & Applications*, 8(1):51–60, 2014.

[42] Subhradeep Roy and Nicole Abaid. Leader-follower consensus modeling representative democracy. *Proceedings of CDSR'15 - International Conference on Control, Dynamic Systems, and Robotics*, 2015.

[43] Francesco Sorrentino, Mario di Bernardo, Franco Garofalo, and Guanrong Chen. Controllability of complex networks via pinning. *Physical Review E*, 75(4):046103, 2007.

[44] Louis M Pecora and Thomas L Carroll. Master stability functions for synchronized coupled systems. *Physical Review Letters*, 80(10):2109, 1998.

[45] Maurizio Porfiri and Francesca Fiorilli. Node-to-node pinning control of complex networks. *Chaos: An Interdisciplinary Journal of Nonlinear Science*, 19(1):013122, 2009.

[46] Daniel J Stilwell, Erik M Bollt, and D Gray Roberson. Sufficient conditions for fast switching synchronization in time-varying network topologies. *SIAM Journal on Applied Dynamical Systems*, 5(1):140–156, 2006.

[47] Jun Zhao, David J Hill, and Tao Liu. Synchronization of complex dynamical networks with switching topology: a switched system point of view. *Automatica*, 45(11):2502–2511, 2009.

[48] Pietro DeLellis, Mario di Bernardo, and Maurizio Porfiri. Pinning control of complex networks via edge snapping. *Chaos: An Interdisciplinary Journal of Nonlinear Science*, 21(3):033119, 2011.

[49] Maurizio Porfiri, Daniel J Stilwell, and Erik M Bollt. Synchronization in random weighted directed networks. *IEEE Transactions on Circuits and Systems I: Regular Papers*, 55(10):3170–3177, 2008.

[50] Maurizio Porfiri, Daniel J Stilwell, Erik M Bollt, and Joseph D Skufca. Random talk: Random walk and synchronizability in a moving neighborhood network. *Physica D: Nonlinear Phenomena*, 224(1):102–113, 2006.

[51] Maurizio Porfiri. Stochastic synchronization in blinking networks of chaotic maps. *Physical Review E*, 85(5):056114, 2012.

[52] Igor Belykh, Mario di Bernardo, Jurgen Kurths, and Maurizio Porfiri. Evolving dynamical networks. *Physica D: Nonlinear Phenomena*, 267:1–6, 2014.

[53] Nicole Abaid and Maurizio Porfiri. Synchronous dynamics over numerosity-constrained stochastic networks. In *Applications of Chaos and Nonlinear Dynamics in Science and Engineering-Vol. 2*, pages 95–121. Springer, 2012.

[54] Michael L Mezey. *Representative democracy: legislators and their constituents*. Rowman & Littlefield Publishers, 2008.

[55] Xiangbo Feng, Kenneth Loparo, Yuandong Ji, and Howard Jay Chizeck. Stochastic stability properties of jump linear systems. *IEEE Transactions on Automatic Control*, 37(1):38–53, 1992.

[56] Maurizio Porfiri. A master stability function for stochastically coupled chaotic maps. *EPL (Europhysics Letters)*, 96(4):40014, 2011.

[57] Maurizio Porfiri. Stochastic synchronization in blinking networks of chaotic maps. *Physical Review E*, 85(5):056114, 2012.

[58] Stephan G Reebs. Can a minority of informed leaders determine the foraging movements of a fish shoal? *Animal Behaviour*, 59(2):403–409, 1999.

[59] Larissa Conradt, J Krause, Iain D Couzin, and Timothy J Roper. "Leading according to need" in self-organizing groups. *The American Naturalist*, 173(3):304–312, 2009.

[60] Jens Krause and Graeme D Ruxton. *Living in groups*. OUP Oxford, 2002.

[61] Iain D Couzin, Jens Krause, Nigel R Franks, and Simon A Levin. Effective leadership and decision-making in animal groups on the move. *Nature*, 433(7025):513–516, 2005.

[62] Staffan Tamm. Bird orientation: single homing pigeons compared with small flocks. *Behavioral Ecology and Sociobiology*, 7(4):319–322, 1980.

[63] David JT Sumpter, Jens Krause, Richard James, Iain D Couzin, and Ashley JW Ward. Consensus decision making by fish. *Current Biology*, 18(22):1773–1777, 2008.

[64] Andrew M Simons. Many wrongs: the advantage of group navigation. *Trends in Ecology & Evolution*, 19(9):453–455, 2004.

[65] EA Codling, JW Pitchford, and SD Simpson. Group navigation and the "many-wrongs principle" in models of animal movement. *Ecology*, 88(7):1864–1870, 2007.

[66] Larissa Conradt and Timothy J Roper. Consensus decision making in animals. *Trends in Ecology & Evolution*, 20(8):449–456, 2005.

[67] J Rabol and H Noer. Spring migration in the skylark (*alauda arvensis*) in Denmark: Influence of environmental factors on the flocksize and correlation between flocksize and migratory direction. *Vogelwarte*, 27(1):50–65, 1973.

[68] Lilia Paradis and Qi Han. A survey of fault management in wireless sensor networks. *Journal of Network and Systems Management*, 15(2):171–190, 2007.

[69] Soummya Kar and Jose M. F. Moura. Sensor networks with random links: Topology design for distributed consensus. *IEEE Transactions on Signal Processing*, 56(7):3315–3326, 2008.

Chapter 4

Interactional dynamics of same-sex marriage legislation in the United States

The contents of this chapter have appeared in Royal Society Open Science 4 (6), 170130.

4.1 Abstract

Understanding how people form opinions and make decisions is a complex phenomenon that depends on both personal practices and interactions. Recent availability of real-world data has enabled quantitative analysis of opinion formation, which illuminates phenomena that impact physical and social sciences. Public policies exemplify complex opinion formation spanning individual and population scales, and a timely example is the legalization of same-sex marriage in the United States. Here, we seek to understand how this issue captures the relationship between state laws and Senate representatives subject to geographic and ideological factors. Using distance-based correlations, we study how physical proximity and state-government ideology may be used to extract patterns in state-law adoption and senatorial support of same-sex marriage. Results demonstrate that proximal states have similar opinion dynamics in both state-laws and senators' opinions, and states with similar state-government ideology have analogous senators' opinions. Moreover, senators' opinions drive state-laws with a time lag. Thus, change in opinion not only results from negotiations among individuals, but also reflects inherent spatial and political similarities and temporal delays. We build a social impact model of state-law adoption in light of these results, which predicts the evolution of state-laws legalizing same-sex marriage over the last three decades.

4.2 Introduction

No issue in the United States has demonstrated the complex interaction between political and social life like same-sex marriage. June 26, 2015 was a historic moment when the United States became one of 22 countries to legalize same-sex marriage across the 50 states. The decision was made by the Supreme Court, and prior to that, there were 37 states to legalize same-sex marriage independently [1]. Among these 37 states, same-sex marriage was legalized in 26 states by court decisions, in eight states by state legislature, and in three states by popular vote. Clearly, the courts played an important role in the process of legalization of same-sex marriage. The opinion of the senators on this issue has also shifted to support over years. The first polling vote among the senators was on Sep 10, 1996, where the topic was to introduce Defense of Marriage Act (DOMA), which defines marriage as the union between one man and one woman and to prohibit same-sex marriage. A total of 14 senators among 100 were against DOMA, however only four supported same-sex marriage. Since then, the opinion of the senators on this issue has evolved, and in 2014 there were 57 senators who were in support of same-sex marriage. State legislatures, popular vote, and the courts have made remarkable changes over the past two decades in laws defining whether marriage is limited to relationships between a man and a woman or may be extended to same-sex couples.

The public support for gay rights has also increased over the years[2, 3, 4]. A Gallup Poll demonstrates this shift [5]. For instance in 1996, 68% of individuals in the United States opted to vote against the legalization of same-sex marriage, whereas in 2016, 61% of individuals opted to vote in favor of legalization of same-sex marriage. Religious affiliations have substantially influenced the increasing public support for same-sex couples, as demonstrated in a study of data until 2010[2]. However, political affiliation has stronger influence (almost five times more) as compared to the religious affiliations [2]. The major shift in opinions among individuals has been attributed to increased interaction with same-sex couples via interpersonal[6, 7, 8, 9] or parasocial contacts[10, 11]. Recent support is also due to younger people favoring legalization of same-sex marriage compared to older generations[12].

Although significant studies have been done to determine the factors that play important roles in the increasing public support, research on the evolution of senators' opinions, state-law on the issue of same-sex marriage, and the relationships between these two indicators of public opinion is limited. A first study on the diffusive process underlying senators shifting from opposing to supporting same-sex marriage can be found in [13], but only a limited data set is considered and the roles of the individual factors mitigating the diffusion of opinions are not isolated. Specifically, this study calculates a likelihood for senators in 2013 to change their opinions based on personal characteristics (e.g. political party, re-election status), home state voting history and laws (e.g. previous presidential election results, state-wide legalization of same-sex marriage), interactions with other senators (e.g. the number of senators who announce support for same-sex marriage that year), and political climate (e.g. announcements by the president and US Supreme Court)[13]. Here, we explore the opinion

formation of senators and state-law as they evolve over 19 years preceding the national legalization of same-sex marriage and attempt to identify factors mitigating interactions between senators and states that may have affected the dynamics. In other words, we neglect individual variations among senators and states and seek to define interaction patterns that best describe the observed opinion dynamics.

Interactions between agents drive opinion dynamics in real-world scenarios, which have been studied from both modeling and data-based perspectives. In the literature, a variety of mathematical models have been proposed to study opinion formation in a social group. These mathematical models incorporate protocols motivated from real-world phenomena, and are important to understand the dynamics of opinion formation and for their predictive power. A review of such mathematical models can be found in [14]. For example, the "voter model" [15, 16, 17, 18] represents the voters and their interactions as nodes and edges, respectively, in a network and the conditions to reach consensus are studied. Other well studied models include the "majority rule model", [19, 20, 21] where the agents share binary opinions and group decision is determined by the position of the majority; the "compromise model", [22] where the agents interact randomly in a pairwise manner, and update if their opinions are within a given threshold; the "Deffuant model", [23] where the agents share continuous, rather than discrete binary, opinions and interactions occur if two agents' opinions are sufficiently close to each other; the "Sznajd model", [24] which assumes that the opinion of an agent is driven by the opinions of its neighbors; and the "social impact model", [25, 26] which is based on a psychological theory that considers the influence of the group size, their convincing power, and the distance from a target opinion. Here, distance can refer to either physical (spatial proximity) or psychological metrics (closeness in terms of personal opinion).

In addition to the theoretical exploration of these mathematical models, the recent availability of large datasets has motivated the empirical analysis of opinion dynamics based on the real-world phenomenon, for example, Indian [27] and Brazilian elections [28]. To study the Brazilian election results, a network-based model is applied along with the assumption of the Sznajd model, in the sense that a small group of individuals influences the opinion of their nearest neighbors if and only if they share common opinions among themselves. The model shows a good agreement with the observed voter distribution from the Brazilian elections dataset [29]. Furthermore, a prospective experiment has been performed to demonstrate that opinion formation among individuals is subject to social influences[30]; for example, when an individual lacks knowledge, the more susceptible she is to seek information from others to update her beliefs. Similarly, in an online experiment [31], three main types of individuals are identified based on opinion update processes, namely stubborn individuals (who do not change their opinions), compromising individuals (who negotiate with their neighbors' opinions), and conforming individuals (who ignore their own opinion and take on opinions of their neighbors). For group-level behavior, a study of synchronized clapping in a concert hall uses a "random field Ising model" to find that the emergence of collective behavior is induced by a combination of imitation and social pressure [32]. Opinion formation using different kinetic models is further studied in [33], where using the presidential election results in the

state of Arizona it has been shown that the citizens tend to live in neighborhood with similar political belief. The above mentioned real-world examples suggest that opinion formation at the individual and group level is the result of a complex negotiation based on multiple social factors. Public policies are perfect examples of such complex opinion formation that aggregates interactions across multiple social scales. Consequently, we target the timely issue of same-sex marriage in the United States to provide evidence that the geographical and ideological similarities are significant contributors to the senators' opinions and the state-law adoption.

In the present work, we study the issue of same-sex marriage from data on state-law adoption and senatorial support from 1996 to 2014. We perform a correlational analysis to capture interdependence between these data and factors that may mitigate opinion dynamics. We hypothesize that two external factors impact the dynamics of the state-law and the senators' opinions, namely topological distances between the states, which capture the influence of geographic proximity, and state-government ideology, which condenses beliefs driving social and political policy. We investigate the effect of these factors on both the state-law and the senators' opinions using distance-based correlations. Distance-based correlation, as defined in Gallos et al. [34], has been an effective tool to unfold the topological dependencies of real-world phenomena, for example, the spread of obesity [34], cascading failures [35], motor vehicle deaths [36], and traffic percolation [37]. Defining distance in terms of topology and ideology, we anticipate that both the state-law, and the senators from states that are topologically closer exhibit comparable trends. On the other hand, we expect that the senators sharing similar ideology display comparable patterns, while sorting states by ideology may provide weaker correlation among their laws. Drawing on the results of the data-based analysis, we model the evolution of state-law using a distance-based social impact model, with which we seek to identify when states switch from banning to legalizing same-sex marriage. The present study seeks to uncover and model this real-world phenomenon and has two-fold contributions. First, we unravel the components that may have affected the opinion dynamics, and second, we build a protocol which captures these driving factors, and verify its predictive power with the real-world dataset. The two-way approach of the problem not only identifies the presence of driving factors, but also validates the dynamics in a predictive model.

4.3 Results and Discussion

State-law and senators' opinions

State-law and senators opinions reflect the position of the individual states and the senators, respectively, on the issue of same-sex marriage which we categorize as "support", "oppose" or "ambiguous" for the senators, and "legal", "ban" or "neither legal nor ban" for the state-law. The definition of these terms and the methods for data collection are further

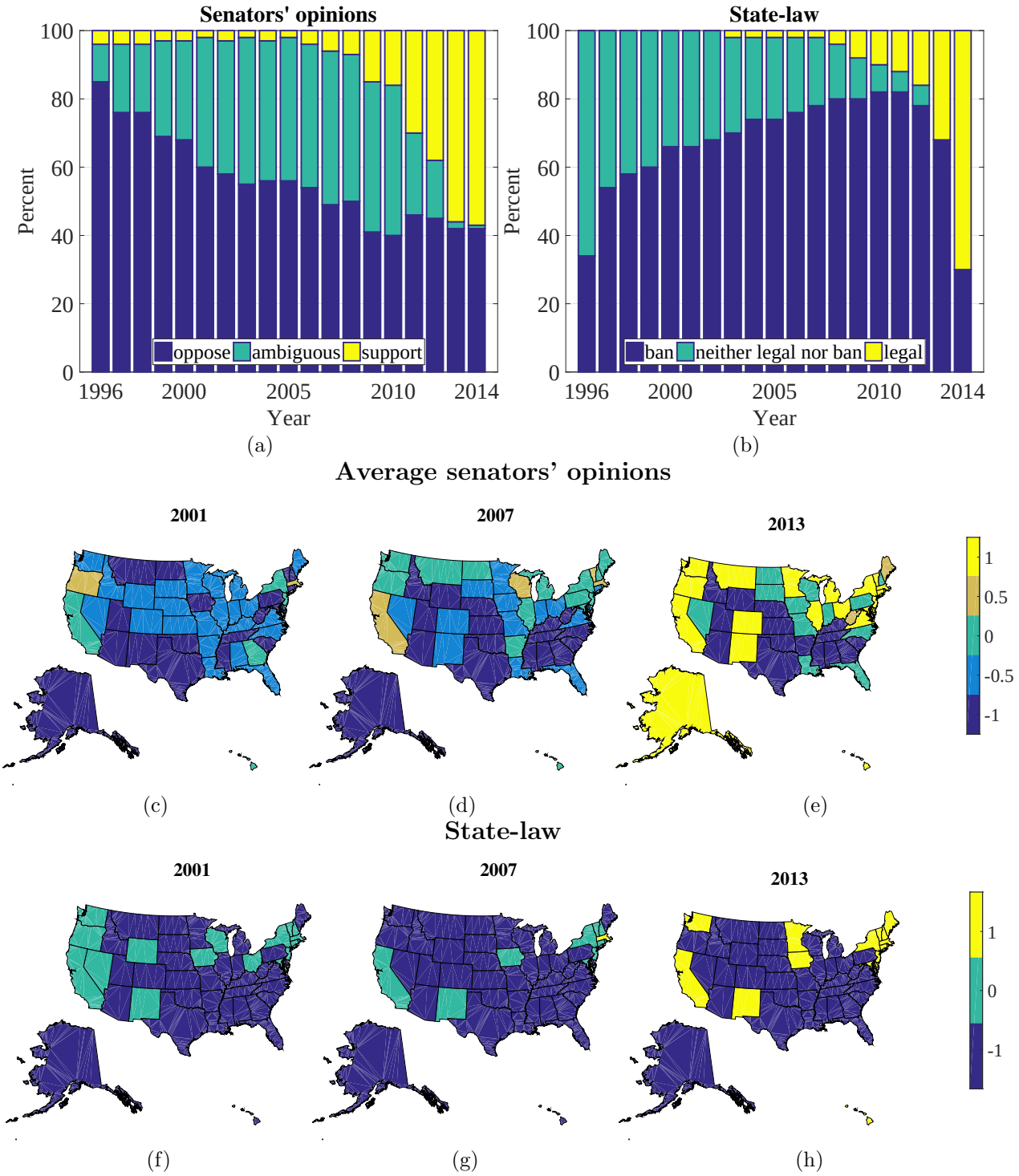

Figure 4.1: Distribution of (a) senators' opinions and (b) state-law on the issue of same-sex marriage over time. (c)-(h) Snapshots of the data for three representative years, 2001, 2007, and 2013 with showing (c)-(e) average senators' opinions and (g)-(h) state-law. Both the bar plots and the maps are created using MATLAB, version R2016a (https://www.mathworks.com/).

elaborated in the Method section. We assign values for the state-law of state i for year t as $x_{\text{state}}(i,t) \in \{-1,0,1\}$ if state i has legalized ($x_{\text{state}} = 1$), banned ($x_{\text{state}} = -1$) or neither legalized nor banned ($x_{\text{state}} = 0$) same-sex marriage. Similarly, we assign values to the senators' opinions for each year from 1996 to 2014 as $1, -1$ or 0 if the particular senator supports, opposes or is ambiguous on the issue of same-sex marriage. Averaging the opinions of the two senators representing each state where each senator can assume values from $\{-1,0,1\}$, we define $x_{\text{sen}}(i,t) \in \{-1,-0.5,0,0.5,1\}$ as the average senators' opinions for state i in year t.

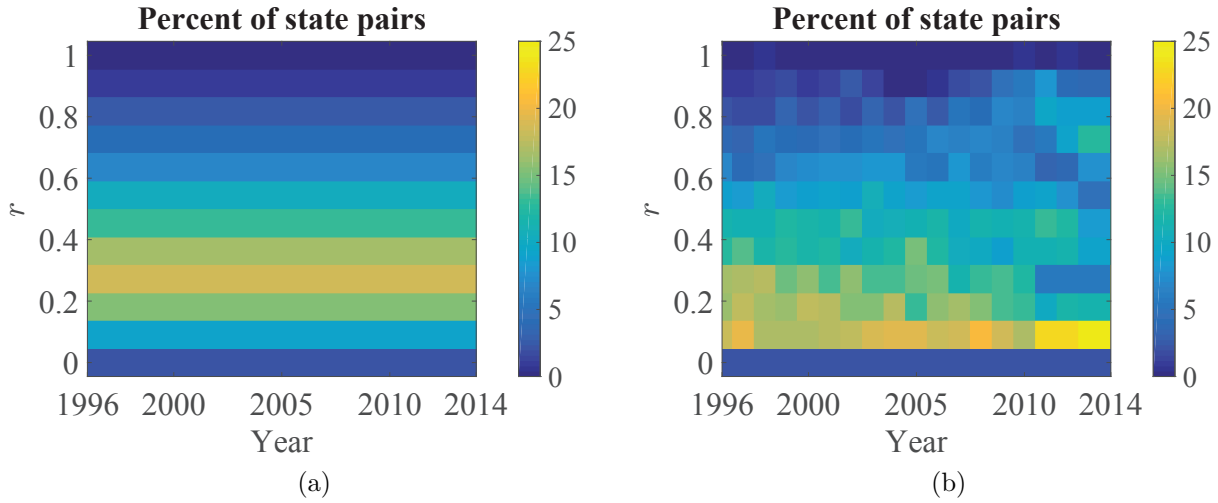

Figure 4.2: Percentage of state pairs that are separated at a given distance, r, computed based on (a) topological distance and (b) ideological distance from the year 1996 to 2014.

The data are shown in Figures 4.1a and 4.1b, where we present the distribution of state-law and senators' opinions over time, and in Figures 4.1c to 4.1h, where we present snapshots of the data for three representative years, namely 2001, 2007, and 2013. We observe in Figure 4.1a that ambiguity among the senators first grows from opposing same-sex marriage, and then converts to support in recent years. However, Figure 4.1b shows that strong laws emerge monotonically over time either in support of or banning same-sex marriage. Comparing Figure 4.1a and 4.1b, we see that support among the senators initiated earlier than the state-laws to admit same-sex marriage.

Distance-based correlation

Following from Gallos et al. [34], we compute a distance-based correlation function to quantify the influences of two distance metrics on the senators' opinions and the state-law. The two distance metrics are defined in terms of the geographic topology and state-government

ideology. For the topological distance, the states are considered as nodes in a network and pairs of states sharing physical boundaries are linked by an edge. Then the topological distance between a pair of states is defined as the shortest path between them over this network. Based on the geography of the United States, the maximum distance obtained between a pair of states is found to be 11, which we use to normalize all topological distances r between 0 and 1. The percentage of the state pairs that are separated at a topological distance r is presented in Figure 4.2a.

The ideological distance is defined as a metric in $[0, 100]$ based on state-government ideology from the database in [38], which is further described in the Methods section. The normalized ideological distances are combined in twelve equally spaced bins between 0 and 1 to allow comparison with topological distances and are presented in Figure 4.2b. Since the topological distance is fixed, the percentage of state pairs separated at a given distance is constant over time, whereas the ideology being dynamic has percentages that change over time. Selecting either topology or ideology to set the normalized distance $r \in [0, 1]$, we define the distance-based correlation function $C(r)$ introduced in [34] as

$$C(r,t) = \frac{1}{\sigma(t)^2} \frac{\sum_{i,j=1}^{N} (x_*(i,t) - \bar{x}_*(t))(x_*(j,t) - \bar{x}_*(t))\delta(r_{ij}, r)}{\sum_{i,j=1}^{N} \delta(r_{ij}, r)}, \tag{4.1}$$

where N is the number of states used in the analysis, x_* is either x_{state} or x_{sen}, $\bar{x}_*$ and σ^2 are the mean and variance of x_* over all states in a given year, r_{ij} is the measured distance between state i and state j in terms of either ideology or topology, and the function δ is the Kronecker delta that selects states at distance r as set by the argument of the function C. It is worth mentioning that r_{ij} is constant for all years when topological distances are considered; however its value changes in the case of ideological distances. Similar to the commonly-used Pearson correlation coefficient, large values of $C(r)$ denote strong correlation among states separated by a distance of r, and values close to zero denote weak correlation among these states. Also, positive values of $C(r)$ imply positive correlations, while negative values indicate negative correlations. Figure 4.3 shows the distance-based correlation coefficients for state-law and average senators' opinions computed using topological and ideological distances.

When distance is defined in terms of geography, pairs of states and senators separated by short distances show positive correlations, with more pronounced correlations for state-laws than senators' opinions. In Figure 4.3a and 4.3b, we observe that both the state-law and the average senators' opinions display positive correlations at $r = 0.1$ and $r = 0.2$. Moreover, the small-distance positive correlations generally increase in time, initiating earlier in the state-law than the average senators' opinions. In addition, state-laws show stronger correlations than senators as time increases. Hence, nearby state pairs are more similar both with respect to state-law and average senators' opinions in recent years. However, correlations decrease as the topological distance increases in both cases, and goes to zero at about $r = 0.4$ for the state-law, and at $r = 0.3$ for the average senators' opinions. At $r > 0.5$ we observe long-distance negative correlations in both cases, however these

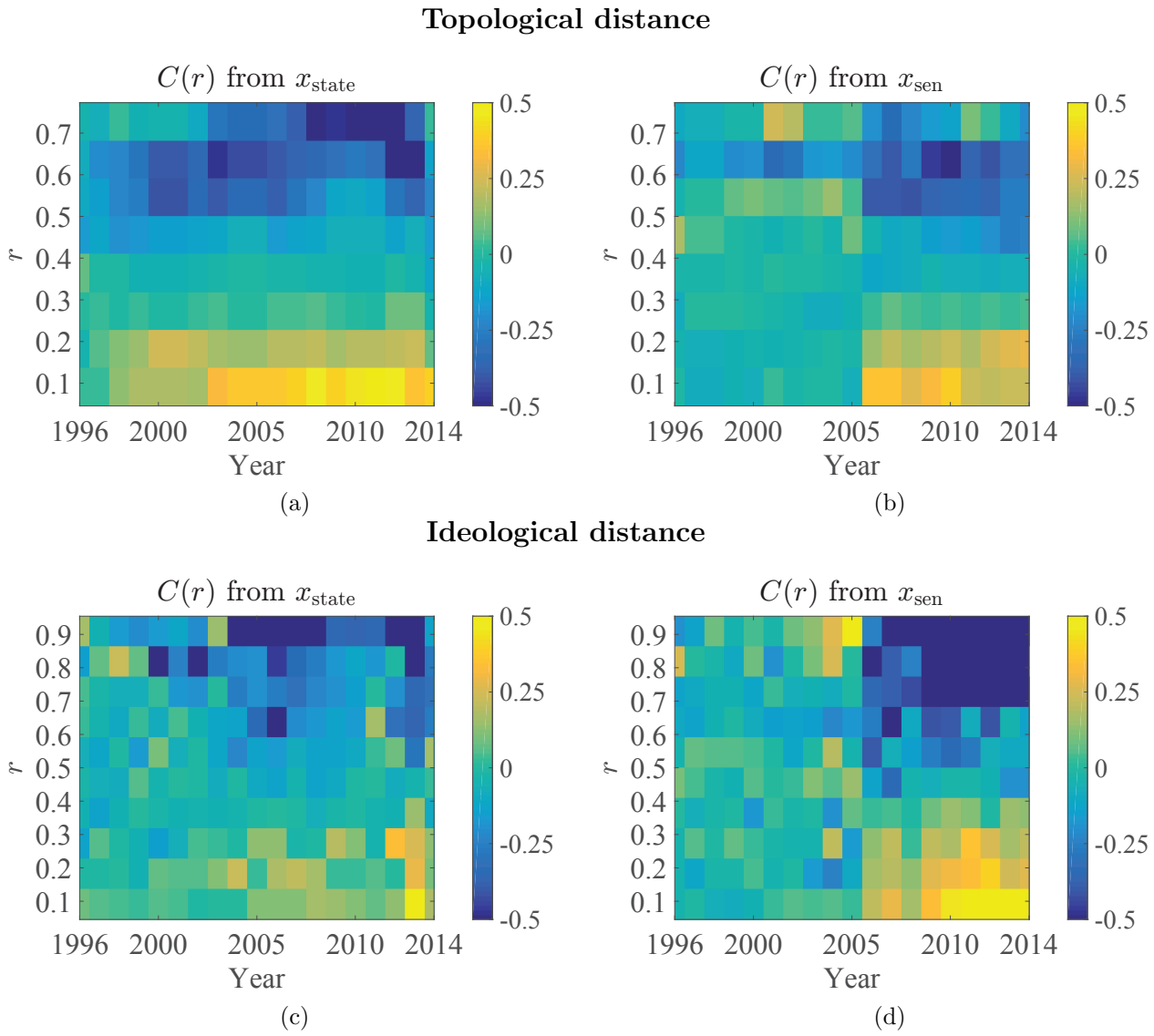

Figure 4.3: Distance-based correlation for (a) state-law and (b) average senators' opinions computed using topological distances with r varying from 0 to 0.7. Distance-based correlation for (c) state-law and (d) average senators' opinions computed using ideological distances with r varying from 0 to 0.9.

are more pronounced in the state-law in recent years. We note that r is varied from 0.1 to 0.7 since number of state pairs which are topologically distant from each other at $r > 0.7$ is very small, see Figure 4.2a. Specifically, less than 8.16% of state pairs are separated by distances greater than $r = 0.7$. These results suggest that the impact of the physically proximal states is evident in both state-law and senator's opinions, but is more pronounced in state-law.

When distance is defined in terms of ideology, pairs of states and senators separated by short distances show no positive correlations except for senators in recent years; long-distance pairs show negative correlations in both cases. Figure 4.3c shows that the state-law for the states with similar ideology display correlation near zero. However, small-distance positive correlation is strong for average senators' opinions in the year range 2007 to 2014 as seen in Figure 4.3d. In the same year range, we also observe long-distance negative correlation among the senators who are ideologically far from each other. It is note-worthy that this negative correlation should not be neglected since number of state-pairs that are ideologically distant are not trivial as seen in Figure 4.2b (20.88% of state pairs averaged over years 2008 to 2014 are separated by distances greater than $r = 0.7$). These results indicate that state-government ideology has a significant influence on the opinion of the senators in recent years. In particular, the senators who are ideologically close hold similar opinions on same-sex marriage, whereas those are ideologically distant have different view-points. This long-distance negative correlation has also been captured to some extent in the state-law and starting earlier (starting from year 2000) than that of the average senators' opinion.

To summarize, we observe recent polarization in the state-law when topological distances are used (Figure 4.3a), and in the average senators' opinions when ideological distances are used (Figure 4.3d). Additionally comparing Figures 4.3a and 4.3d, polarization is more extreme in the average senators' opinions with ideological distances.

Control experiment

To further verify the results in terms of the correct identification of the factors, we randomly permute the values for the time series of both the state-law and the senators' opinions within each year. This ensures that the mean and standard deviations used in equation (4.1) are maintained, but the individual state and senator dynamics are scrambled. We compute the distance-based correlation $C(r, t)$ of the scrambled data considering both topological and ideological distances.

The observed effects for state-laws and senators' opinions result from interactions, rather than an average change in support or legalization. The results as shown in Figure 4.4 demonstrate that the distance-based correlation converges to zero immediately from $r = 0.1$ for both state-laws and senators' opinions using ideological and topological distances. This verifies that $C(r, t)$ captures individual and interactional dynamics beyond a mere increase in overall percentage support for same-sex marriage. This

suggests that topological and ideological factors provide an explanation for the previously observed correlations.

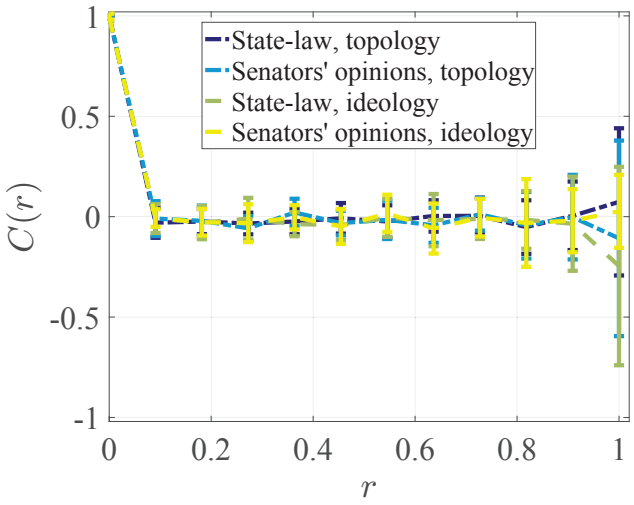

Figure 4.4: Mean distance-based correlation values for randomly permuted state-law and senators' opinions with respect to the states using both topological and ideological distances. Points indicate the mean value and error bars denote one standard deviation over the entire year range.

Mutual dependence of the state-law and the average senators' opinions

To study the interdependence of the state-law and the average senators' opinions, we compute the cross-correlation of the two time series after lagging them in time. Other existing tools that can be used to detect the interdependence include transfer entropy[39, 40, 41] and event synchronization[42]. However, we choose cross-correlation as it has been used to detect the directionality of opinion flow in a real-world phenomenon[43]. For this analysis, we concatenate the time series of either state-law or the average senators' opinions from each state to build an amalgamated dataset. For example, to build the one-year lagged time series of the state-law from the year 1996 to 2013, we first delete the values of all the fifty states of the year 2014, then we concatenate the time series of each state in succession, starting from Alabama ending with Wyoming. It is important to note that here we include Alaska and Hawaii, as the cross-correlation analysis is independent of whether or not states share boundaries with each other. In a similar fashion, we build the dataset for the average senators' opinions. To compare one-year lagged state-law with unlagged average senators' opinions, we compute the Pearson correlation coefficient R of the state-law from 1996 to 2013

with that of the average senators' opinions from year 1997 to 2014 for all the fifty states. This process is repeated for lags of 5 years on both the states and senators.

State-laws show maximum correlation with senators' opinions lagged in time, suggesting that opinions flow from senators' opinions to state-laws. Figure 4.5 presents the correlation coefficient for the two time-series, when compared with different year ranges. Interestingly, the correlation coefficient is maximum when state-law time-series, chosen from 1997 to 2014, is compared with the average senators' opinions time-series, chosen from 1996 to 2013. In other words, the state-law time-series shows maximum dependence on the time-series of the average senators' opinions with a difference of a year when the state-law is allowed to follow the senators' opinions. A summary of results is shown in Figure 4.6, which shows the correlation values for lags of one year, two years and without any lag. For the unlagged version, a two-way directed arrow is used to represent the mutual dependencies on each other, whereas for the lagged version one-way directed arrow is used to show the influence of the past values of either state-law or average senators' opinions on that of the present values.

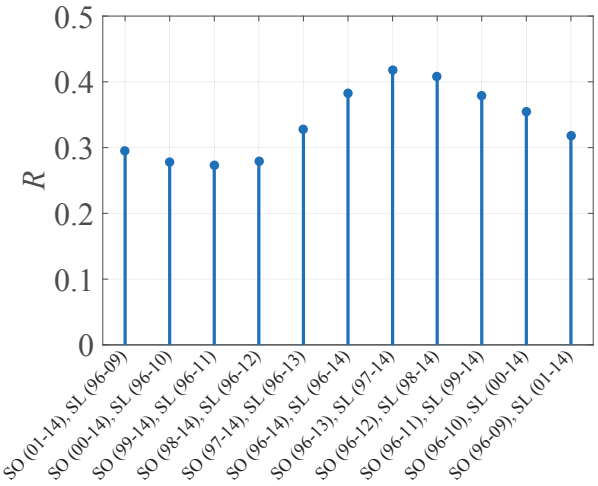

Figure 4.5: Correlation coefficient of the lagged time-series of the average senators' opinions and the state-law. The horizontal axis denotes the two time-series that are compared; "SO" stands for average senators' opinions, "SL" stands for state-law, and the time ranges of the two times series is in the parentheses.

Social impact model

From the dataset, we observe that the state-law and the average senators' opinions are both dependent on the topological distances, average senators' opinions are dependent on

the ideological distances, and the state-law shows maximum dependence on the average senators' opinions from one year prior. Hence, we seek to model the state-law as it varies with both the topological distances and the average senators' opinions. We select a distance-based opinion dynamics model drawing on impact theory[26] to study the dynamics of the state-law in terms of initiation of legislation legalizing same-sex marriage. With this motive, we classify the state-law in two groups as "legalized" and "not-legalized" same-sex marriage thus eliminating the possibility of ambiguity used in the previous analyses.

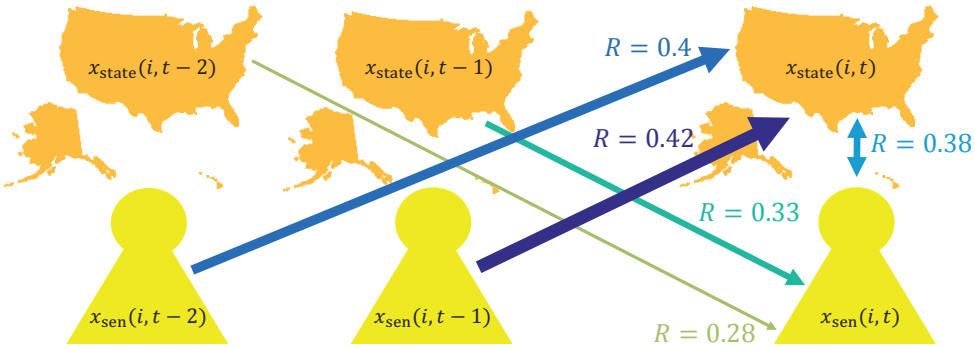

Figure 4.6: Schematic representation demonstrating the correlation coefficients for state-laws and senators' opinions with lags of one year, two years and without any lag. The correlation coefficient is maximum when one-year lagged average senators' opinions (from the year 1996 to 2013) are compared to state-law (from the year 1997 to 2014),with a value of $R = 0.42$. Maps are created using MATLAB, version R2016a (https://www.mathworks.com/).

In the model, state i in year t assumes binary opinions $\hat{x}_{\text{state}}(i,t) = \{-1, 1\}$, which correspond to states where same-sex marriage is legalized ($\hat{x}_{\text{state}} = 1$) or not legalized ($\hat{x}_{\text{state}} = -1$). To capture the social pressure that state i experiences from all other states in year t, we define the impact $I(i,t)$ given by

$$I(i,t) = \left[\sum_{j=1}^{N} \frac{1}{{r_{ij}}^{\alpha}}(1 - \hat{x}_{\text{state}}(i,t)\hat{x}_{\text{state}}(j,t))\right] - \left[\sum_{j=1}^{N} \frac{1}{{r_{ij}}^{\alpha}}(1 + \hat{x}_{\text{state}}(i,t)\hat{x}_{\text{state}}(j,t))\right], \quad (4.2)$$

where $N = 48$ is the number of states used in the model (omitting Hawaii and Alaska because they do not share physical borders with any other states), and α is a constant exponent that indicates how fast the impact decreases with the pairwise state distances r_{ij}. In our model, we choose r_{ij} as the topological distances that have been used in the distance-based correlation analysis, which has been shown to influence state-law. Note that the first sum in equation (4.2) denotes a persuasive impact from the states who hold opposite opinions than state i, and the second sum denotes a supportive impact from the states who share the same opinions. By definition, positive impact $I(i,t) > 0$ signifies a pressure in favor of opinion change for state i. The opinion then updates as follows,

$$\hat{x}_{\text{state}}(i, t+1) = -\text{sign}\left[\hat{x}_{\text{state}}(i,t)I(i,t) + wx_{\text{sen}}(i,t)\right]. \quad (4.3)$$

In the traditional social impact model, the second summand in the argument of the sign function is reserved for a random variable representing noise. However, we use the average senators' opinions here based on the relationship between senators and states evidenced by the time-lagged correlations.

We use this model to capture the dynamics of the state-law by identifying the states that initiate legalization of same-sex marriage, with the two factors (topological distance and a year-lag average senators' opinions) provided as the input parameters. To make the dataset consistent with the model parameters for comparison of results, we replace the zero values of x_{state} with negative ones in order to convert the data to binary values. We choose the initial condition for $\hat{x}_{\text{state}}$ as the state-law for N states for the year 1996, and allow it to update for the next year following equations (4.2) and (4.3). We simulate the model for 18 years, that is, until the end of year 2014. The free parameters, α and weight w, are tuned to fit the model to the dataset by allowing α to vary from 0 to 10 with an increment of 0.05, and w to vary from -20 to 0 with an increment of 0.05. We compare the $\hat{x}_{\text{state}}$ values with the binary state-law data for all states and for all years using root mean square error to quantify the error. The optimal range of the parameter values correspond to values that minimizes the error.

To study the dependence of the root mean square error on w and α, we compute the contour plot in Figure 4.7a. Root mean square error value equal to 0.585 corresponds to the case when the $\hat{x}_{\text{state}}$ values are all equal to -1 for all years and for all states which is considered as a control condition. In other words, the control condition is that $\hat{x}_{\text{state}}$ values remain the same as the initial condition and never change. This condition sustains at positive values of w, whereas only the negative values allow $\hat{x}_{\text{state}}$ to switch in equation (4.3), and initiate the legalization. To understand parameter values that give systems with less error than this control condition, the value 0.585 is set as a ceiling for the root mean square error. Figure 4.7a demonstrates the domain of the parameter values that result in improved error, with the root mean square error value equal to 0.585 are omitted and are set to white on the plot. The minimum value of the root mean square error obtained is equal to 0.468. Corresponding to this minimum value we get three configurations of $\hat{x}_{\text{state}}$ denoted by type I, type II and type III as shown in Figure 4.7a with diamond, squares and circles, respectively. In Figure 4.7b, we plot the $\hat{x}_{\text{state}}$ values for type II configuration with $\alpha = 2.35$, and $w = -17.8$, and compare it with the state-law and the average senators' opinions.

In Figure 4.7b, we observe that the update protocol (4.2) and (4.3) identifies states that shift from banning to legalizing same-sex marriage in the dataset. The model identifies 23 states that switch to legalizing same-sex marriage in the end of 19 years in comparison to 33 states with respect to the state-law data at the end of year 2014. However, there are 2 false positives, namely in states 20 (Michigan), and 33 (Ohio). This means that there are 12 states that the update protocol fails to identify, but of these, 11 states have switched from banning to legalizing same-sex marriage in 2014. We comment that the failure in identification of the 12 states may be because the protocol in few states identifies the switch with an inherent lag. Overall, this simple model is capable of capturing the complex dynamics of the state-law

adoption based on two input parameters, namely the topological distance and a year-lag average senators' opinions, which we have determined to be the driving factors from the correlation analysis. Nevertheless, the physical significance of the optimal α and w values is as yet unclear.

Table 4.1: Sensitivity and specificity values for type I, II, and III configurations from 1996 to 2014.

Year	1996-2002	2003-2007	2008	2009	2010	2011	2012	2013	2014
Sensitivity (Type I)	NA	0	0	0	0.60	0.83	0.88	0.87	0.64
Specificity (Type I)	1	1	0.98	0.96	0.91	0.9	0.85	0.94	0.87
Sensitivity (Type II)	NA	0	0	0.50	0.60	0.83	0.88	0.87	0.64
Specificity (Type II)	1	1	0.98	0.96	0.91	0.88	0.83	0.94	0.87
Sensitivity (Type III)	NA	0	0	0	0.20	0.33	0.50	0.67	0.40
Specificity (Type III)	1	1	1	1	1	1	0.98	0.97	1

To quantify the performance of the model by comparing all three optimal configurations over all years, we use sensitivity and specificity measures [44]. Sensitivity is defined as the ratio of the number of states legalizing same-sex marriage that the model correctly identifies (true positives) and the total number of states that legalize same-sex marriage from the dataset in a specific year. On the other hand, specificity is defined as the ratio of the number of states not-legalizing same-sex marriage that the model correctly identifies (true negatives) and the total number of states that do not legalize same-sex marriage from the dataset in a specific year. Sensitivity and specificity measure the true positive rate and true negative rate, respectively, scaled between zero to one, where the value one corresponds to a perfect predictor model. The results are summarized in Table 4.1. Note that the first state to legalize same-sex marriage was in 2003, hence we do not have sensitivity values in prior years. Comparing the sensitivity values corresponding to each year, we see that type I and II perform similarly for all years, except in 2009, where sensitivity for type II is 0.5 in comparison to a value zero for type I. The sensitivity values for type I and II increase over years, and are greater than 0.8 in the year range 2011 to 2013 denoting a reasonably good performance in identifying the true positives. However for type III, sensitivity values are small in 2010 and 2011, and gradually increase over years. For each type, we observe that the specificity values are greater than 0.8, in particular type III has values close to one for all years. In other words, type III is almost perfect in identifying the true negatives. Note that in each type, sensitivity values decrease in 2014, since there were 18 states that actually legalized same-sex marriage in comparison to a total of 15 states in the end of 2013. Synthesizing these results, we can see that, while opinion formation is more complex in reality and certainly has random components, this simple update protocol works well in predicting the states that switch from banning to legalizing same-sex marriage.

We directly compare the simulation results and with the data in Figure 4.7b, where we also add the average senators' opinions. These results show that the inclusion of the average

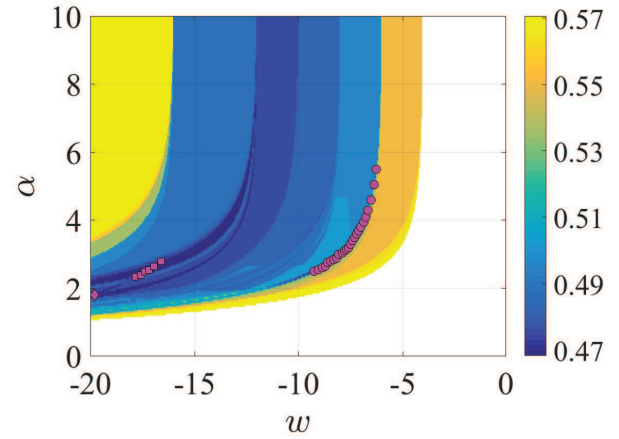

(a)

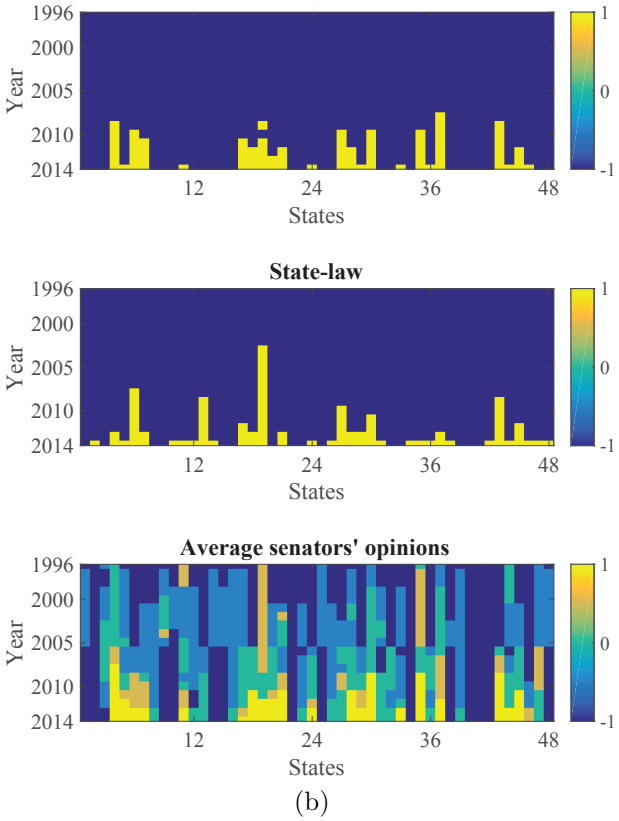

(b)

Figure 4.7: (a) Contour plot of root mean square error between model generated and state-law data, with weight w and α varying. Diamond (type I), squares (type II) and circles (type III) correspond to the minimum of the root mean square error equal to 0.468. (b) For comparison, $\hat{x}_{\text{state}}$ of type II, state-law and the average senators' opinions are plotted for all years and states.

senators' opinions in our update protocol does not solely govern the $\hat{x}_{\text{state}}$ values. We observe noticeable discrepancies between the $\hat{x}_{\text{state}}$ values and the average senators' opinions, confirming the result is driven by both the distance-based measure of the state-law and the average senators' opinions.

4.4 Conclusion

The present study supports the hypothesis that the physical proximity has a strong influence on both the state-law and the senators' opinions, whereby the states and the senators that are close in terms of geography tend to have similar state-law and senators opinions, respectively, whereas the states that are far tend to have different state-law. In addition to the physical proximity, the state-government ideology is also found to be a predictor of the senators' opinions, since the senators who share close ideology had similar opinions and the senators who are ideologically distant had opposite opinions. The effect of state-government ideology on the state-law is observed in terms of long-distance negative correlation, specifically that the state-law in the states that are ideologically far have different state-laws. However, states with similar ideologies do not have similar laws. All these results are more pronounced in recent years. In addition, the analysis reveals that the state-law shows maximum dependence on the senators' opinions from one year prior. A distance-based social impact model is able to capture the evolution of the state-laws and shows a good predictive power in terms of correctly identifying the states that switch from banning to legalizing the same-sex marriage. To summarize, we understand public policy adoption is generally complex and depends on a variety of external factors. In our present study, we target same-sex marriage to identify these factors, which in future may be considered to understand or model other public policies that propagate via social and political change.

4.5 Methods

Here, we explain in detail how we build the dataset for the senators' opinions and the state-law. There are two senators representing each state and, when combined for 50 states, there are 100 senators nationally. The senators may be reassigned at least every four years through the election process. For each year from 1996 to 2014, we assign values $1, -1$ or 0 to each of these senators if the particular senator supports, opposes, or is ambiguous, respectively, on the issue of same-sex marriage in that year. A particular senator is said to be ambiguous if he/she neither support nor oppose same-sex marriage. We only consider the senators during their period of tenure, and after that we consider the opinion of the new senator, modifying the opinion value accordingly. We choose 26th of December of each year to log the opinion of the senators for that specific year, regardless of whether a senator is reassigned within the year. The data are collected from the list of supporters of same-

sex marriage from different sources (for example, personal candidate/senator websites, news media, and Wikipedia) and each supporter is identified with the first mention of support, opposition, or ambiguity publicly on this issue. If a particular senator is identified as a supporter, then for all successive years the senator is considered as a supporter until the end of his or her tenure. We rely on the available data over the internet on news and senators' websites to build the dataset.

The data for the state-law on the issue of same-sex marriage across 50 states are collected from internet sources. Similar to senators' opinions we assign values for state-law as $1, -1$ or 0 if that particular state has legalized, banned, or neither banned nor legalized same-sex marriage, respectively.

We define distances between states based on two measures: a topological measure, which is based on the geography of state borders, and an ideological measure, based on the political ideology of state officials. The topological data used in the present study is based on building a network where states are vertices and the states sharing a common physical boundary are linked with an edge. Shortest paths over this network define topological distances between state pairs. We exclude Alaska and Hawaii from the distance-based correlation analysis using topological distance since neither share physical boundaries with the remaining states.

The state-government ideology data that we use in our present study is created by William Berry et al. [45]. The data is updated through 2013, and can be found in [38]. We use the ADA/COPE measure of state-government ideology for our study. For the year 2014, we use the state-government ideology same as that of 2013. The state-government ideology data measures the mean position of the elected public officials in a state on a liberal-conservative continuum, weighted based on the power they have over public policy decisions. The score ranges from zero, representing the most conservative value, to one hundred, representing the most liberal position. Similar to topological distances, we normalize the score between zero and one for the ideological distances. Note that we exclude Alaska and Hawaii in our study where we use topological distance, particularly in the distance-based correlation analysis and in the model, because it is defined based on whether states share physical boundaries or not. However, we retain these two states in cross-correlation analysis and in the distance-based correlation analysis using ideological distance, which is independent of this fact. The numerical analysis is performed using MATLAB, version R2016a.

4.6 References

[1] State-by-state history of banning and legalizing gay marriage, 1994-2015. Available at http://gaymarriage.procon.org/view.resource.php?resourceID=004857.

[2] Dawn Michelle Baunach. Changing same-sex marriage attitudes in America from 1988 through 2010. *Public Opinion Quarterly*, 76(2):364–378, 2012.

[3] Paul R Brewer. *Value war: Public opinion and the politics of gay rights*. Rowman & Littlefield Publishers, 2007.

[4] Jeni Loftus. America's liberalization in attitudes toward homosexuality, 1973 to 1998. *American Sociological Review*, pages 762–782, 2001.

[5] Gay and lesbian rights. Available at http://www.gallup.com/poll/1651/gay-lesbian-rights.aspx.

[6] Jeremiah J Garretson. Exposure to the lives of lesbians and gays and the origin of young people's greater support for gay rights. *International Journal of Public Opinion Research*, 27(2):277–288, 2015.

[7] Bob Altemeyer. Changes in attitudes toward homosexuals. *Journal of Homosexuality*, 42(2):63–75, 2002.

[8] Joshua J Dyck and Shanna Pearson-Merkowitz. To know you is not necessarily to love you: The partisan mediators of intergroup contact. *Political Behavior*, 36(3):553–580, 2014.

[9] Sue Ann Skipworth, Andrew Garner, and Bryan J Dettrey. Limitations of the contact hypothesis: Heterogeneity in the contact effect on attitudes toward gay rights. *Politics & Policy*, 38(5):887–906, 2010.

[10] Edward Schiappa, Peter B Gregg, and Dean E Hewes. Can One TV Show Make a Difference? a Will & Grace and the Parasocial Contact Hypothesis. *Journal of Homosexuality*, 51(4):15–37, 2006.

[11] Edmon W Tucker and Miriam Potocky-Tripodi. Changing heterosexuals' attitudes toward homosexuals: A systematic review of the empirical literature. *Research on Social Work Practice*, 16(2):176–190, 2006.

[12] Alison Keleher and Eric Ran Smith. Growing support for gay and lesbian equality since 1990. *Journal of Homosexuality*, 59(9):1307–1326, 2012.

[13] Sean M Theriault and Herschel F Thomas. The diffusion of support for same-sex marriage in the US Senate. *PS: Political Science & Politics*, 47(04):824–828, 2014.

[14] Claudio Castellano, Santo Fortunato, and Vittorio Loreto. Statistical physics of social dynamics. *Reviews of Modern Physics*, 81(2):591, 2009.

[15] Peter Clifford and Aidan Sudbury. A model for spatial conflict. *Biometrika*, 60(3):581–588, 1973.

[16] Richard A Holley and Thomas M Liggett. Ergodic theorems for weakly interacting infinite systems and the voter model. *The Annals of Probability*, pages 643–663, 1975.

[17] Claudio Castellano, Vittorio Loreto, Alain Barrat, Federico Cecconi, and Domenico Parisi. Comparison of voter and glauber ordering dynamics on networks. *Physical Review E*, 71(6):066107, 2005.

[18] Vishal Sood, Tibor Antal, and Sidney Redner. Voter models on heterogeneous networks. *Physical Review E*, 77(4):041121, 2008.

[19] Serge Galam. Minority opinion spreading in random geometry. *The European Physical Journal B-Condensed Matter and Complex Systems*, 25(4):403–406, 2002.

[20] Claudio J Tessone, Raul Toral, Pau Amengual, Horacio S Wio, and Maxi San Miguel. Neighborhood models of minority opinion spreading. *The European Physical Journal B-Condensed Matter and Complex Systems*, 39(4):535–544, 2004.

[21] R Lambiotte. How does degree heterogeneity affect an order-disorder transition? *EPL (Europhysics Letters)*, 78(6):68002, 2007.

[22] Maurizio Porfiri, EM Bollt, and DJ Stilwell. Decline of minorities in stubborn societies. *The European Physical Journal B*, 57(4):481–486, 2007.

[23] Guillaume Deffuant, David Neau, Frederic Amblard, and Gerard Weisbuch. Mixing beliefs among interacting agents. *Advances in Complex Systems*, 3(01n04):87–98, 2000.

[24] K Sznajd-Weron. Sznajd model and its applications. *Acta Physica Polonica. Series B*, 35(8):2537–2547, 2005.

[25] Bibb Latane. The psychology of social impact. *American Psychologist*, 36(4):343, 1981.

[26] Maciej Lewenstein, Andrzej Nowak, and Bibb Latane. Statistical mechanics of social impact. *Physical Review A*, 45(2):763, 1992.

[27] MC Gonzalez, AO Sousa, and HJ Herrmann. Opinion formation on a deterministic pseudo-fractal network. *International Journal of Modern Physics C*, 15(01):45–57, 2004.

[28] RN Costa Filho, MP Almeida, JE Moreira, and JS Andrade. Brazilian elections: voting for a scaling democracy. *Physica A: Statistical Mechanics and its Applications*, 322:698–700, 2003.

[29] Americo T Bernardes, Dietrich Stauffer, and Janos Kertesz. Election results and the Sznajd model on Barabasi network. *The European Physical Journal B-Condensed Matter and Complex Systems*, 25(1):123–127, 2002.

[30] Morton Deutsch and Harold B Gerard. A study of normative and informational social influences upon individual judgment. *The Journal of Abnormal and Social Psychology*, 51(3):629, 1955.

[31] Abhimanyu Das, Sreenivas Gollapudi, and Kamesh Munagala. Modeling opinion dynamics in social networks. In *Proceedings of the 7th ACM international conference on Web search and data mining*, pages 403–412, 2014.

[32] Quentin Michard and J-P Bouchaud. Theory of collective opinion shifts: from smooth trends to abrupt swings. *The European Physical Journal B-Condensed Matter and Complex Systems*, 47(1):151–159, 2005.

[33] Bertram During and Marie-Therese Wolfram. Opinion dynamics: inhomogeneous boltzmann-type equations modelling opinion leadership and political segregation. In *Proc. R. Soc. A*, volume 471, page 20150345. The Royal Society, 2015.

[34] Lazaros K Gallos, Pablo Barttfeld, Shlomo Havlin, Mariano Sigman, and Hernan A Makse. Collective behavior in the spatial spreading of obesity. *Scientific Reports*, 2:454, 2012.

[35] Li Daqing, Jiang Yinan, Kang Rui, and Shlomo Havlin. Spatial correlation analysis of cascading failures: congestions and blackouts. *Scientific Reports*, 4:5381, 2014.

[36] Nicole Abaid, James Macinko, Diana Silver, and Maurizio Porfiri. The effect of geography and citizen behavior on motor vehicle deaths in the united states. *PLoS One*, 10(4), 2015.

[37] Feilong Wang, Daqing Li, Xiaoyun Xu, Ruoqian Wu, and Shlomo Havlin. Percolation properties in a traffic model. *EPL (Europhysics Letters)*, 112(3):38001, 2015.

[38] Richard C Fording. State ideology data.

[39] Jakob Runge, Jobst Heitzig, Vladimir Petoukhov, and Jurgen Kurths. Escaping the curse of dimensionality in estimating multivariate transfer entropy. *Physical Review Letters*, 108(25):258701, 2012.

[40] Carsten Grabow, James Macinko, Diana Silver, and Maurizio Porfiri. Detecting causality in policy diffusion processes. *Chaos: An Interdisciplinary Journal of Nonlinear Science*, 26(8):083113, 2016.

[41] Sachit Butail, Violet Mwaffo, and Maurizio Porfiri. Model-free information-theoretic approach to infer leadership in pairs of zebrafish. *Physical Review E*, 93(4):042411, 2016.

[42] R Quian Quiroga, Thomas Kreuz, and Peter Grassberger. Event synchronization: a simple and fast method to measure synchronicity and time delay patterns. *Physical Review E*, 66(4):041904, 2002.

[43] Mate Nagy, Zsuzsa Akos, Dora Biro, and Tamas Vicsek. Hierarchical group dynamics in pigeon flocks. *Nature*, 464(7290):890–893, 2010.

[44] Brani Vidakovic. Sensitivity, specificity, and relatives. In *Statistics for Bioengineering Sciences*, pages 109–130. Springer, 2011.

[45] William D Berry, Evan J Ringquist, Richard C Fording, and Russell L Hanson. Measuring citizen and government ideology in the american states, 1960-93. *American Journal of Political Science*, pages 327–348, 1998.

Chapter 5

Extracting information flow between flying bat pairs using model-free methods

This manuscript is ready to be submitted for possible publication in a peer-reviewed journal.

5.1 Abstract

Social animals exhibit collective behavior wherein they negotiate to reach an agreement, for example to coordinate motion and synchronize migration. Bats are unique among such social animals in that they use active sensory echolocation or "bio-sonar", that is, they emit ultrasonic waves and sense echoes to detect and navigate surroundings. In real bat swarms, understanding navigational leadership roles in light of their unique sensing capabilities is a challenge, and quantitative assessment of leadership has not been explored rigorously. Given the broadcast nature of bio-sonar, the active sensing of one individual can directly influence the motion of others, making the directionality of leadership unclear. Here, we seek to understand navigational leadership in bats from direct observation of bat swarms in flight. Pairs of bats were continuously tracked in a mountain cave in Shandong Province, China, from which three-dimensional path points are extracted and converted to one-dimensional curvature time series. We utilize two recent methods from dynamical systems and information theory, namely convergent cross mapping and transfer entropy, to extract causal relationships between pairs of time series. These tools identify the direction of information transfer between a pair of bats flying together, which allows us to answer the question of whether individuals fly independently of each other or interact to plan flight paths. We find that the identified causal relationships between bats is sensitive to the selected mathematical tools, their parameters and the behavior these animals exhibit.

5.2 Introduction

Animal groups such as bird flocks [1], fish schools [2] and insect swarms [3] frequently exhibit coordination often referred to as 'collective behavior' that results from social interactions among individuals. In nature, social animals take advantage of collective behavior to locate food sources [4], avoid predators [5], and find a mate [6]. Interaction among the individuals is a strong determinant of collective behavior whereby information propagates across the group enabling decision making. In particular, individual members in the group act based on local information available from the interaction with neighbors. This information diffuses to the entire group, and the result may be the group-level coordination. Quantitative assessment of the information exchange within animal groups is extremely challenging and hence has attracted researchers from different disciplines. One approach to study interactions is by using numerical simulations which rely on a priori assumptions of the nature of interactions among the individuals. However, a deeper understanding regarding the nature of unknown interactions in animal groups triggers the need for an alternate approach which directly uses data from laboratory or field experiments. For such datasets, identification of a dominant direction of information flow allows for defining the influential members in the group, and hence leader-follower relationships which are observed within social groups, for example, fish schools [7], pigeon flocks [8], and human crowds [9].

The detection of information exchange in a pair of individuals is a particular challenge for organisms who use active sensory systems [10, 11]. A fitting example of active sensing animals is bats, who are particularly effective users of echolocation or "bio-sonar", wherein they emit ultrasonic waves and sense echoes to navigate and hunt in the dark [12]. The use of active sensing poses both advantages and limitations. Particularly, active sensing promotes information sharing wherein one individual bat may eavesdrop and use the reflected signal from its peer to sense obstacles or detect the food source. Moreover active sensing allows bats to potentially send information forward in space, whereas vision or passive sensing may not. However, an inevitable challenge in active sensing within a group is jamming, which occurs when multiple bats are using echolocation and each individual's calls become difficult to distinguish, which leads to misinterpretation of their environment. Biological literature provides evidence of such jamming in bats and tests different strategies that bats adopt to avoid misinterpretation, like frequency modulation [13] or vocalization cessation [14]. It is worth noting that bats have been observed to purposefully jam conspecifics during competition for food [15]. Thus, bats certainly act differently in group than alone and, in many situations, this can benefit their survival.

Given the above, we hypothesize that active sensing of one bat influences the motion of the other which we define as leadership. In this framework, quantitative assessment of interaction and identification of the navigational leadership roles in real bat swarms is a challenge and a quantitative study is less explored in literature [11]. Here, we seek to understand if bats fly independently of each other or interact to plan flight paths from direct observation of bat swarms. To answer this question we focus on trajectories of pairs of bats where one bat

is positioned in front and the other in the rear, and we identify the dominant direction of information flow using model-free methods.

A classical approach to identify leader-follower interactions is by computing cross-correlation between time series of two trajectories for a range of time lags and looking for a maximum in correlation value that exists at some non zero lag. Then the leading time series is identified as leader and the lagged time series as follower. Cross-correlation has been applied in detecting leadership in animal group motion, for example to find hierarchy in pigeon flocks [8]. However, the major limitation in cross-correlation is that it assumes a linear dependence, and is sensitive to noise which is typical in real-world systems. Moreover, the cross-correlation measure is symmetric and hence is not appropriate to detect lag-lead relationships in systems with feedback. Alternative methods are model-free approaches that do not assume behaviors a priori and are capable of identifying non-linear relationships. Increasingly popular among these methods are transfer entropy (TE) [16] and convergent cross map (CCM). Transfer entropy is an information-theoretic approach and measures information exchange between two or more random variables, whereas convergent cross map is grounded on dynamical systems theory and has the potential to detect directional causation between two time series [17]. Transfer entropy has already found its applications in different fields, including neuroscience [18], finance [19], social media [20], climate networks [21], whereas CCM is relatively new but already demonstrated successful applications in diverse settings [17, 22, 23, 24]. Recently, information theoretic approaches and particularly transfer entropy have received increasing interest in studying interactions in animal group motion, for example, in fish [25, 26, 27], crabs [28], meerkats [29], and insect swarms [30]. On the contrary, in spite of being qualified as a potential framework in detecting information flow or causality, CCM has not previously been used in the context of animal groups.

In this work, we use these analytical tools to formally measure the strength of influence of one individual on another by quantifying directional coupling. This study uses field data from animal motion to investigate the reliability of using these methods. Particularly, we target systems of bats because of their use of active sensing which makes them a unique example of pairwise interaction. To investigate the navigational leadership roles in pairs of flying bats, we use the data of bat trajectories as filmed on summers of 2014 and 2015 in a cave in Shandong Province, China. In the year 2014, the bat trajectories are filmed in absence of any obstacles. In the year 2015, we further use a control strategy on the bats' flight paths by implementing obstacles in the form of thin films arranged in vertical maze, with the aim of compelling the pairs of bats to interact in avoiding the novel obstacles.

5.3 Materials and Methods

In this section, we present a brief demonstration of the different analytical tools, namely, transfer entropy, convergent cross map, and cross correlation, that are used in the present study to detect information exchange from time series data of bat pairs. In addition, we

explain our experimental setup and the method of data collection.

5.3.1 Tools to detect interactions:

We use two model-free methods, namely TE and CCM, to identify interactions in pairs of bats flying together. These tools are capable of identifying a dominant direction of information flow and hence can detect the causal variable. Here, we start by explaining briefly how these methods work and then demonstrate with an example.

Convergent cross map: CCM was first introduced in [17] and is based on an algorithm that compares the ability of lagged components of one time series variable to estimate the dynamics of another. Given two time series, $X(t)$ and $Y(t)$ where t denotes the time index and in the case of unidirectional causality ($X \rightarrow Y$), the behavior of the causal variable (X) leaves a signature on the affected variable (Y). Hence, the past values of Y can better estimate the values of X at the corresponding times. This idea is implemented by constructing a shadow manifold from time-delayed projections of each time series independently. A more detailed description of the algorithm can be found in the supplementary materials of [17] and in [31] which can be summarized as follows. We first construct a shadow manifold of X, called M_X where we build an E dimensional vector of the form $(X(t), X(t-\tau), X(t-2\tau), \cdots, X(t-(E-1)\tau))$, where E and τ are embedding dimension and time-delay, respectively at each point $X(t)$ in X. The first vector is created at $t = 1 + (E-1)\tau$ and the last is at $t = L$, where L is the library size. Similarly, a shadow manifold of Y, called M_Y is constructed independently. Next, a cross-mapped estimate of $Y(t)$ is obtained by locating the contemporaneous lagged-coordinate vector on M_X using a nearest neighbor technique. Finally, cross map (or cross estimate) skill is evaluated by computing Pearsons correlation coefficient between Y and estimated Y. The negative correlation values are converted to zeros and are treated as insignificant indicating that CCM estimate lacks information about the dynamics of the other variable. Hence, the CCM values range in between 0 and 1 and is unit less. The cross map estimation improves with increased library size and converges to a constant value. CCM identifies the causal variable by the asymptotic value of cross map estimation. CCM in the present study is implemented using rEDM package in R [32], where the lag (τ) used for attractor reconstruction is set to 1 by default, and the optimal embedding dimension E is evaluated following Simplex Projection method [33].

Transfer entropy: Thomas Schreiber [34] formalised the idea of transfer entropy to measure the information flow between two time series based on Shannon entropy. Shannon entropy is a measure of expected value of the information associated with the occurrence of an event and is defined as follows

$$H(X) = -\sum_{x \in \mathbb{X}} \Pr[x] \log_2 \Pr[x],$$

where $\Pr[x]$ is the probability density function for a variable X taking the value x and $\mathbb{X}$

refers to the set containing all possible realizations of X. Transfer entropy extends this concept to compare the entropy in one time series given some knowledge of another time series; information is said to flow between time series if the entropy of one decreases by conditioning the other. TE from Y to X, $T_{Y\to X}$, computes information transfer from Y to X by measuring degree of uncertainty resolved to predict the future of X from its present, using the additional knowledge of Y at present. Hence, transfer entropy from Y to X is defined as

$$T_{Y\to X} = \sum_{\substack{x(t+1)\in\mathbb{X}(t+1),\\ x(t)\in\mathbb{X}(t),\\ y(t)\in\mathbb{Y}(t)}} \Pr[x(t+1), x(t), y(t)] \log \frac{\Pr[x(t+1)|x(t), y(t)]}{\Pr[x(t+1)|x(t)]},$$

where $\Pr[x(t+1)|x(t)]$ and $\Pr[x(t+1)|x(t), y(t)]$ denote the probability of $x(t+1)$ conditioned on only $x(t)$ or both $x(t)$ and $y(t)$, and $\Pr[x(t+1), x(t), x(t)]$ denotes joint probability. Depending upon the logarithm base selected, unit of TE can either be bits (base 2) or nats (base e). In absence of influence of Y, $\Pr[x(t+1)|x(t), y(t)] = \Pr[x(t+1)|x(t)]$, and hence $T_{Y\to X}$ equals zero. By construction, transfer entropy is an asymmetric quantity as $T_{Y\to X}$ is not equal to $T_{X\to Y}$ in general, and the idea is used to identify the dominant direction of information flow, and hence to infer causality. Transfer entropy can also be expressed in terms of conditional entropy as $T_{Y\to X} = H(X(t+1)|X(t)) - H(X(t+1)|X(t), Y(t))$, where $H(X)$ is the Shannon entropy. The probability distribution function used in these definitions can be calculated by using different techniques [35], for example, partitioning each time series variable into finite number of discrete bins and then computing the relative frequency of occupancy of the samples in the bin (binning estimators); using a kernel function that measures similarity between pairs of samples given resolution or kernel width r (kernel-estimators); or the recent Kraskov, Stogbauer, and Grassberger (KSG) method which uses dynamically altered kernel width in terms of K nearest-neighbours (k_{nn}). We have used the JIDT (Java Information Dynamics Toolkit) [36], which is an open-source code to implement various information-theoretic measures from time series data. In all analysis, unless otherwise noted, we use the KSG method of computing TE since it has been shown to decrease errors in PDF estimation [37], and the unit is in nats.

Cross correlation: Both of the above mentioned tools use model-free approaches to identify causality or information flow, and hence have been identified as superiors in comparison to the classical cross correlation approach particularly for nonlinear dynamics. Nevertheless, we compute cross correlation for reference. Cross correlation relies on the idea of identifying relationships between one time series variable and lagged version of the other. Specifically, it computes correlation between two time series for range of time lags, and identifies a maximum in correlation value at some non zero lag. Then the leading variable is identified as causal driver. The major limitations of cross correlation is that it assumes linear dependence and is sensitive to noise [27]. Cross correlation values may assume positive and negative values ranging in between 0 and 1, and is a unitless quantity.

Example: We consider a simple model system of two coupled logistic difference equations

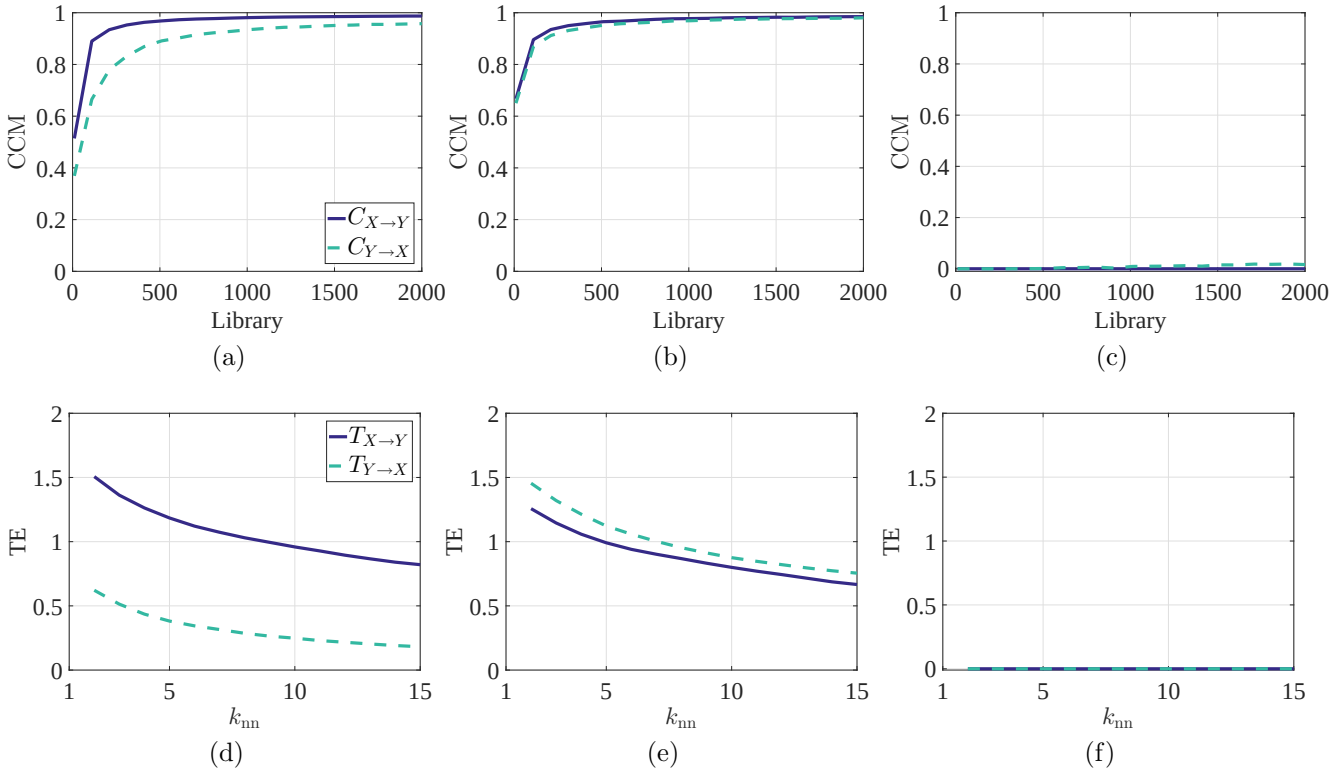

Figure 5.1: CCM is implemented on time series data from logistic equations with (a) unidirectional coupling (X driving Y), (b) bidirectional coupling , and (c) no coupling. TE is implemented on the same time series data with (d) unidirectional coupling (X driving Y), (e) bidirectional coupling , and (f) no coupling.

as follows:

$$X(t+1) = X(t)[3.65 - 3.65X(t) - \alpha Y(t)],$$
$$Y(t+1) = Y(t)[3.77 - 3.77Y(t) - \beta X(t)],$$

where α and β denote the influence of Y on X, and the influence of X on Y, respectively. We choose the same initial conditions for X and Y and are set to 0.02. We further consider three scenarios, first with bidirectional coupling where we assign α and β to be of same value, second, with X driving Y by choosing $\beta > \alpha$, and third, in absence of coupling by fixing $\beta = \alpha = 0$. We apply the above tools in each case to examine their performance in distinguishing bidirectional from unidirectional coupling by identifying the causal variable, and to verify if they can recognize the lack of coupling.

We choose $\alpha = \beta = 0.5$ for bidirectional causality, and $\alpha = 0.15$ and $\beta = 0.5$ for X driving Y. Figure 5.1 demonstrates the results. Comparing Figures 5.1b and 5.1a, we observe CCM distinguishes bidirectional causality from the unidirectional one. In the case of bidirectional causality, there is no difference in relative skill in cross map estimates and both converge to same value close to 1 with increasing library size. However, in the case of X driving Y, there is difference in the convergence where $C_{X\to Y}$ converges to a higher value than $C_{Y\to X}$, which we interpret as meaning the causal variable as X. Transfer entropy on the other hand computes the information flow as a function of input parameter to the KSG method for building the PDF, k_{nn}. Comparing Figures 5.1e and 5.1d, we observe that there is noticeable difference in the information transfer in the unidirectional coupling as $T_{X\to Y}$ is greater than $T_{Y\to X}$ for all values of k_{nn}, whereas in the bidirectional case the difference in the transfer entropy values is lost. It is important to note that causality is identified by the relative difference in TE values. On the contrary, the asymptotic value of the cross-map skill in CCM is an indicator of the causal variable since these numbers are bounded. However, real-world data being an approximation of dynamics occurring in higher dimensions, the asymptotic value of CCM is usually less than one as in the example in [17]. Interestingly, the absence of coupling is correctly identified by both the tools as shown in Figures 5.1c and 5.1f. To summarize, we verify both these tools have the potential to capture the information exchange between time series data and can identify the causal variable, at the same time both the tools are identified reliable in not providing false positives.

5.3.2 Experimental setup and data collection:

In our present study we investigate the navigational leadership roles in a pair of flying bats by using the flight trajectory data of bats filmed in summers of 2014 and 2015 in a cave on Mount Lian Tai in Shandong Province, China. This cave served as a roost to a colony of approximately 2000 Myotis bats. In 2014, the bat trajectories were filmed in absence of any obstacles. In 2015, we introduced obstacles in bats' flight paths by arranging thin films in vertical maze to compel the pairs of bats to coordinate in the presence of novel obstacles.

A total of 30 pairs of bats (10 pairs from 2014, and 20 pairs from 2015) are tracked as

they fly through the capture volume, which refers to the three-dimensional volume within which the bat trajectories are filmed. The capture volume was a cave entrance which bats navigated to exit the cave after sunset, and is approximately 12 meter portion of the cave "hallway". Three-dimensional coordinates of bat trajectories from the raw video data were extracted from multiple camera views of the capture volume using a custom Matlab script and proprietary and open source calibration scripts [38, 39]. Pairs are selected if two bats fly together in the tracking volume and we refer them as bat 1 and bat 2 corresponding to the one that enters the capture volume first and second, respectively. To attain one-dimensional time series representation from three-dimensional trajectory coordinates, we choose the metric as curvature since it is a reflective of bat's steering. Moreover, the curvature based time series have previously been used in the study of animal behavior for example in the study of laboratory insects [40].

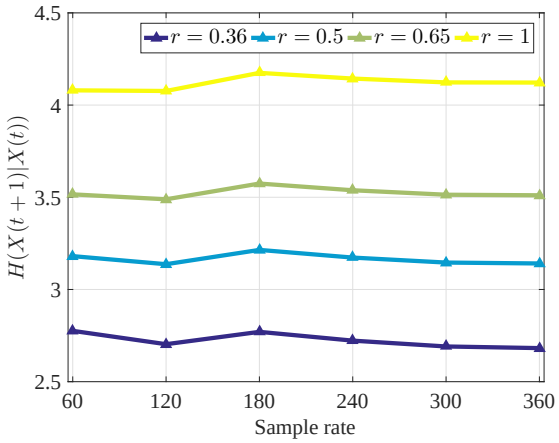

Figure 5.2: Conditional entropy as calculated for a range of sample rates for different choice of kernel widths (r).

Two different camera set ups have been used in filming the videos of bats' flights for the two summers, in particular, six GoPro cameras with infrared filters in 2014 [41], and three thermal cameras in 2015. The GoPro cameras have a frame rate of 60 Hz, whereas the thermal cameras have frame rate of at least 25 Hz. In order to attain consistent rate of sampling for both years' data, we first fit a third order spline through three-dimensional coordinates and re-sample in time at six different sample rates, ranging from 60Hz to 360Hz. Next, we differentiate the spline to generate the three components of velocity and acceleration data at each point. Curvature values at each point are calculated using the following relation,

$$a_n = a - a_t = a - \frac{a \cdot v}{||v||^2} v, \qquad \rho = \frac{||a_n||}{||v||^2},$$

where a, a_n, a_t are acceleration, normal acceleration and tangential acceleration vectors, respectively, v is the velocity vector and ρ is curvature.

For the analysis, we concatenate the curvature time series of each bat 1 and bat 2 from all 30 pairs to build an amalgamated dataset. We select a value for the sampling rate by plotting the conditional entropy $H(X(t)|X(t-1))$, as computed on the amalgamated dataset, as a function of sampling rate. The peak in conditional entropy dictates the best choice of sampling rate [27]. Figure 5.2 demonstrates conditional entropy as calculated for different sample rates. To calculate conditional entropy we have used kernel estimators, and the value r in Figure 5.2 corresponds to the kernel width, which is an input parameter to evaluate PDF. We choose kernel estimator as it is the only available estimator that the present version of JIDT have to calculate the conditional entropy [42]. For four different choices of r, we identify a peak corresponding to sample rate of 180Hz, which we use in further analysis.

Considering the two experiments, we notice that we can categorize the bat pair trajectories in three groups based on flight behaviors as follows. The first 10 bat pairs are flying in absence of any externally provided obstacles or maze and traverse the capture volume, hence we group them together and refer as "No-Maze" (NM). The flight paths of remaining 20 bat pairs fly in the presence of the obstacle maze, and we observe that they either both traverse the maze or both avoid it by turning. We categorize the trajectories within this data as the 14 bat pairs who traverse and denote them as "Maze Cross"(MC), and the 6 pairs that do not traverse and denote them as "Maze Turn"(MT).

5.3.3 Data analysis:

As detailed above, bat 1 is the bat which first enters the capture volume and bat 2 follows. Hence there exists a portion of the time series when one of the bats is filmed to fly by itself in the capture volume. In order to perform TE, CCM and cross correlation, we use only the portion of the time series data when both bats are in the capture volume.

Before implementing TE and CCM, we categorize 30 pairs of bat data in four groups, and three of which are according to bats' flight behavior as detailed in Method section. For each group we build the time series data using an ensemble method [43, 44], which refers to stacking time series together. In the first group, we build an ensemble time series data for bat 1 by concatenating curvature time series over 30 pairs, and we refer them as "All". We similarly build an ensemble time series data for bat 2, independent to that of bat 1. For the other three groups we choose the pairs that belong to NM, MC and MT, and concatenate likewise.

To understand the statistical significance of the following results, we define a control condition for our analysis within each group to verify the significance of the results obtained. The rationale of using a control condition is that there is no standard threshold value for TE and CCM to distinguish causality above the noise level. For the control condition, we manufacture 20 randomly shuffled ensembles within each group, and, in each shuffled ensemble, partners are scrambled. That is to say, each bat 1 is compared to a bat 2, but not a bat with which it coincided in time. In doing so we encounter time series of different lengths

for which we select the time series corresponding to larger library size and the shorter one are stacked with zeros in the end to make it of same size. Next we implement the tools and perform a test of significance to compare our experimental results to these controls. The main idea is to distinguish pairwise interaction above the effect of external factors, which may involve the geometry of the cave itself. We hypothesize that the pairwise interaction will involve additional information exchange above similarities in trajectories due to the fact that all the bats are leaving the cave and hence exhibit similar flight paths. Ensemble time series from actual bat pairs and shuffled pairs are normalized to zero mean and unit variance before analysis.

5.4 Results

We compute TE, CCM and cross correlation on ensembled data considering all pairs and additionally on 3 subgroups categorized by behavior as shown in Figure 5.3. For TE measurement we fix k_{nn} value equal to 5, so that the resolution width in estimating transfer entropy is neither too large nor too small. Sensitivity of results to this parameter will be discussed below. On the other hand, CCM relies on the asymptotic value of convergence to infer causality, and hence we focus on the statistical significance at the maximum library size. We denote transfer entropy (CCM) from bat 1 to bat 2 and from bat 2 to bat 1 as $T_{1\to2}$ ($C_{1\to2}$) and $T_{2\to1}$ ($C_{2\to1}$), respectively, and for control condition as $T^c_{1\to2}$ ($C^c_{1\to2}$) and $T^c_{2\to1}$ ($C^c_{2\to1}$). Significance above the control condition is computed in terms of percentile and results that belong outside 95 percentile of the shuffled distribution is denoted by red circles. The shaded regions refer to mean $\pm$ one standard deviation of the control condition for bat 1 and bat 2. For all bats, TE demonstrates bidirectional information transfer between bats 1 and 2 in Figure 5.3a and significance above the control condition is observed in either direction. However, statistical significance is not reached when CCM and cross correlation are implemented on all pairs as observed in Figures 5.3b and 5.3c.

Analysis by behavior unravels significant results with respect to control condition when NM pairs are considered. For NM pairs, TE recognizes unidirectional information exchange from bat 2 to 1, and statistical insignificance in the opposite direction. Interestingly, CCM display strong causal coupling and recognizes bat 2 as the leader, which is consistent with TE results. Significance is also identified in the cross correlation result for NM pairs. In other words, both TE and CCM identify bat 2 as the leader when bat pairs fly in absence of externally provided obstacles, whereas cross correlation provides evidence of pairwise correlated trajectories. When bat pairs in presence of obstacles (MC and MT) are considered, the indication of unidirectional information exchange varies and consistency between the TE and CCM results are also lost. In particular, comparing Figures 5.3b and 5.3a, CCM reveals bat 2 as the leader for MC pairs as opposed to bidirectional coupling in TE results, and no causal coupling in MT pairs confronting bidirectional coupling as demonstrated in TE results. In addition, from Figure 5.3c, cross correlation fails to indicate statistical significance

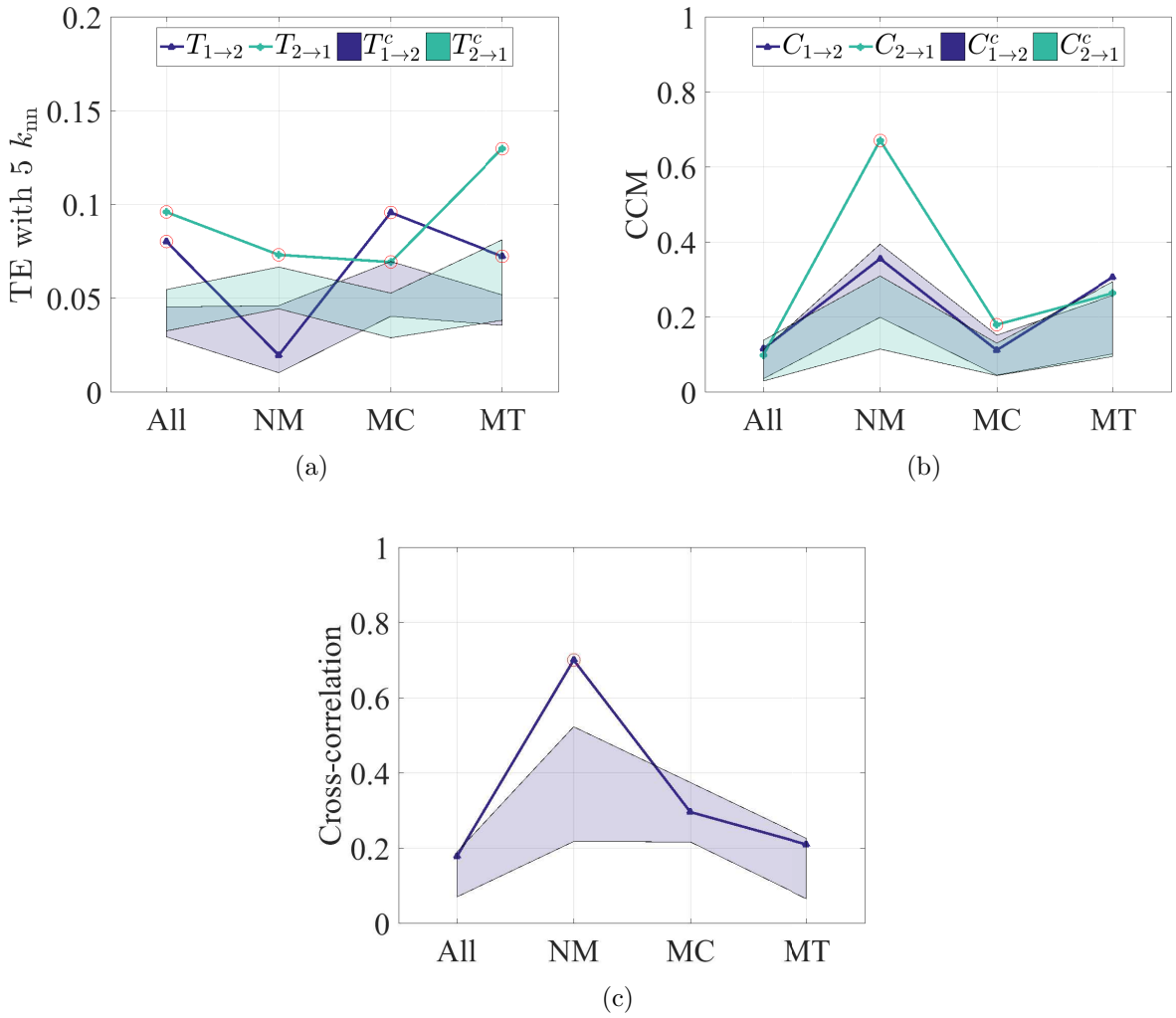

Figure 5.3: Results of implementation of (a) TE, (b) CCM and (c) cross correlation on ensembled time series data are summarized. Control conditions are shown as mean ± one standard deviation in the shaded regions. Markers circled in red are used to refer results that belong outside 95 percentile of the control condition. TE, CCM and cross correlation are implemented on ensembled time series data for all bat pairs ($N = 30$), NM pairs ($N = 10$), MC pairs ($N = 14$) and MT pairs ($N = 6$), where N denotes number of pairs present in each category. We use k_{nn} value equal to 5 for TE measurement, and asymptotic value of convergence at the maximum library size for CCM.

for both MC and MT pairs.

In order to identify the sensitivity of the TE results to the parameter choice used in the analytical tool, we vary k_{nn} from 2 to 15 as shown in Figure 5.4. We anticipate statistical significance may not be obtained for large and small values of k_{nn}, which may effect the estimation of PDFs. Figure 5.4a demonstrates bidirectional information transfer between bats 1 and 2 for all bats, and significance in the results is observed in either direction for entire range of k_{nn} values. Hence the results for all pairs are insensitive to the resolution width used in the estimation of TE. Splitting by behavior, we observe TE results are sensitive to choice of k_{nn} values as shown in Figures 5.4b to 5.4d. Specifically considering NM pairs, the significant result is observed in $T_{2\to1}$ for k_{nn} values greater than 4 as evidenced from Figure 5.4b, and $T_{1\to2}$ loses significance at higher values of k_{nn} in both MC and MT pairs. However, from Figures 5.4c and 5.4d, we witness significance in the transfer entropy results from bat 2 to 1 ($T_{2\to1}$) across all choice of k_{nn} values. Hence, fixing k_{nn} equal to 5 in Figure 5.3a is a reasonable choice as large and small values of k_{nn} may result in degenerated PDF estimation.

Similarly, we compute CCM on experimental data and with control conditions at different library sizes in Figure 5.5. It should be noted that the estimation of significance at intermediate library sizes is not conclusive in terms of identifying the causal variable, as CCM relies on the asymptomatic value of convergence. We observe from Figures 5.5b and 5.5c that CCM from bat 2 to 1 converges to high value in NM pair and to low value in MC pair with increased library size, reflecting strong and weak unidirectional causal coupling, respectively. Also, we can observe that the time series used are long enough to result in convergence in each of these plots.

5.5 Discussion

Results in TE and CCM support our hypothesis that pairwise interactions involve additional information exchange above control similarities in trajectories. TE clearly captures significant bidirectional information exchange between bat pairs in all, MC and MT pairs, and significant unidirectional information exchange from rear to front bat in NM pairs. Thus the results support our hypothesis that bats interact to plan flight paths, instead of the presence of clear similarities in the trajectories of bats that do not fly together. It is important to note that an alternative control condition can be used where the manufactured data can be shuffled in time. However, that control is very liberal and leads to zero mean and standard deviation close to zero, revealing statistical significance in our results for four different choices of bat categories when TE and CCM are implemented. But we have chosen a relatively conservative control condition in order to capture the information exchange above the effect of cave geometry and similarity in bat trajectories. CCM on the other hand identifies leadership in rear bat for both NM and MC pairs, and no indication of leadership in other choices.

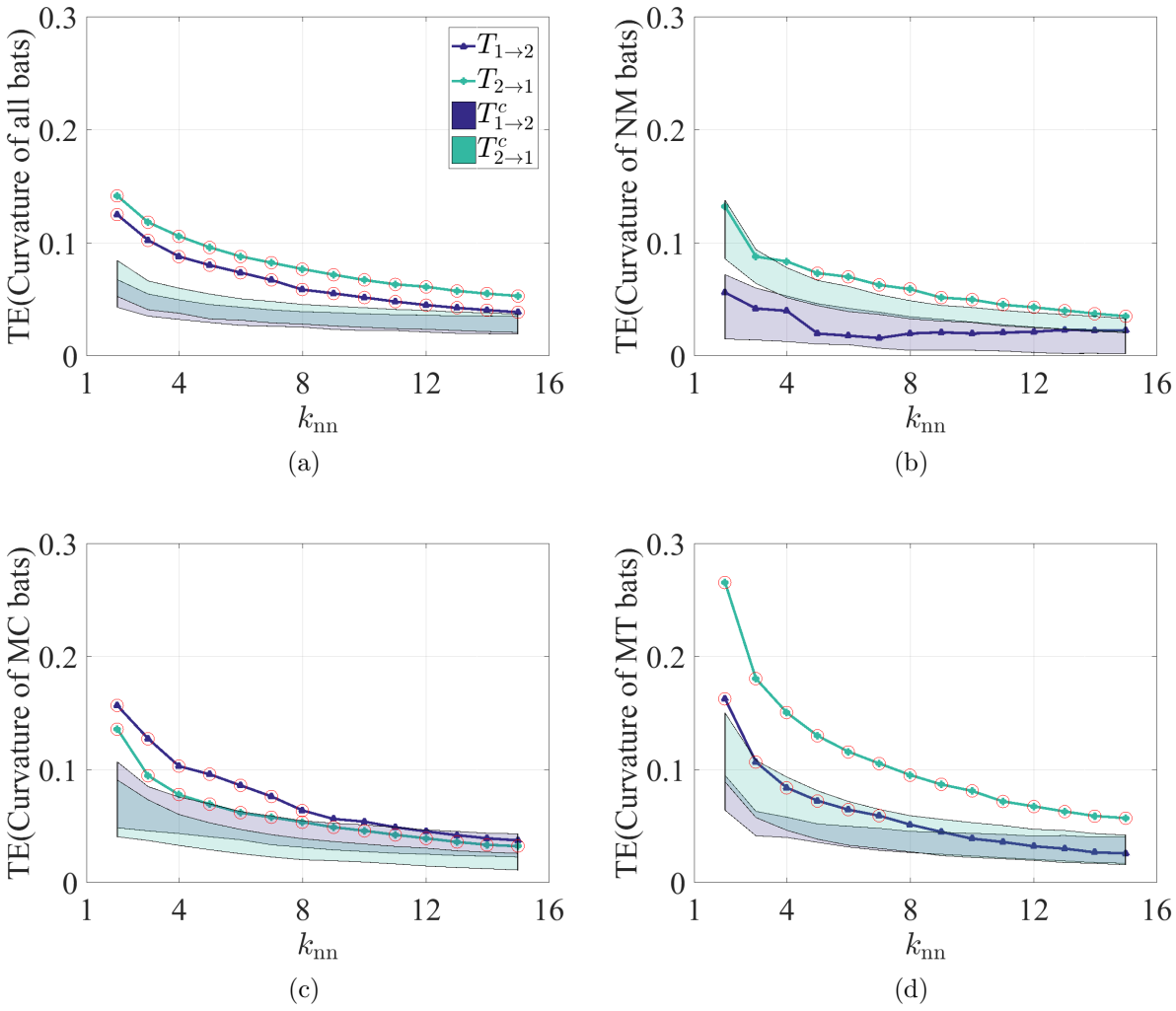

Figure 5.4: Information flow in terms of transfer entropy is calculated using curvature based time series. $T_{1\to2}$ and $T_{2\to1}$ are calculated for varying values for k_{nn}. Control conditions $T^c_{1\to2}$ and $T^c_{2\to1}$ are shown as mean $\pm$ one standard deviation in the shaded regions. Markers circled in red are used to refer results that belong outside 95 percentile of the control condition. TE is implemented on ensembled time series data for (a) all bat pairs ($N = 30$), (b) NM pairs ($N = 10$), (c) MC pairs ($N = 14$) and (d) MT pairs ($N = 6$), where N denotes number of pairs present in each category.

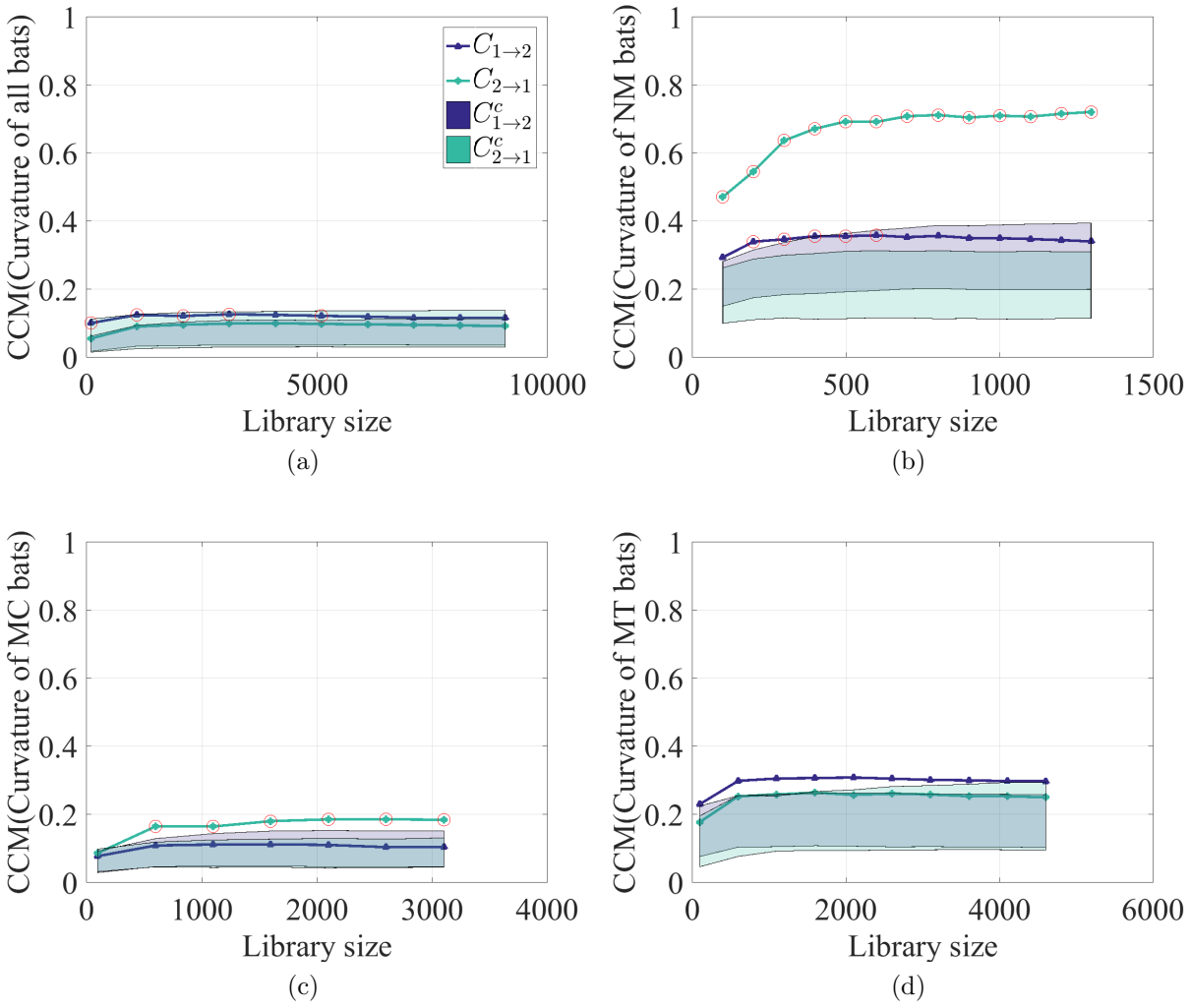

Figure 5.5: To detect dominant direction of information flow we implement CCM using curvature based time series. $C_{1\to2}$ and $C_{2\to1}$ are calculated by increasing library sizes. Control conditions $C^c_{1\to2}$ and $C^c_{2\to1}$ are shown as mean $\pm$ one standard deviation in the shaded regions. Markers circled in red are used to refer results that belong outside 95 percentile of the control condition. CCM is implemented on ensembled time series data for (a) all bat pairs ($N = 30$), (b) NM pairs ($N = 10$), (c) MC pairs ($N = 14$) and (d) MT pairs ($N = 6$), where N denotes number of pairs present in each category.

Rear bat drives the front bat when bat pairs fly in absence of obstacles. We identify bat 2 or the rear bat as the leader according to both TE and CCM when bat pairs traverse in absence of obstacles. The result may be counter-intuitive, however information propagating from rear to front individual is prevalent and has been identified in animal group motion, for example in a study with meerkats [29]. This is particularly possible in bats as they are effective user of active sensing, wherein the information from the rear bat may discharge forward in space and hence to the front bat.

TE and CCM are two different metrics in identifying causality. The primary difference in our TE and CCM results is due to the fact that these are two different indicators of pairwise interaction, and use fundamentally different approaches. TE measures information transfer whereas CCM identifies causal variable. Distinction between TE and causal effect has been discussed in [45]. Particularly, TE with the assumption of traditional 1st order Markov process [34] means current position of one bat is only affected by the values of one time step prior which may be overcome by incorporating the idea of information storage [46]. On the contrary, CCM is a tool to detect the causal variable, and should not be confused as an indicator of information transfer. In other words, TE picks up the traces of significant information exchange whereas CCM inspects the dominant influence between a pair of time series variables. Additionally, TE is grounded on the idea of reduction in uncertainty in prediction using information from the causal variable, whereas CCM identifies causality by finding traces of influence in the history of one time series by another. As a result, it is not surprising that the results differ as we use two different tools.

TE is sensitive to the choice of independent variables used. To explore the sensitivity of TE results to the choice of independent variable, we adopt the multivariate functionality where three-dimensional coordinates of bat trajectories can be used to determine the information flow between two bats. The multivariate functionality in TE poses both advantages and limitations. The advantage being raw data can be used without converting to one-dimensional time series as there is no unique choice of one-dimensional variable, whereas the limitation is the procedure requires large library of dataset to build three-dimensional PDFs. Figure 5.6 shows the results. Bidirectional information exchange is noted when all 30 pairs and MC bats are considered as in Figures 5.6a and 5.6c, whereas unidirectional information exchange is observed for MT bats as in Figure 5.6d. Interestingly, even the evidence of interaction is lost for NM pairs in Figure 5.6b as the TE results are not significant above the control condition. One possible reason is that the three-dimensional implementation of TE is a data hungry process, and hence the lack of enough data to build three-dimensional PDFs in NM pairs may be the cause in insignificant results. However, it is clear TE results are sensitive to choice of independent variables used in analysis, which may lead to inconsistent results.

Here we present a comparison with previous work. In the previous work, a preliminary study was performed with NM pairs of bats, where TE was implemented and a binning approach was used for PDF estimation[41]. Unlike in the present study, an ensembled approach was not used, and instead analysis on each pair was performed separately. In addition

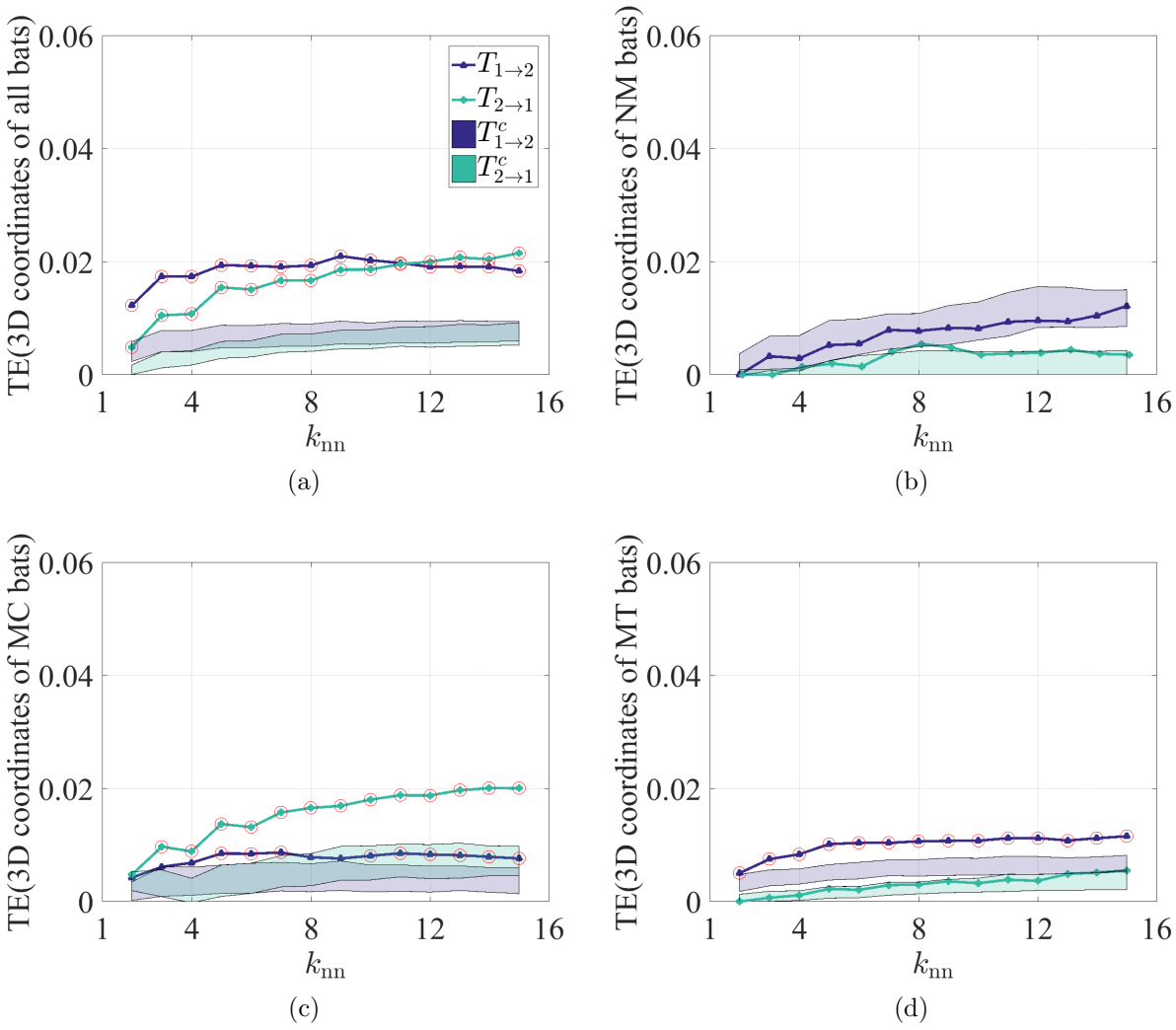

Figure 5.6: Information flow in terms of transfer entropy is calculated using three-dimensional coordinates of bat trajectories. $T_{1\to2}$ and $T_{2\to1}$ are calculated for varying values for k_{nn}. Control conditions $T^c_{1\to2}$ and $T^c_{2\to1}$ are shown as mean $\pm$ one standard deviation in the shaded regions. Markers circled in red are used to refer results that belong outside 95 percentile of the control condition. TE is implemented on ensembled time series data for (a) all bat pairs ($N = 30$), (b) NM pairs ($N = 10$), (c) MC pairs ($N = 14$) and (d) MT pairs ($N = 6$), where N denotes number of pairs present in each category.

a path coupling hypothesis was used with time-delay modifications retaining Markovianity of the process. The idea of time delay was to take into account the response time in adjusting bat's trajectory based on information received from the other bat. Trends suggested a leader-follower interaction between the front bat and the rear bat, although statistical significance was not achieved due to the small number of pairs used in the analysis. In the present extension, we introduce a novel experimental setup by implementing obstacles in the form vertical maze in bats' flight paths, in order to investigate if bats perform higher information exchange in coordinating with peers. In addition, we have used JIDT toolkit to implement TE with KSG method which is superior in correctly estimating PDFs compared to classical binning approach [37]. Furthermore, we have also implemented CCM and cross correlation, which were not explored in the earlier study, which support the directed information transfer we find with our method. To understand if bats rely on echolocation compared to other sensing cues a study was performed in [11], where an approach called heading delay which is similar to cross correlation was used in leader-follower pairs. However, it was not identified if the leader bats occupy rear or frontal position, which is investigated in the present work.

To conclude, in the present study, we investigate if pairs of bats fly independently or they interact to plan their flight paths. To answer this question, we collect the three-dimensional trajectories of bats flying in pairs. We use a novel experimental strategy by providing obstacles in their flight path to examine the change in pairwise interaction as compared to when obstacles are absent. To quantify information exchange from the bats' curvature time series, we implement two model free approaches, namely TE and CCM along with classical cross correlation. Although TE has been previously used to detect information exchange among individuals, CCM has been applied for the first time in context to animal group motion. TE provides evidences of information exchange in a pair of individuals, whereas CCM identifies leadership from rear to front bat when analysis is performed by flight behavior. Driving from rear may appear to be counter-intuitive to passive sensing users, although the use of active sensing in bats has the possibility to propagate information forward in space. Finally, we show that the identified coupled relationships between bats is sensitive to the selected mathematical tools, their parameters and the behavior these animals exhibit.

5.6 References

[1] Michele Ballerini, Nicola Cabibbo, Raphael Candelier, Andrea Cavagna, Evaristo Cisbani, Irene Giardina, Vivien Lecomte, Alberto Orlandi, Giorgio Parisi, and Andrea Procaccini. Interaction ruling animal collective behavior depends on topological rather than metric distance: Evidence from a field study. *Proceedings of the National Academy of Sciences*, 105(4):1232–1237, 2008.

[2] Roland W Tegeder and Jens Krause. Density dependence and numerosity in fright stimulated aggregation behaviour of shoaling fish. *Philosophical Transactions of the Royal Society of London. Series B: Biological Sciences*, 350(1334):381–390, 1995.

[3] John Stodart Kennedy. The migration of the desert locust (schistocerca gregaria forsk.). i. the behaviour of swarms. ii. a theory of long-range migrations. *Philosophical Transactions of the Royal Society of London B: Biological Sciences*, 235(625):163–290, 1951.

[4] Tony J Pitcher, Anne E Magurran, and Ian J Winfield. Fish in larger shoals find food faster. *Behavioral Ecology and Sociobiology*, 10(2):149–151, 1982.

[5] Birgitta Sillen-Tullberg and Olof Leimar. The evolution of gregariousness in distasteful insects as a defense against predators. *American Naturalist*, pages 723–734, 1988.

[6] David P Cowan. Group living in the european rabbit (oryctolagus cuniculus): mutual benefit or resource localization? *The Journal of Animal Ecology*, pages 779–795, 1987.

[7] Iain D Couzin, Christos C Ioannou, Guven Demirel, Thilo Gross, Colin J Torney, Andrew Hartnett, Larissa Conradt, Simon A Levin, and Naomi E Leonard. Uninformed individuals promote democratic consensus in animal groups. *Science*, 334(6062):1578–1580, 2011.

[8] Mate Nagy, Zsuzsa Akos, Dora Biro, and Tamas Vicsek. Hierarchical group dynamics in pigeon flocks. *Nature*, 464(7290):890–893, 2010.

[9] John RG Dyer, Anders Johansson, Dirk Helbing, Iain D Couzin, and Jens Krause. Leadership, consensus decision making and collective behaviour in humans. *Philosophical Transactions of the Royal Society B: Biological Sciences*, 364(1518):781–789, 2009.

[10] Mark E Nelson and Malcolm A MacIver. Sensory acquisition in active sensing systems. *Journal of Comparative Physiology A*, 192(6):573–586, 2006.

[11] Zhaodan Kong, Nathan Fuller, Shuai Wang, Kayhan Ozcimder, Erin Gillam, Diane Theriault, Margrit Betke, and John Baillieul. Perceptual modalities guiding bat flight in a native habitat. *Scientific reports*, 6, 2016.

[12] Raphael Arlettaz, Gareth Jones, and Paul A Racey. Effect of acoustic clutter on prey detection by bats. *Nature*, 414(6865):742–745, 2001.

[13] Nachum Ulanovsky, M Brock Fenton, Asaf Tsoar, and Carmi Korine. Dynamics of jamming avoidance in echolocating bats. *Proceedings of the Royal Society of London. Series B: Biological Sciences*, 271(1547):1467–1475, 2004.

[14] Chen Chiu, Wei Xian, and Cynthia F Moss. Flying in silence: echolocating bats cease vocalizing to avoid sonar jamming. *Proceedings of the National Academy of Sciences*, 105(35):13116–13121, 2008.

[15] Aaron J Corcoran and William E Conner. Bats jamming bats: Food competition through sonar interference. *Science*, 346(6210):745–747, 2014.

[16] Fatimah Abdul Razak and Henrik Jeldtoft Jensen. Quantifying 'causality' in complex systems: understanding transfer entropy. *PloS one*, 9(6):e99462, 2014.

[17] George Sugihara, Robert May, Hao Ye, Chih-hao Hsieh, Ethan Deyle, Michael Fogarty, and Stephan. Munch. Detecting causality in complex ecosystems. *Science*, 338(6106):496–500, 2012.

[18] Raul Vicente, Michael Wibral, Michael Lindner, and Gordon Pipa. Transfer entropy - a model-free measure of effective connectivity for the neurosciences. *Journal of computational neuroscience*, 30(1):45–67, 2011.

[19] Thomas Dimpfl and Franziska Julia Peter. Using transfer entropy to measure information flows between financial markets. *Studies in Nonlinear Dynamics and Econometrics*, 17(1):85–102, 2013.

[20] Greg Ver Steeg and Aram Galstyan. Information transfer in social media. In *Proceedings of the 21st international conference on World Wide Web*, pages 509–518. ACM, 2012.

[21] Jaroslav Hlinka, David Hartman, Martin Vejmelka, Jakob Runge, Norbert Marwan, Jurgen Kurths, and Milan Palus. Reliability of inference of directed climate networks using conditional mutual information. *Entropy*, 15(6):2023–2045, 2013.

[22] Joseph C McBride, Xiaopeng Zhao, Nancy B Munro, Gregory A Jicha, Frederick A Schmitt, Richard J Kryscio, Charles D Smith, and Yang Jiang. Sugihara causality analysis of scalp eeg for detection of early alzheimer's disease. *NeuroImage: Clinical*, 7:258–265, 2015.

[23] Florian Dost. A non-linear causal network of marketing channel system structure. *Journal of Retailing and Consumer Services*, 23:49–57, 2015.

[24] M Cyrus Maher and Ryan D Hernandez. Causemap: fast inference of causality from complex time series. *PeerJ*, 3:e824, 2015.

[25] Emanuele Crosato, Li Jiang, Valentin Lecheval, Joseph T Lizier, X Rosalind Wang, Pierre Tichit, Guy Theraulaz, and Mikhail Prokopenko. Informative and misinformative interactions in a school of fish. *arXiv preprint arXiv:1705.01213*, 2017.

[26] Sachit Butail, Fabrizio Ladu, Davide Spinello, and Maurizio Porfiri. Information flow in animal-robot interactions. *Entropy*, 16(3):1315–1330, 2014.

[27] Sachit Butail, Violet Mwaffo, and Maurizio Porfiri. Model-free information-theoretic approach to infer leadership in pairs of zebrafish. *Physical Review E*, 93(4):042411, 2016.

[28] Takenori Tomaru, Hisashi Murakami, Takayuki Niizato, Yuta Nishiyama, Kohei Sonoda, Toru Moriyama, and Yukio-Pegio Gunji. Information transfer in a swarm of soldier crabs. *Artificial Life and Robotics*, 21(2):177–180, 2016.

[29] Thomas O Richardson, Nicolas Perony, Claudio J Tessone, Christophe AH Bousquet, Marta B Manser, and Frank Schweitzer. Dynamical coupling during collective animal motion. *arXiv preprint arXiv:1311.1417*, 2013.

[30] Warren M Lord, Jie Sun, Nicholas T Ouellette, and Erik M Bollt. Inference of causal information flow in collective animal behavior. *IEEE Transactions on Molecular, Biological and Multi-Scale Communications*, 2(1):107–116, 2016.

[31] James M McCracken and Robert S Weigel. Convergent cross-mapping and pairwise asymmetric inference. *Physical Review E*, 90(6):062903, 2014.

[32] Available at `http://deepeco.ucsd.edu/resources/`.

[33] Ethan R Deyle, Michael Fogarty, Chih-hao Hsieh, Les Kaufman, Alec D MacCall, Stephan B Munch, Charles T Perretti, Hao Ye, and George Sugihara. Predicting climate effects on pacific sardine. *Proceedings of the National Academy of Sciences*, 110(16):6430–6435, 2013.

[34] Thomas Schreiber. Measuring information transfer. *Physical Review Letters*, 85(2):461, 2000.

[35] Angeliki Papana and Dimitris Kugiumtzis. Evaluation of mutual information estimators for time series. *International Journal of Bifurcation and Chaos*, 19(12):4197–4215, 2009.

[36] Joseph T Lizier. Jidt: An information-theoretic toolkit for studying the dynamics of complex systems. *arXiv preprint arXiv:1408.3270*, 2014.

[37] Alexander Kraskov, Harald Stogbauer, and Peter Grassberger. Estimating mutual information. *Physical review E*, 69(6):066138, 2004.

[38] Tomas Svoboda, Daniel Martinec, Tomas Pajdla, Jean-Yves Bouguet, Tomas Werner, and Ondrej Chum. Multi-camera self-calibration. *Czech Technical University, Prague, Czech Republic. tt http://cmp. felk. cvut. cz/ svoboda/SelfCal*, 2003.

[39] Jean-Yves Bouguet. Camera calibration toolbox for matlab. *Public Domain Internet Software*, 2013.

[40] James G Puckett, Douglas H. Kelley, and Nicholas T Ouellette. Searching for effective forces in laboratory insect swarms. *Scientific Reports*, 4, 2014.

[41] Nicholas Orange and Nicole Abaid. A transfer entropy analysis of leader-follower interactions in flying bats. *European Physical Journal: Special Topics*, 224(17):3279–3293, 2015.

[42] *Based on personal email conversation with Dr. Joseph T.entropy, the author of JIDT toolkit, confirmed the use of kernel estimator to evaluate conditional entropy with the present version of JIDT.*

[43] Michael Wibral, Raul Vicente, and Joseph T Lizier. *Directed information measures in neuroscience*. Springer, 2014.

[44] Patricia Wollstadt, Mario Martinez-Zarzuela, Raul Vicente, Francisco J Diaz-Pernas, and Michael Wibral. Efficient transfer entropy analysis of non-stationary neural time series. *PloS one*, 9(7):e102833, 2014.

[45] Joseph T Lizier and Mikhail Prokopenko. Differentiating information transfer and causal effect. *The European Physical Journal B-Condensed Matter and Complex Systems*, 73(4):605–615, 2010.

[46] Michael Wibral, Joseph T Lizier, Sebastian Vogler, Viola Priesemann, and Ralf Galuske. Local active information storage as a tool to understand distributed neural information processing. 2014.

Chapter 6

Conclusions

In this dissertation, we have addressed a two-scale approach to study interactions- one in larger scale, where we study the information exchange in a group and how it enables the group to reach a common decision, and the other in a smaller scale, where we investigate the directionality of the information exchange between pairs of individuals. Particularly, in the large scale approach, we use stochastic consensus and synchronization protocols to study collective behavior that rely on a priori assumptions that individuals seek agreement on a quantity of interest through iterated negotiations. In the small scale approach, we explore two real-world datasets, first, to study opinion formation in humans taking an example from public policy issue and, second, to directly observe how individuals in bat swarms perform pairwise interactions to plan their flight paths.

6.1 Research summary

In Chapter 2, we define a composite model over a stochastically-switching network capturing both collaborative and antagonistic interactions among the agents and study stochastic consensus and synchronization protocols. We consider a general class of agents, so-called conspecifics, which encompasses a wide range of protocols explored in the literature, ranging from Erdős-Rényi random networks to numerosity-constrained networks. The symmetry in the definitions of these random interaction networks enables us to compute closed form expressions for consensus conditions and convergence speed, which are generally lacking in the literature. The theoretical results are validated and discussed using numerical simulations. We find that, for certain selections of system parameters, the presence of antagonistic interactions permits consensus in systems that would not reach accordance otherwise. The results of the present work may find applications in real-world networks, where antagonistic interactions are prevalent, for example international relations, online social media sites, neural networks, and biologically inspired robotic interactions.

In Chapter 3, we study leader-follower consensus and synchronization protocols where both leaders and followers negotiate their states over a stochastically-switching network. The model is inspired by the phenomenon of numerosity, which limits the perception of exact numbers, and have been shown to play an important role in the collective behavior exhibited by animal groups. We derive a closed form expression for the asymptotic convergence factor that provides a necessary and sufficient condition for convergence and is used to study the expected decay rate of disagreement among agents. These results are validated with Monte Carlo simulations. Finally, we explore the dependence of the asymptotic convergence factor on model parameters, which are group size, proportion of leaders, numerosity, and persuasibility using numerical simulations. We find that the system achieves consensus faster with a higher proportion of leaders but this convergence rate is achieved only when all individuals are more stubborn during the decision making process. In addition, increasing the population size necessitates increasing the connectedness of each individual to maintain the systems ability to reach consensus, when the proportion of leaders is kept constant.

In Chapter 4, we target the legalization of same-sex marriage in the United States to understand how this issue captures the relationship between state laws and Senate representatives as it depends on geographic and ideological factors. Using a distance-based correlation metric, we demonstrate how physical proximity and state-government ideology may be used to extract patterns in state-law adoption and senatorial support of same-sex marriage. Results demonstrate that proximal states have a strong similarity in both the state-law and the senators opinions, and states with similar state-government ideology are predictors of the senators opinions. Moreover, we find from a time-lagged correlation that state-laws show maximum dependencies on senators opinions from one year prior. Thus, change in opinion is not only a result of negotiations among the individuals, but also reflects inherent spatial and political similarities. We build a social impact model of state-law adoption in light of these results and verify its predictive power.

In Chapter 5, we choose the system of bats, who are effective users of active sensing, to investigate navigational leadership roles as they fly in pairs. For each bat in the pair, we compute a curvature-based time series from three dimensional trajectories that are captured in a field experiment in a mountain cave in Shandong Province, China. We explore two recent tools from dynamical systems to extract causal relationships between these time series, namely transfer entropy and convergent cross mapping. These tools identify the direction of information transfer between a pair of bats flying together, which allows us to answer the question of whether individuals fly independently of each other or interact to plan flight paths. We find that the identified causal relationships between bats is sensitive to the selected mathematical tools and parameters.

6.2 Future work

This dissertation has demonstrated how interactions can be studied using mathematical modeling, at the same time reveals that real-world interactions are even more complex and lend themselves to further study. Mathematical modeling provides capabilities to introduce biologically inspired phenomena, for example, the implementation of multiple sensing cues in Chapter 2 has been recently verified in a study with bats [1]. The simultaneous presence of antagonistic and collaborative interactions are identified in social networks [2, 3, 4], however its presence in system of bats is an open question and hence requires evidence from field study. Similarly, the study in Chapter 3, demonstrated increased proportion of leaders and stubbornness help in faster decision making at group level which can be verified by adopting real-world leader follower examples as in a system of robots or in representative democracy.

To understand or model public policies, the state-law adoption model provided in Chapter 4 may be considered, and its predictive power can be verified. The distance-based correlation along with topological and ideological distances introduced can be used to detect additional factors that drive real-world opinion dynamics.

Moreover, in the study of bats as in Chapter 5, we identify leadership from rear bat which requires further investigation. The causality detecting methods used in capturing this counter-intuitive phenomenon can also be tested using self-propelled particle models [5], where the information exchange can be set to flow from rear to front individual. The trajectories generated with this modeling approach can be used as a test bed in verifying the ability of these causality detecting methods to correctly identify the rear bat as the leader. Recently new method called Causation Entropy [6] has been introduced to detect causality, which can also be implemented in the study to verify the consistency in the results observed. Furthermore, it has been recently pointed out that bats can imprint the presence of an obstacle in its spatial memory [1] enabling their robust flight. This evidence sets the future direction to use bat trajectory data from other dates in our study since we have abundant video recordings of bat pairs from several other days. Presently, our results reveal leadership from rear bat which is destroyed as obstacles are introduced, and hence it will be interesting to see if the leadership is regained as the bats get aware of the presence of the obstacles.

6.3 References

[1] Zhaodan Kong, Nathan Fuller, Shuai Wang, Kayhan Ozcimder, Erin Gillam, Diane Theriault, Margrit Betke, and John Baillieul. Perceptual modalities guiding bat flight in a native habitat. *Scientific reports*, 6, 2016.

[2] David Easley and Jon Kleinberg. *Networks, crowds, and markets: Reasoning about a highly connected world*. Cambridge University Press, 2010.

[3] Tibor Antal, Paul L Krapivsky, and Sidney Redner. Social balance on networks: The dynamics of friendship and enmity. *Physica D: Nonlinear Phenomena*, 224(1):130–136, 2006.

[4] Michael Szell, Renaud Lambiotte, and Stefan Thurner. Multirelational organization of large-scale social networks in an online world. *Proceedings of the National Academy of Sciences*, 107(31):13636–13641, 2010.

[5] Yuan Lin and Nicole Abaid. Modeling perspectives on echolocation strategies inspired by bats flying in groups. *Journal of theoretical biology*, 387:46–53, 2015.

[6] Pileun Kim, Jonathan Rogers, Jie Sun, and Erik Bollt. Causation entropy identifies sparsity structure for parameter estimation of dynamic systems. *Journal of Computational and Nonlinear Dynamics*, 12(1):011008, 2017.

Appendix A

Appendix for Chapter 3

A.1 Table

A.2 Spectrum of G

It can be verified that G has at most twelve distinct eigenvalues and corresponding eigenspaces. The eigenvectors from the eigenspaces have the form $\boldsymbol{v} = [\boldsymbol{v}_1{}^T \boldsymbol{v}_2{}^T \cdots \boldsymbol{v}_N{}^T]^T$ and satisfy the eigenvalue equation $G\boldsymbol{v} = \lambda\boldsymbol{v}$. The eigenvalues are given as follows:

$$\lambda_1 = \epsilon^2\kappa_2 n + \sqrt{\epsilon^4\kappa_3 n^2 - \epsilon^3\kappa_5 n^2 + \epsilon^2\kappa_4 n^2} - \epsilon\kappa_1 n + 1, \tag{A.1a}$$

$$\lambda_2 = \epsilon^2\kappa_7 n - \epsilon\kappa_6 n + 1, \tag{A.1b}$$

$$\lambda_{3,12} = \gamma_1 + (r_{3,12})\gamma_5, \tag{A.1c}$$

$$\lambda_4 = \theta_1 + \theta_6 - \theta_{29} - \theta_{34}, \tag{A.1d}$$

$$\lambda_5 = \theta_{15} + \theta_{20} - \theta_{86} - \theta_{91}, \tag{A.1e}$$

$$\lambda_6 = \epsilon^2\kappa_2 n - \sqrt{\epsilon^4\kappa_3 n^2 - \epsilon^3\kappa_5 n^2 + \epsilon^2\kappa_4 n^2} - \epsilon\kappa_1 n + 1, \tag{A.1f}$$

$$\lambda_{7,8} = \tau_9 + (r_{7,8})\tau_{10}, \tag{A.1g}$$

$$\lambda_9 = \theta_{15} + \theta_{17} - l\left(\theta_{48} + \theta_{50}\right) + (l-1)\left(\theta_{86} + \theta_{88}\right), \tag{A.1h}$$

$$\lambda_{10} = \theta_1 + \theta_3 - \theta_{29} - \theta_{31}, \tag{A.1i}$$

$$\lambda_{11} = 0. \tag{A.1j}$$

where $\kappa_1 \ldots \kappa_7, \gamma_1, \gamma_5, \tau_9, \tau_{10}$ can be found in Appendix A.3, $r_{3,12}$ are the two solutions r of the quadratic equation:

$$(\gamma_2 + \gamma_3 + \gamma_7) + r(\gamma_4 + \gamma_6 + \gamma_8 + \gamma_5 - \gamma_1) - r^2(\gamma_5) = 0$$

and $r_{7,8}$ are the two solutions r of the quadratic equation:

$$\tau_1 + \tau_3 + r(\tau_2 + \tau_5 + \tau_6 + \tau_8 - \tau_9) - r^2(\tau_{10}) = 0.$$

From the expressions it can be further verified that all of the eigenvalues are real. The eigenspaces corresponding to these eigenvalues are

$$\Gamma^{(1),(6)} = \Bigg\{ v \in \mathbb{R}^{N^2} : v_i = (\mu_1 - \mu_2)e_i + \mu_2 1_f + \mu_3 1_l \text{ with } (\mu_1 - \mu_2) + f\mu_2 + l\mu_3 = 0,$$

$$\frac{\mu_3}{\mu_2} = r_{1,6} \text{ when } i \in \mathcal{F} \text{and } v_i = \mu_3 1_f + \mu_4 1_l \text{ with } f\mu_3 + l\mu_4 = 0 \text{ when } i \in \mathcal{L} \Bigg\}; \tag{A.2a}$$

$$\Gamma^{(2)} = \Bigg\{ v \in \mathbb{R}^{N^2} : v_i = (\mu_1 - \mu_2)e_i + \mu_2 1_f + \mu_3 1_l \text{ with } (\mu_1 - \mu_2) + f\mu_2 + l\mu_3 = 0, \frac{\mu_2}{\mu_3} = {r_2}^{(1)}$$

when $i \in \mathcal{F}$ and $v_i = \mu_3 1_f + \mu_4 1_l + (\mu_5 - \mu_4)e_i$ with $f\mu_3 + l\mu_4 + (\mu_5 - \mu_4) = 0$,

$$\frac{\mu_3}{\mu_4} = {r_2}^{(2)} \text{ when } i \in \mathcal{L} \Bigg\}; \tag{A.2b}$$

$$\Gamma^{(3)} = \Bigg\{ v \in \mathbb{R}^{N^2} : v_i = \sum_{k=f+1}^{N} \mu_k e_k \text{ with } \sum_{j=f+1}^{N} \mu_j = 0 \text{ when } i \in \mathcal{F} \text{ and } v_i = \mu_i 1_f + \sum_{k=f+1}^{N} \beta_k^i e_k$$

with $\beta_{f+m}^{f+m} = (r_3)\,\mu_{f+m},\ \beta_{f+m}^{f+n}(m \neq n) = \left(\dfrac{f + r_3}{2 - l}\right)(\mu_{f+n} + \mu_{f+m})$ where $m, n \in \mathcal{L}$

when $i \in \mathcal{L} \Bigg\}$; (A.2c)

$$\Gamma^{(4)} = \Bigg\{ v \in \mathbb{R}^{N^2} : v_i = \sum_{j=f+1}^{N} \mu_j^i e_j \text{ with } \sum_{j=f+1}^{N} \mu_j^i = 0, \sum_{i=1}^{f} \mu_j^i = 0 \text{ when } i \in \mathcal{F} \text{ and}$$

$$v_i = \sum_{j=1}^{f} \mu_j^i e_j \text{ with } \sum_{j=1}^{f} \mu_j^i = 0,\ \sum_{i=f+1}^{N} \mu_j^i = 0 \text{ when } i \in \mathcal{L} \Bigg\}; \tag{A.2d}$$

$$\Gamma^{(5)} = \Bigg\{ v \in \mathbb{R}^{N^2} : v_i = 0 \text{ when } i \in \mathcal{F} \text{ and } v_i = \sum_{k=f+1}^{N} \mu_k^i e_k \text{ with } \sum_{k=f+1}^{N} \mu_k^i = 0,$$

$$\sum_{i=f+1}^{N} \mu_k^i = 0,\ \mu_i^i = 0 \text{ when } i \in \mathcal{L} \Bigg\}; \tag{A.2e}$$

$$\Gamma^{(7),(8)} = \Bigg\{ v \in \mathbb{R}^{N^2} : v_i = (\mu_i)\,1_l + \sum_{k=1}^{f} \beta_k^i e_k \text{ with } \beta_k^k = (r_{7,8})\,\mu_k,\ \beta_m^n(m \neq n) =$$

$$\left(\frac{l + r_{7,8}}{2 - f}\right)(\mu_n + \mu_m) \text{ where } m, n \in \mathcal{F} \text{ and } \sum_{j=1}^{f} \mu_j = 0 \text{ when } i \in \mathcal{F}$$

$$\text{and } v_i = \sum_{k=1}^{f} \mu_k e_k \text{ when } i \in \mathcal{L} \Bigg\}; \tag{A.2f}$$

$$\Gamma^{(9)} = \Bigg\{ v \in \mathbb{R}^{N^2} : v_i = (\mu_i)\, 1_l + \sum_{k=1}^{f} \beta_k^i e_k \text{ with } \beta_k^k = 0, \beta_m^n (m \neq n) = \left(\frac{l}{f}\right)(\mu_m - \mu_n)$$

$$\text{where } m, n \in \mathcal{F} \text{ and } \sum_{j=1}^{f} \mu_j = 0 \text{ when } i \in \mathcal{F} \text{ and } v_i = \sum_{k=1}^{f} \mu_k e_k \text{when } i \in \mathcal{L} \Bigg\}; \tag{A.2g}$$

$$\Gamma^{(10)} = \Bigg\{ v \in \mathbb{R}^{N^2} : v_i = \sum_{k=1}^{f} \mu_k^i e_k \text{ with } \mu_i^i = 0,\ \sum_{k=1}^{f} \mu_k^i = 0, \sum_{i=1}^{f} \mu_k^i = 0 \text{ when } i \in \mathcal{F}$$

$$\text{and } v_i = 0 \text{ when } i \in \mathcal{L} \Bigg\}; \tag{A.2h}$$

$$\Gamma^{(11)} = \Bigg\{ v \in \mathbb{R}^{N^2} : v = \omega \otimes 1_N \text{ and } v = 1_N \otimes \omega, \omega \in \mathbb{R}^N \Bigg\}; \tag{A.2i}$$

$$\Gamma^{(12)} = \Bigg\{ v \in \mathbb{R}^{N^2} : v_i = \sum_{k=f+1}^{N} \mu_k e_k \text{ with } \sum_{j=f+1}^{N} \mu_j = 0 \text{ when } i \in \mathcal{F} \text{ and } v_i = \nu_i 1_f +$$

$$\sum_{k=f+1}^{N} \beta_k^i e_k \text{ with } \beta_{f+n}^{f+m} = -\left(\frac{f}{l}\right)(\mu_{f+n} + \nu_{f+m}) \text{ and } \sum_{j=f+1}^{N} \nu_j = 0 \text{ where } m, n \in \mathcal{L} \text{ when } i \in \mathcal{L} \Bigg\}. \tag{A.2j}$$

We comment that we do not provide explicit expressions for r_1, r_6, ${r_2}^{(1)}$, and ${r_2}^{(2)}$ due to their highly intractable forms. However, the eigenvectors corresponding to the eigenspaces $\Gamma^{(1)}$, $\Gamma^{(2)}$, and $\Gamma^{(6)}$ can be shown to satisfy the eigenvalue equation $G\boldsymbol{v} = \lambda \boldsymbol{v}$ without the expressions for these ratios. These expressions can be recovered by substituting both eigenvalues and eigenspaces provided here into the eigenvalue equation. It can be checked that the eigenspaces $\Gamma^{(1)}$, $\Gamma^{(2)}$, and $\Gamma^{(6)}$ are mutually linearly independent, as are the triplet $\Gamma^{(7)}$, $\Gamma^{(8)}$, and $\Gamma^{(9)}$ and the pair $\Gamma^{(3)}$ and $\Gamma^{(12)}$. The rest of the eigenspaces are orthogonal to each other. Counting the number of degrees of freedom for eigenvectors in each eigenspace, we find the following eigenspace dimensions: 1 for $\Gamma^{(1)}$, $\Gamma^{(2)}$, and $\Gamma^{(6)}$; $l-1$ for $\Gamma^{(3)}$; $2(l-1)(f-1)$ for $\Gamma^{(4)}$; $(l-1)(l-2)-1$ for $\Gamma^{(5)}$; $f-1$ for $\Gamma^{(7)}$, $\Gamma^{(8)}$, and $\Gamma^{(9)}$; $(f-1)(f-2)-1$ for $\Gamma^{(10)}$; $2N-1$ for $\Gamma^{(11)}$; and $2l-2$ for $\Gamma^{(12)}$. Since the eigenspaces are all pairwise linearly independent, their direct sum has dimension N^2, that is, G has N^2 linearly independent eigenvectors. Thus G has a spectrum comprised of $\{\lambda_i\}_{i=1}^{12}$ and is diagonalizable.

A.3 Parameters

The parameters used in (3.15) and in (A.1) are

$$\alpha_1 = \epsilon^2 n^2 \left(\frac{f-1}{(N-1)^2}+1\right) - \epsilon n;\;\; \alpha_2 = \alpha_1 + \frac{\epsilon^2 n^2 N}{(N-1)^2};\;\; \alpha_3 = \frac{\epsilon^2 l n^2}{(l-1)(N-1)} + \theta_6;$$

$$\alpha_4 = \frac{\epsilon^2 n^2 (f-2N)}{(N-1)^2} + \frac{\epsilon n}{N-1};\;\; \alpha_5 = \frac{\epsilon^2 n^2 (f-N)}{(N-1)^2} + \frac{\epsilon n}{N-1};\;\; \alpha_6 = \frac{\epsilon n}{N-1} +$$

$$\epsilon^2 n^2 \left(\frac{f}{(N-1)^2} + \frac{l-2}{(l-1)(N-1)} - \frac{1}{l-1} - \frac{1}{N-1}\right);\;\; \alpha_7 = \frac{\epsilon l n}{(l-1)N} +$$

$$\frac{\epsilon^2 l n^2 \left(\frac{f}{N-1} - \frac{N-1}{l-1} + \frac{l-2}{l-1} - 1\right)}{(l-1)N};\;\; \theta_1 = \frac{(N-1)(1-\epsilon n)}{N} - \frac{\epsilon n (f-1)}{N(N-1)};$$

$$\theta_2 = \frac{\frac{\alpha_1 f}{N} + (f-1)\theta_{11} - \theta_1}{N};\;\; \theta_3 = \alpha_1 + \theta_{11};\;\; \theta_4 = -\left(\frac{\alpha_1}{N} + \theta_{11}\right);\;\; \theta_5 = -\frac{\theta_3}{N};$$

$$\theta_6 = \frac{\epsilon^2 l n^2 \left(\frac{f-1}{N-1} + N - 1\right)}{(l-1)N} - \frac{\epsilon l n (N-1)}{(l-1)N};\;\; \theta_7 = -\frac{\theta_6}{l};\;\; \theta_8 = -\frac{\Delta_1 \epsilon^2}{N};\;\; \theta_9 = \frac{-f\theta_8 - \theta_{10}}{N};$$

$$\theta_{10} = \frac{\Delta_1 \epsilon^2}{N-1};\;\; \theta_{11} = -\frac{\Delta_1 \epsilon^2}{N(N-1)};\;\; \theta_{15} = \theta_1 - \frac{\epsilon n}{N-1};\;\; \theta_{16} = \frac{\alpha_2 f}{N^2} + \frac{f\theta_{11}}{N} - \frac{\theta_{15}}{N};$$

$$\theta_{17} = \alpha_2 + \theta_{11};\;\; \theta_{18} = -\left(\frac{\alpha_2}{N} + \theta_{11}\right);\;\; \theta_{19} = -\frac{\theta_{17}}{N};\;\; \theta_{20} = \alpha_3 + \theta_{26};\;\; \theta_{21} = -\left(\frac{\alpha_3}{l} + \theta_{26}\right);$$

$$\theta_{23} = \frac{-f\theta_8}{N} - \frac{l\theta_{27}}{N} - \frac{\theta_{24}}{N};\;\; \theta_{24} = \frac{\Delta_2 \epsilon^2 l}{(l-1)N};\;\; \theta_{26} = -\frac{\theta_{24}}{l};\;\; \theta_{27} = -\frac{\Delta_2 \epsilon^2}{N};\;\; \theta_{28} = \frac{(l-2)\theta_{26}}{N};$$

$$\theta_{29} = \frac{2\epsilon n}{N-1} - \frac{\frac{\epsilon f n}{N-1} + 1}{N};\;\; \theta_{30} = \frac{\frac{\alpha_4 f}{N} + (f-1)\theta_{11} + \theta_{10} - \theta_{29}}{N};\;\; \theta_{31} = \alpha_4 + \theta_{11};\;\; \theta_{32} = -\frac{\alpha_4}{N}$$

$$- \theta_{11};\;\; \theta_{33} = -\frac{\alpha_4 + \theta_{11}}{N};\;\; \theta_{34} = \frac{\epsilon^2 l n^2 \left(\frac{f}{N} - 2\right)}{(l-1)(N-1)} + \frac{\epsilon l n}{(l-1)N};\;\; \theta_{35} = -\frac{\theta_{34}}{l};\;\; \theta_{36} = \Delta_1 \epsilon^2;$$

$$\theta_{37} = \frac{-f\theta_8 - \theta_{10} - \theta_{36}}{N};\;\; \theta_{48} = \frac{1}{N}\left(\frac{\epsilon n (N-f)}{(N-1)} - 1\right);\;\; \theta_{49} = \frac{\frac{\alpha_5 f}{N} + f\theta_{11} + \theta_{10} - \theta_{48}}{N};$$

$$\theta_{50} = \alpha_5 + \theta_{11};\;\; \theta_{51} = -\frac{\alpha_5}{N} - \theta_{11};\;\; \theta_{52} = -\frac{\alpha_5 + \theta_{11}}{N};\;\; \theta_{53} = \theta_{26} + \theta_{72};\;\; \theta_{54} = -\left(\frac{\theta_{72}}{l} + \theta_{26}\right);$$

$$\theta_{56} = \frac{-f\theta_8 - l\theta_{27} - \theta_{24} - \theta_{36}}{N};\;\; \theta_{68} = \frac{\frac{\alpha_5 f}{N} + (f-1)\theta_{11} - \theta_{48}}{N};\;\; \theta_{72} = \frac{\epsilon l n}{(l-1)N}$$

$$- \frac{\epsilon^2 l n^2 (N-f)}{(l-1)N(N-1)};\;\; \theta_{73} = -\frac{\theta_{72}}{l};\;\; \theta_{86} = \frac{\epsilon n}{N}\left(-\frac{f}{(N-1)} + \frac{N-1}{(l-1)} + \frac{2-l}{(l-1)} + 1\right) - \frac{1}{N};$$

$$\theta_{87} = \frac{\frac{\alpha_6 f}{N} + f\theta_{11} - \theta_{86}}{N};\;\; \theta_{88} = \alpha_6 + \theta_{11};\;\; \theta_{89} = -\left(\frac{\alpha_6}{N} + \theta_{11}\right);\;\; \theta_{90} = -\frac{\alpha_6 + \theta_{11}}{N};$$

$$\theta_{91} = \alpha_7 + \theta_{26};\;\; \theta_{92} = -\left(\frac{\alpha_7}{l} + \theta_{26}\right);\;\; \theta_{93} = \Delta_2 \epsilon^2;\;\; \theta_{94} = \frac{-f\theta_8 - l\theta_{27} - \theta_{24} - \theta_{93}}{N};$$

$\theta_{96} = \dfrac{\Delta_2\epsilon^2}{l-1}$; $\theta_{103} = \dfrac{(l-2)\theta_{26}+\theta_{96}}{N}$; $\theta_{12} = \theta_{40} = \theta_{43} = \theta_{44} = \theta_{59} = \theta_{81} = \theta_{82} = \theta_{11}$;
$\theta_{13} = \theta_{14} = \theta_{25} = \theta_{45} = \theta_{46} = \theta_{47} = \theta_{62} = \theta_{66} = \theta_{74} = \theta_{76} = \theta_{77} = \theta_{78} = \theta_{83} = \theta_{84} =$
$\theta_{85} = \theta_{95} = \theta_{100} = 0$; $\theta_{22} = \theta_{41} = \theta_{60} = \theta_{79} = \theta_{98} = \theta_8$; $\theta_{39} = \theta_{42} = \theta_{58} = \theta_{80} =$
$-\theta_{38} = -\theta_{57} = \theta_{10}$; $\theta_{55} = \theta_{36}$; $\theta_{61} = \theta_{99} = \theta_{24}$; $\theta_{63} = \theta_{97} = \theta_{101} = \theta_{26}$; $\theta_{65} = \theta_{28}$;
$\theta_{67} = \theta_{48}$; $\theta_{69} = \theta_{50}$; $\theta_{70} = \theta_{51}$; $\theta_{71} = \theta_{52}$; $\theta_{75} = \theta_9$; $\theta_{102} = \theta_{64} = \theta_{27}$; $\theta_{104} = -\theta_{96}$;
$K_1 = 2n(N-1)(-l+N-1)\left(-l^2N - l(N+2) + N^3 - 3N^2 + 3N - 2\right)$
$+ n^2\left(l^4(N-2) - 2l^3N - l^2\left(2N^3 - 6N^2 + 5N + 2\right) + 2l\left(N^3 - N^2 + N - 2\right) + (N-2)\right.$
$\left.\left(N^2 - N + 1\right)^2\right) + (N-2)(N-1)^2(l-N+1)^2$;
$K_2 = n\left((l-N)\left(l^2(N-2) - lN - N^3 + 3N^2 - 3N + 2\right) - 2l\right) + (N-1)N(-l+N-2)$
$(-l+N-1)$; $K_3 = \left(N^2 - 3N + 2\right)\left(l^2n + l(n-N+1) + n\left(N^2 - N + 1\right) + (N-1)^2\right)$;
$\kappa_1 = \dfrac{f^2 + f(3l-2) + 2l(l-2)}{(N-2)(N-1)}$; $\kappa_2 = \dfrac{K_3}{2(N-2)(N-1)^3}$; $\kappa_3 = \dfrac{K_1}{4(N-2)(N-1)^4}$;
$\kappa_4 = \dfrac{f^2}{(N-1)^2}$; $\kappa_5 = \dfrac{K_2}{(N-2)(N-1)^3}$; $\kappa_6 = \dfrac{2l}{l-1}$; $\kappa_7 = \dfrac{ln}{(l-1)^2} + n + 1$; $\kappa_8 = \kappa_1 - \kappa_6$;
$\kappa_9 = \kappa_7 - \kappa_2$; $\kappa_{10} = \kappa_9^2 - \kappa_3$; $\kappa_{11} = \kappa_8^2 - \kappa_4$; $\kappa_{12} = \kappa_5 + 2\kappa_8\kappa_9$; $\gamma_1 = \theta_{15} + \theta_{17} - \theta_{86} - \theta_{88}$
$+ f\left(\theta_{103} + \theta_{19} - \theta_{26} - \theta_{28} - \theta_{90}\right)$; $\gamma_2 = f\left(\theta_{103} + \theta_{19} - \theta_{21} - \theta_{26} - \theta_{28} - \theta_{90} + \theta_{92}\right)$;
$\gamma_3 = f\left(-\theta_{26} + \theta_{48} + \theta_{72} - \theta_{86} - \theta_{91}\right)$; $\gamma_4 = \theta_{15} + \theta_{20} - \theta_{86} - \theta_{91}$; $\gamma_5 = \gamma_6 = \theta_{23} - \theta_{26} - \theta_{94}$;
$\gamma_7 = -2f\theta_{96}$; $\gamma_8 = -\theta_{93} - \theta_{96}$; $\tau_1 = l\left(-\theta_{29} - \theta_{31} + \theta_{48} + \theta_{50}\right)$; $\tau_2 = \theta_1 - \theta_{29} - \theta_{31} + \theta_3$;
$\tau_3 = \theta_{33}l - \theta_5 l$; $\tau_5 = -\theta_{10} - \theta_{36}$; $\tau_6 = -\theta_{11} - \theta_{37} + \theta_9$; $\tau_8 = \theta_{10}$;
$\tau_9 = \theta_{15} + \theta_{17} - l(\theta_{48} + \theta_{50}) + (l-1)(\theta_{86} + \theta_{88})$; $\tau_{10} = \theta_{10}$.

Table A.1: Terms of $\mathbf{E}[L \otimes L]$

$\boldsymbol{i = j, k = m}$	$k, m \in \mathcal{F}$	$k, m \in \mathcal{L}$	
$i, j \in \mathcal{F}$	n^2	n^2	
$i, j \in \mathcal{L}$	n^2	n^2	
$\boldsymbol{i = j, k \neq m}$	$k \in \mathcal{F}, m \in \mathcal{N}$	$k \in \mathcal{L}, m \in \mathcal{F}$	$k, m \in \mathcal{L}$
$i, j \in \mathcal{F}$	$\dfrac{-n^2}{(N-1)}$	0	$\dfrac{-n^2}{(N-1)}$
$i, j \in \mathcal{L}$	$\dfrac{-n^2}{(N-1)}$	0	$\dfrac{-n^2}{(N-1)}$
$\boldsymbol{i \neq j, k = m}$	$k, m \in \mathcal{F}$	$k, m \in \mathcal{L}$	
$i \in \mathcal{F}, j \in \mathcal{N}$	$\dfrac{-n^2}{(N-1)}$	$\dfrac{-n^2}{(N-1)}$	
$i, j \in \mathcal{L}$	$\dfrac{-n^2}{(N-1)}$	$\dfrac{-n^2}{(N-1)}$	
$i \in \mathcal{L}, j \in \mathcal{F}$	0	0	
$\boldsymbol{i \neq j, k \neq m}$ $\boldsymbol{i = k, j = m}$	$k \in \mathcal{F}, m \in \mathcal{N}$	$k \in \mathcal{L}, m \in \mathcal{F}$	$k, m \in \mathcal{L}$
$i \in \mathcal{F}, j \in \mathcal{N}$	$\dfrac{n}{(N-1)}$	N/A	N/A
$i \in \mathcal{L}, j \in \mathcal{F}$	N/A	0	N/A
$i, j \in \mathcal{L}$	N/A	N/A	$\dfrac{n}{(l-1)}$
$\boldsymbol{i \neq j, k \neq m}$ $\boldsymbol{i = k, j \neq m}$	$k \in \mathcal{F}, m \in \mathcal{N}$	$k \in \mathcal{L}, m \in \mathcal{F}$	$k, m \in \mathcal{L}$
$i \in \mathcal{F}, j \in \mathcal{N}$	$\dfrac{n(n-1)}{(N-1)(N-2)}$	N/A	N/A
$i, j \in \mathcal{L}$	N/A	N/A	$\dfrac{n(n-1)}{(l-1)(l-2)}$
$\boldsymbol{i \neq j, k \neq m}$ $\boldsymbol{i \neq k}$	$k \in \mathcal{F}, m \in \mathcal{N}$	$k \in \mathcal{L}, m \in \mathcal{F}$	$k, m \in \mathcal{L}$
$i \in \mathcal{F}, j \in \mathcal{N}$	$\dfrac{n^2}{(N-1)^2}$	0	$\dfrac{n^2}{(N-1)(l-1)}$
$i, j \in \mathcal{L}$	$\dfrac{n^2}{(N-1)(l-1)}$	0	$\dfrac{n^2}{(l-1)^2}$

Appendix B

3D trajectories and curvatures of bat pairs

The plots of original 3D data of 30 bat trajectory pairs and their corresponding curvature time series are presented here.

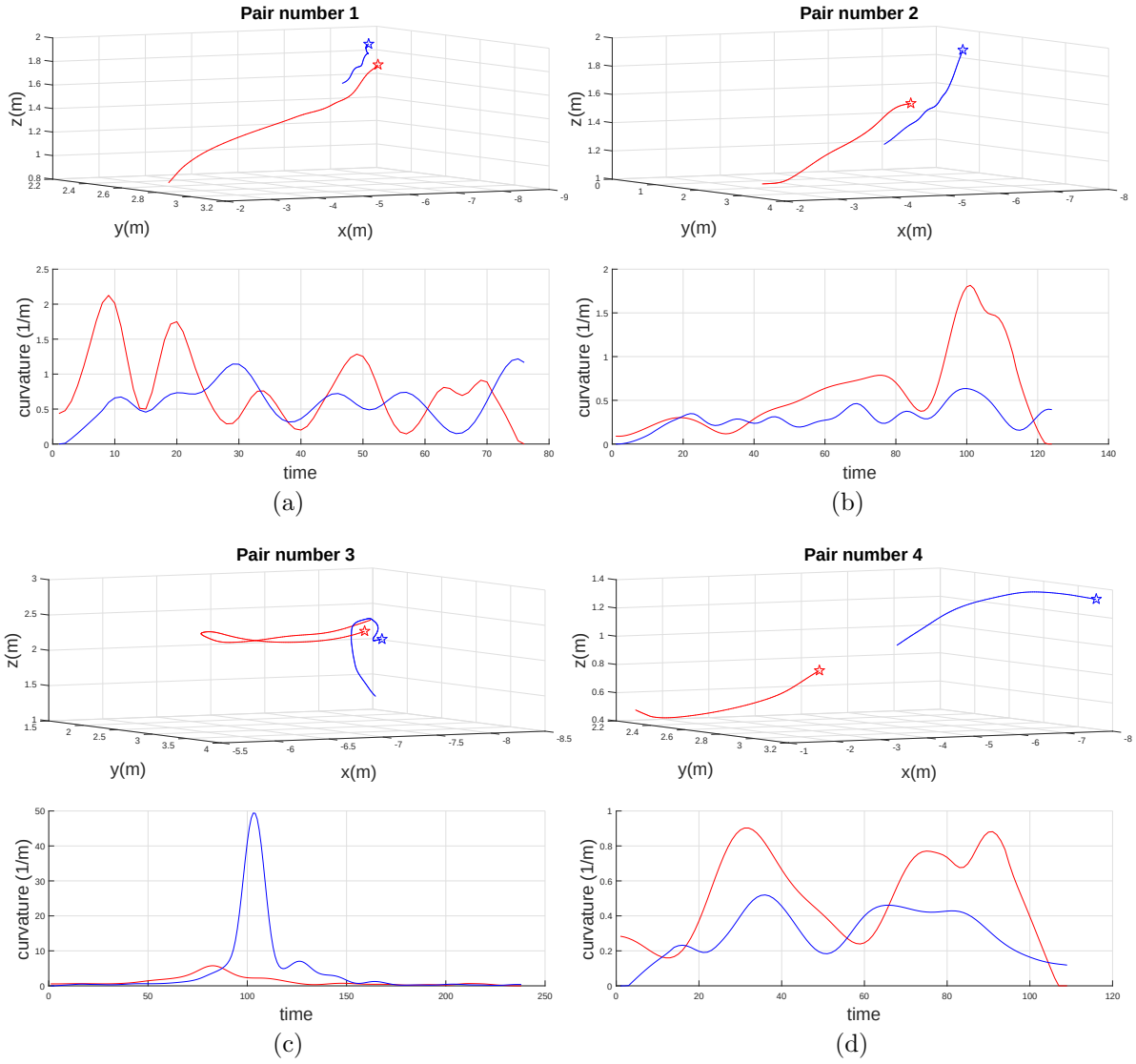

Figure B.1: 3D trajectories and corresponding curvatures of bat pairs from (a) pair number 1, (b) pair number 2, (c) pair number 3, (b) pair number 4. Front and the rear bats are denoted by red and blue lines, respectively, and the symbol star is used to represent the start of the path.

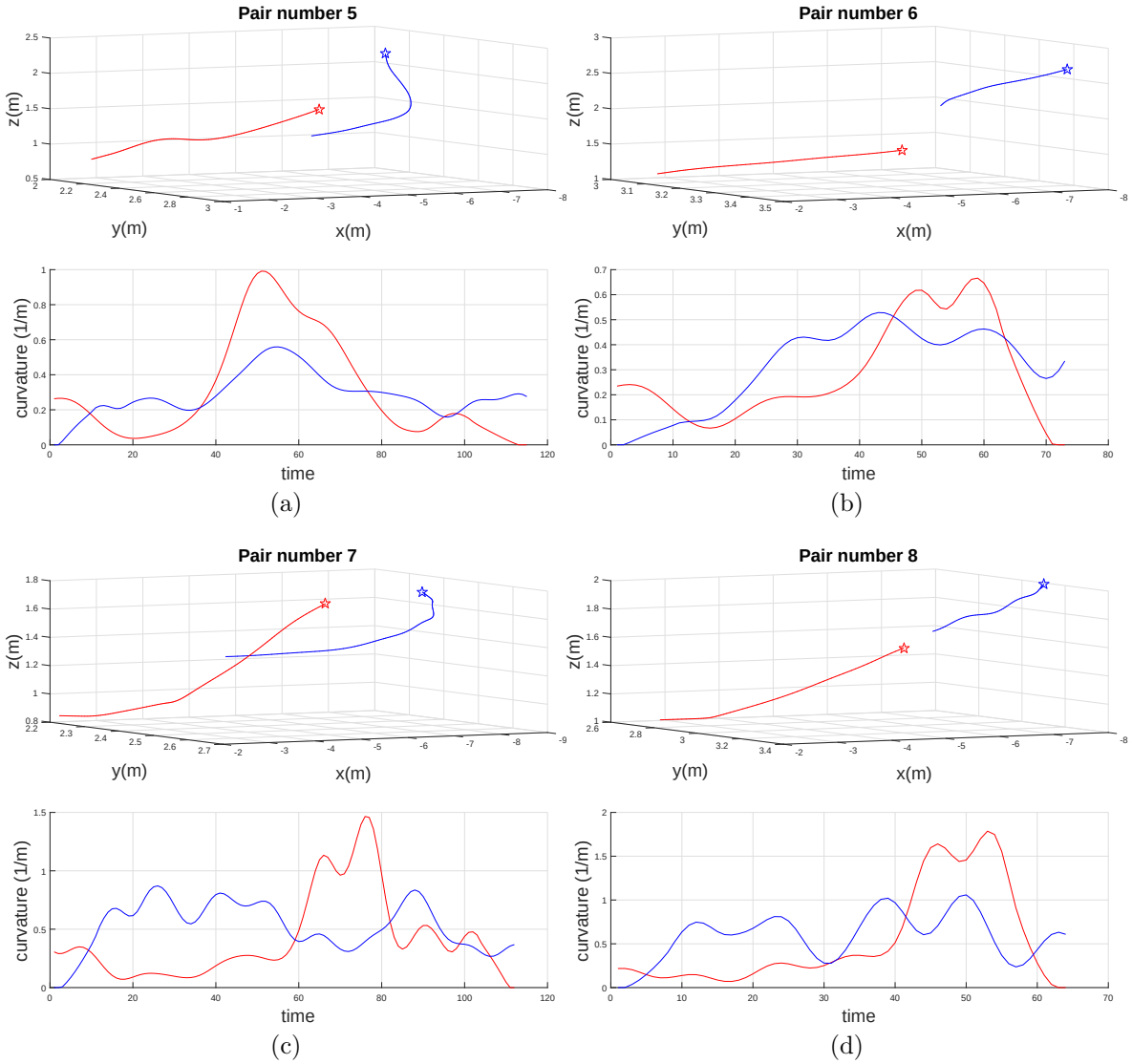

Figure B.2: 3D trajectories and corresponding curvatures of bat pairs from (a) pair number 5, (b) pair number 6, (c) pair number 7, (b) pair number 8. Front and the rear bats are denoted by red and blue lines, respectively, and the symbol star is used to represent the start of the path.

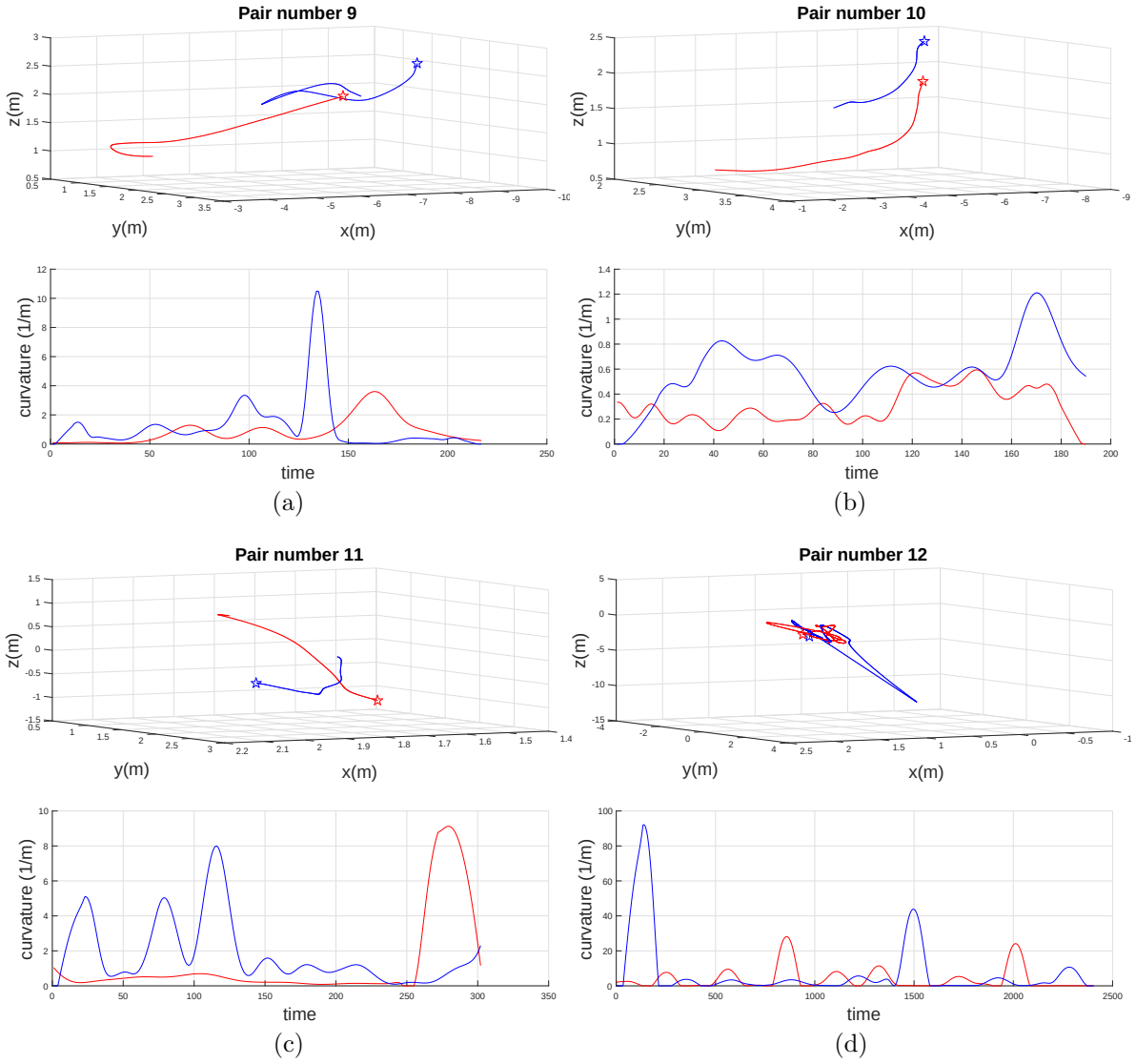

Figure B.3: 3D trajectories and corresponding curvatures of bat pairs from (a) pair number 9, (b) pair number 10, (c) pair number 11, (b) pair number 12. Front and the rear bats are denoted by red and blue lines, respectively, and the symbol star is used to represent the start of the path.

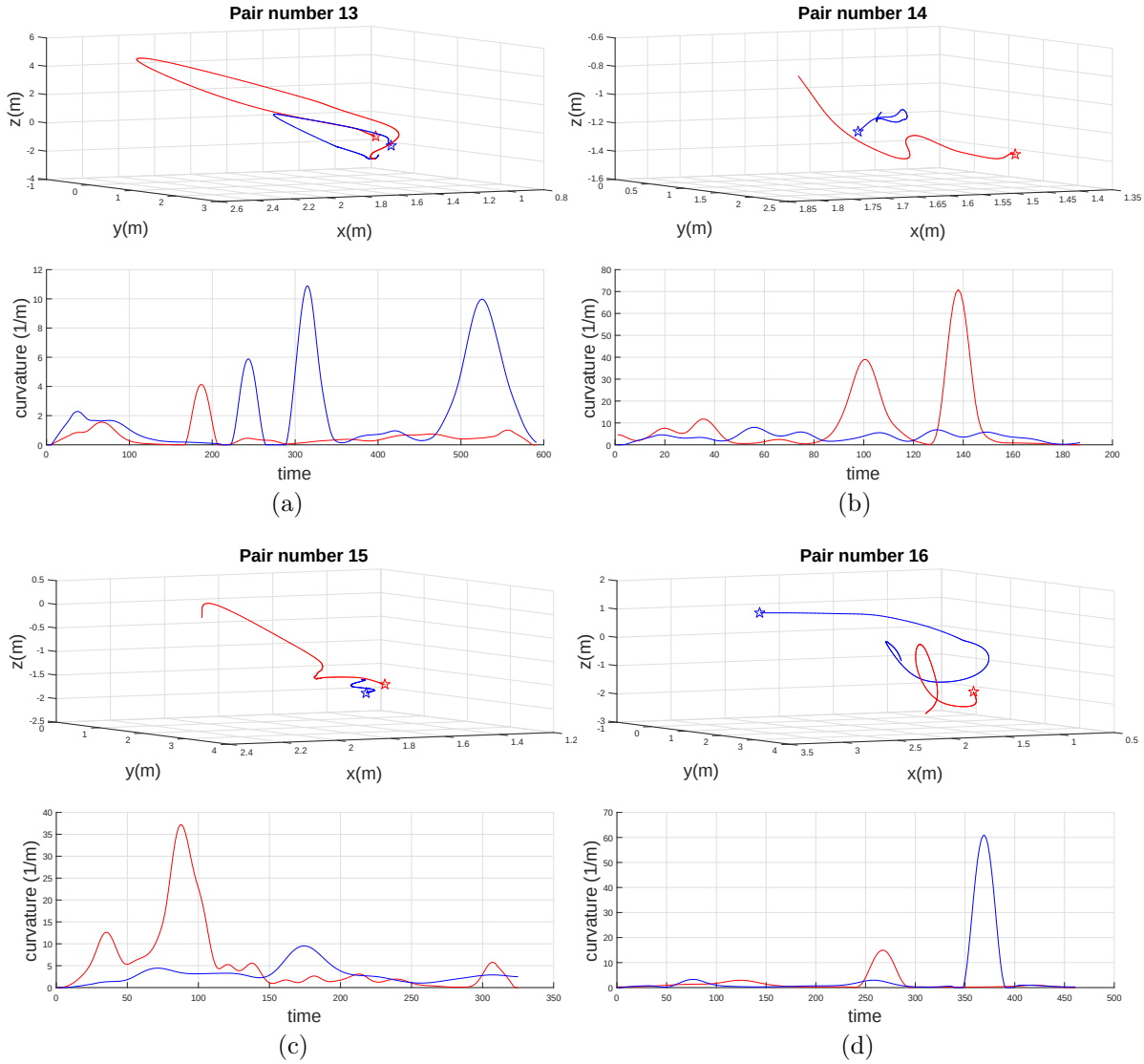

Figure B.4: 3D trajectories and corresponding curvatures of bat pairs from (a) pair number 13, (b) pair number 14, (c) pair number 15, (d) pair number 16. Front and the rear bats are denoted by red and blue lines, respectively, and the symbol star is used to represent the start of the path.

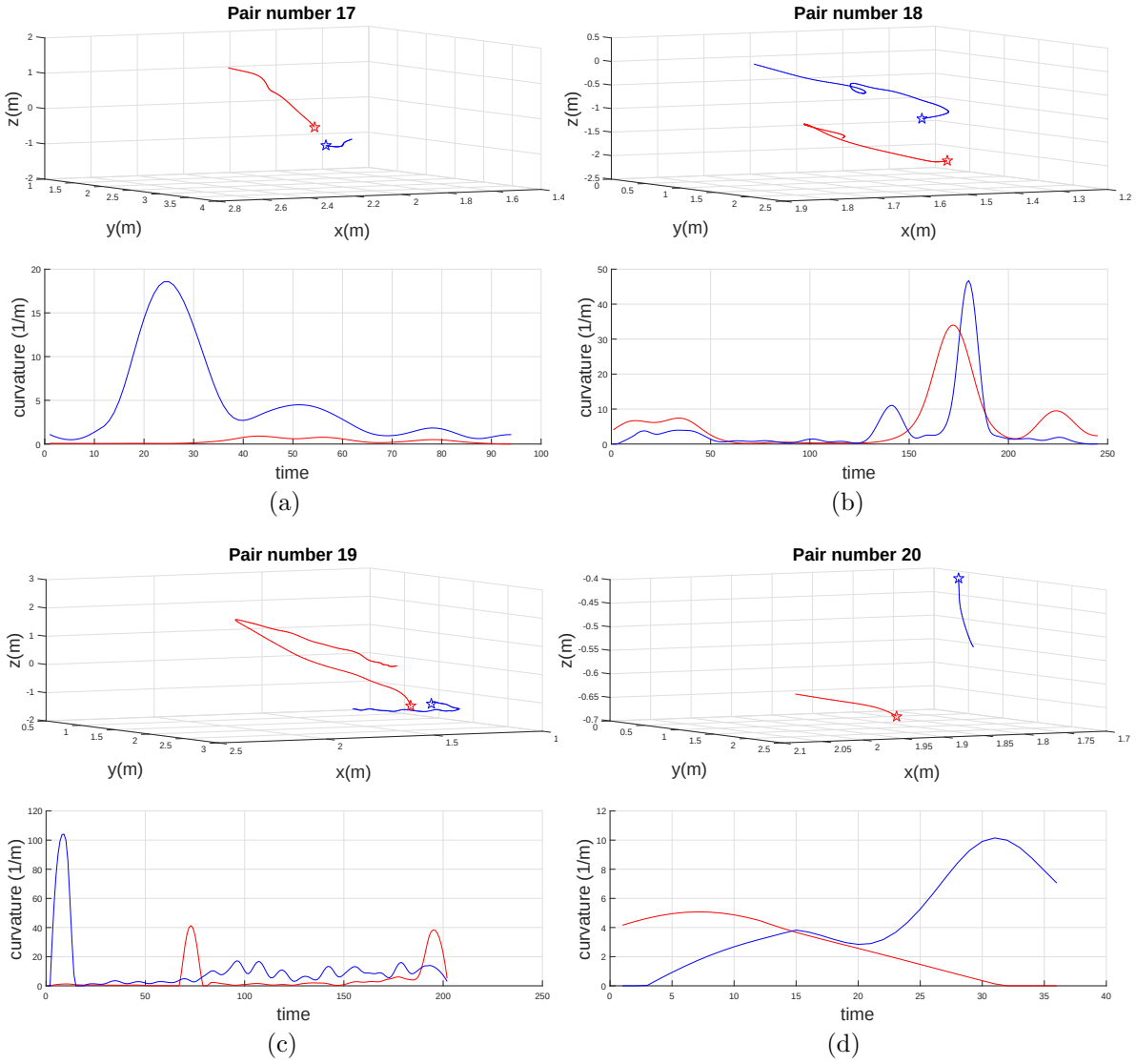

Figure B.5: 3D trajectories and corresponding curvatures of bat pairs from (a) pair number 17, (b) pair number 18, (c) pair number 19, (d) pair number 20. Front and the rear bats are denoted by red and blue lines, respectively, and the symbol star is used to represent the start of the path.

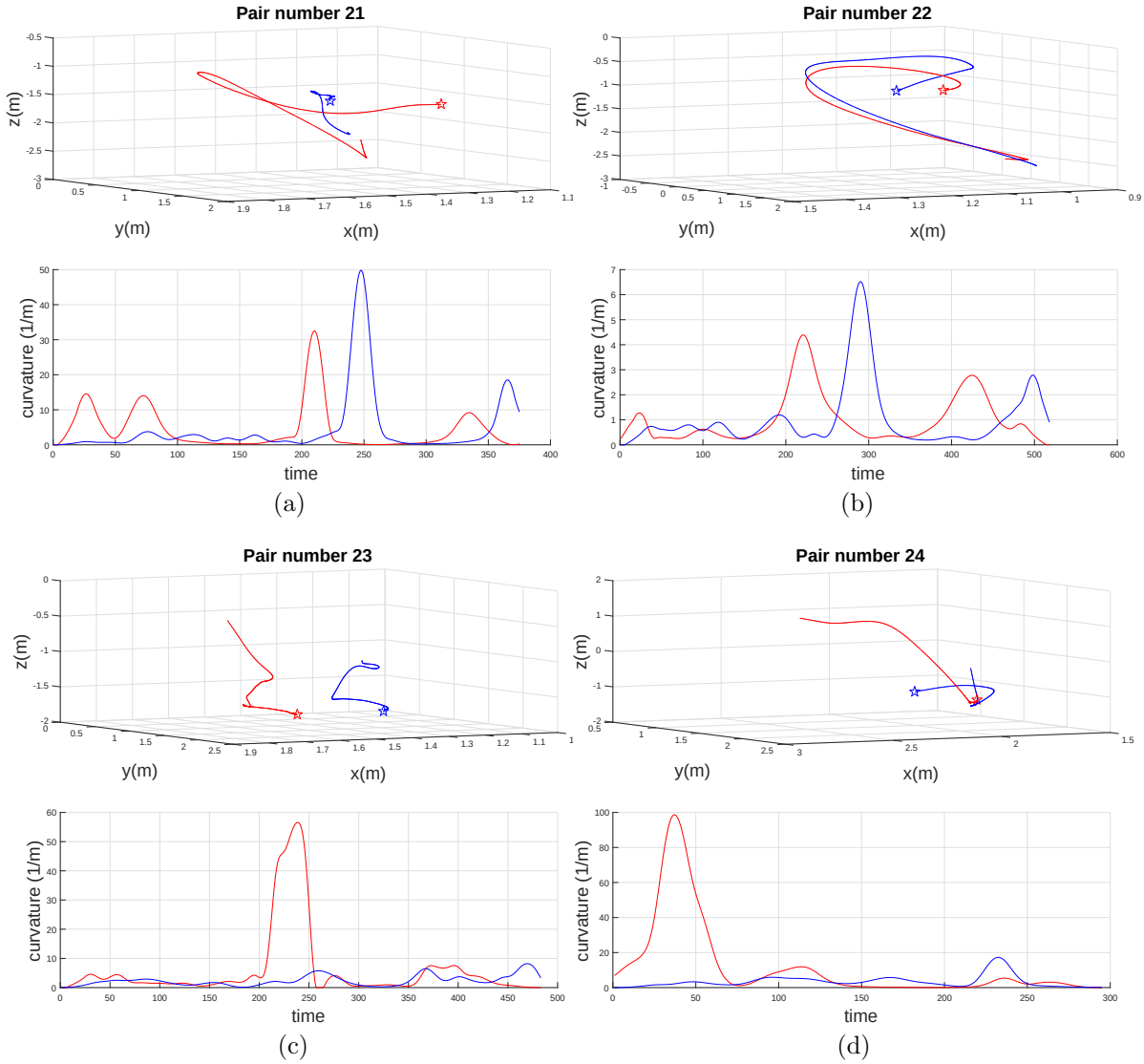

Figure B.6: 3D trajectories and corresponding curvatures of bat pairs from (a) pair number 21, (b) pair number 22, (c) pair number 23, (d) pair number 24. Front and the rear bats are denoted by red and blue lines, respectively, and the symbol star is used to represent the start of the path.

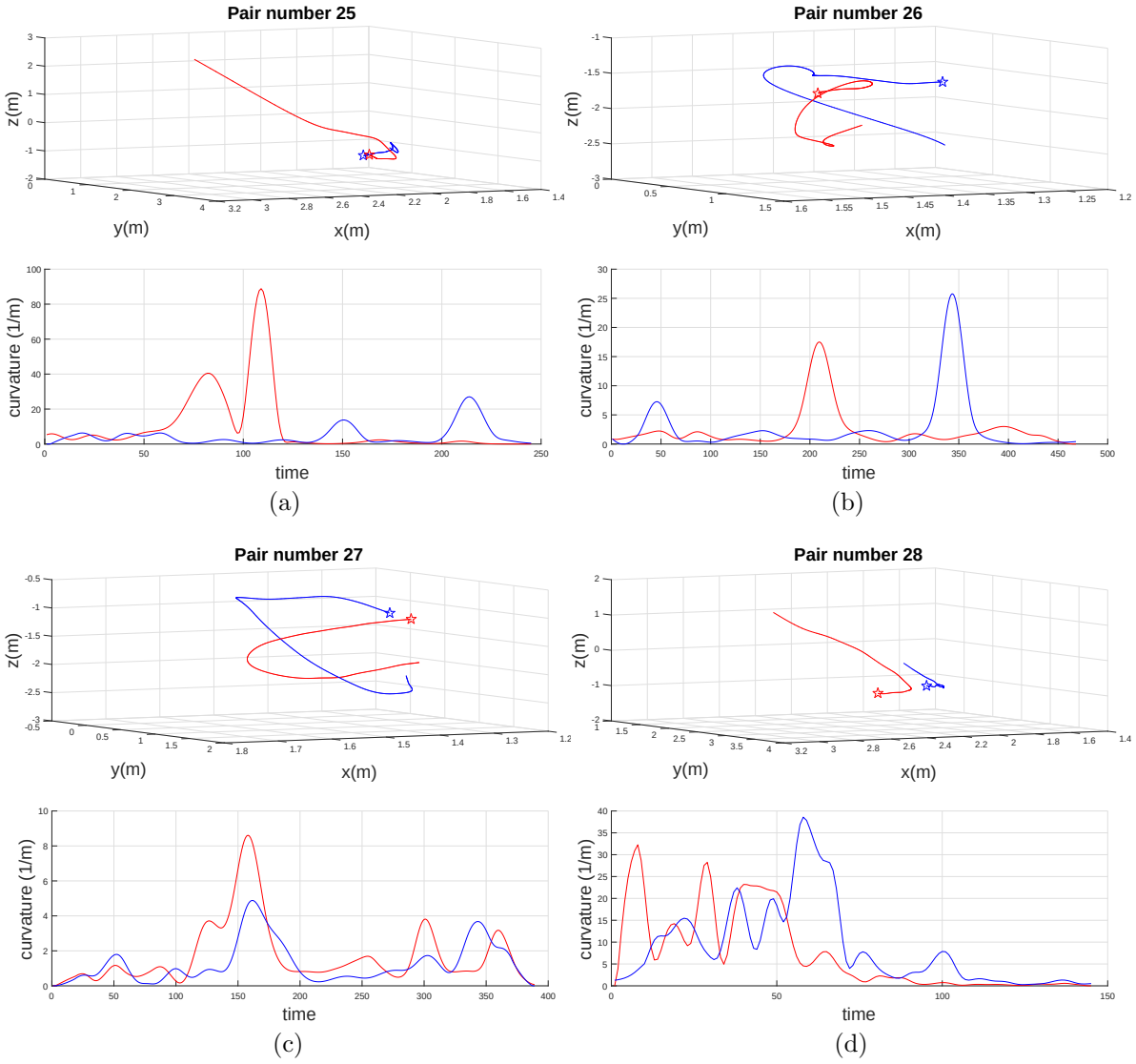

Figure B.7: 3D trajectories and corresponding curvatures of bat pairs from (a) pair number 25, (b) pair number 26, (c) pair number 27, (d) pair number 28. Front and the rear bats are denoted by red and blue lines, respectively, and the symbol star is used to represent the start of the path.

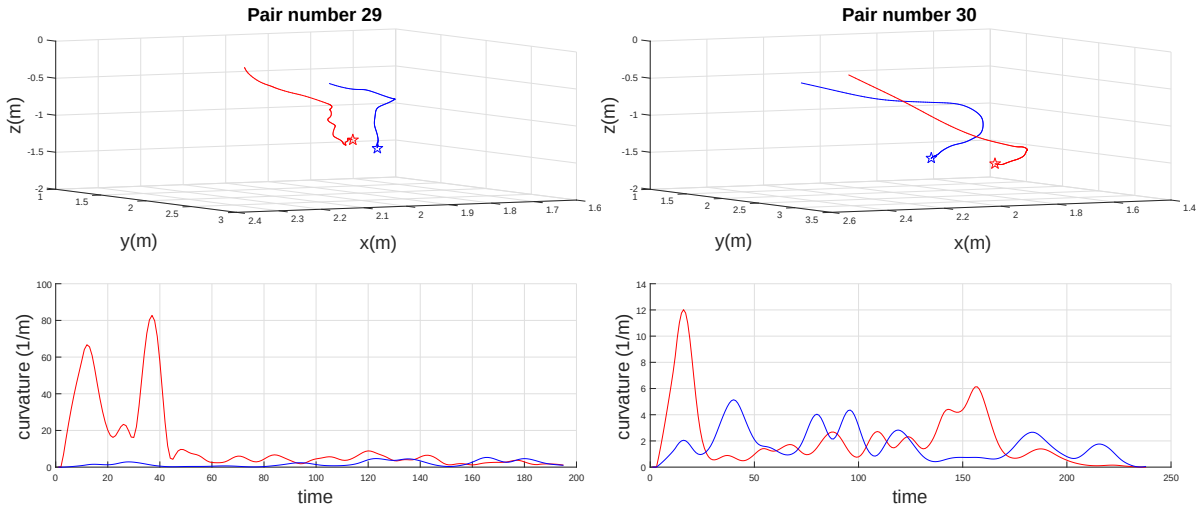

Figure B.8: 3D trajectories and corresponding curvatures of bat pairs from (a) pair number 13, (b) pair number 29, (c) pair number 30. Front and the rear bats are denoted by red and blue lines, respectively, and the symbol star is used to represent the start of the path.

Appendix C

Journal copyright permissions

Chapter 2 is the paper published in IEEE Transactions on Automatic Control which belongs to IEEE. According to the copyright policy from IEEE it does not require individuals working on a thesis to obtain a formal reuse license, however following IEEE copyright/ credit notice should be placed prominently. Detailed information about IEEE copyright information can be found through this link: `https://www.ieee.org/publications_standards/publications/rights/permissions_faq.pdf`. The paper can be found through this link: `http://ieeexplore.ieee.org/abstract/document/7426773/`.

Chapter 3 is the paper published in Chaos: An Interdisciplinary Journal of Nonlinear Science which belongs to American Institute of Physics (AIP). According to the copyright policy from AIP, "AIP Publishing permits authors to include their published articles in a thesis or dissertation. It is understood that the thesis or dissertation may be published in print and/or electronic form and offered for sale on demand, as well as included in a university repository. Formal permission from AIP Publishing is not needed. If the university requires written permission, however, we are happy to supply it." Thus, the permission to include the paper as Chapter 3 is granted. Detailed information about AIP copyright information can be found through this link: `https://publishing.aip.org/authors/copyright-reuse`. The paper can be found through this link: `http://aip.scitation.org/doi/abs/10.1063/1.4967385`.

Chapter 4 is the paper published in the Royal Society Open Science which belongs to Royal Society. According to the copyright policy from Royal Society, the authors can include the articles in a thesis or dissertation provided that this is not to be published commercially. Thus, the permission to include the paper as Chapter 4 is granted. Detailed information about Royal Society copyright information can be found through this link: `https://royalsociety.org/journals/permissions/`. The paper can be found through this link: `http://rsos.royalsocietypublishing.org/content/4/6/170130`.